

**PERMEABILITY OF INTACT SANDSTONES UNDER
DEVIATORIC STRESS STATES**

Natthawat Akkrachattrarat

A Thesis Submitted in Partial Fulfillment of the Requirements for the

Degree of Master of Engineering in Geotechnology

Suranaree University of Technology

Academic Year 2009

ความซึมผ่านของหินทรายภายใต้สภาวะความเค้นเบี่ยงเบน

นายณัฐวัฒน์ อัครนัทรรัตน์

วิทยานิพนธ์นี้เป็นส่วนหนึ่งของการศึกษาตามหลักสูตรปริญญาวิศวกรรมศาสตรมหาบัณฑิต
สาขาวิชาเทคโนโลยีธรณี
มหาวิทยาลัยเทคโนโลยีสุรนารี
ปีการศึกษา 2552

**PERMEABILITY OF INTACT SANDSTONES UNDER
DEVIATORIC STRESS STATES**

Suranaree University of Technology has approved this thesis submitted in partial fulfillment of the requirements for the Master's degree.

Thesis Examining Committee

(Asst. Prof. Thara Lekuthai)

Chairperson

(Assoc. Prof. Dr. Kittitep Fuenkajorn)

Member (Thesis Advisor)

(Dr. Prachaya Tepnarong)

Member

(Prof. Dr. Pairote Sattayatham)

Acting Vice Rector for Academic Affairs

(Assoc. Prof. Dr. Vorapot Khompis)

Dean of Institute of Engineering

ณัฐวัฒน์ อัครฉัตรรัตน : ความซึมผ่านของหินทรายภายใต้สภาวะความเค้นที่ไม่เท่ากัน (PERMEABILITY OF INTACT SANDSTONES UNDER DEVIATORIC STRESS STATES) อาจารย์ที่ปรึกษา : รองศาสตราจารย์ ดร.กิตติเทพ เฟื่องขจร, 101 หน้า

วัตถุประสงค์ของงานวิจัยนี้คือเพื่อศึกษาผลกระทบของความเค้นที่ไม่เท่ากันในแต่ละทิศทางต่อความซึมผ่านของหินพรุน มีการจำลองด้วยระเบียบวิธีเชิงคำนวณเชิงตัวเลขเพื่อศึกษาความซึมผ่านของหินรอบอุโมงค์เดี่ยวและอุโมงค์ขนานรูปทรงกระบอกที่อยู่ใต้สภาวะความเค้นที่ไม่เท่ากัน กิจกรรมที่สำคัญของงานวิจัยนี้ประกอบด้วย การทดสอบอัดน้ำด้วยแรงดันแบบคงที่กับตัวอย่างหินทรายรูปทรงกระบอกภายใต้ความดันรอบข้างและความเค้นที่ไม่เท่ากันที่หลากหลาย ตัวอย่างหินถูกเตรียมจากหินทรายชั้นภูพาน พระวิหาร และภูกระดึง ของกลุ่มหินทรายชุดโคราชซึ่งเป็นตัวแทนของชั้นน้ำบาดาลในภาคเหนือและภาคตะวันออกเฉียงเหนือ หม้อแรงดันได้ถูกนำมาใช้ในการให้ความดันรอบข้างที่คงที่ (อยู่ในช่วงระหว่าง 1, 2 ถึง 3 เมกะปาสกาล) กับตัวอย่างหิน โดยที่ความเค้นในแนวแกนจะเพิ่มขึ้นจนกระทั่งเกิดการวิบัติ ในขณะที่ความเค้นแนวแกนเพิ่มขึ้นได้ทำการตรวจวัดความซึมผ่านของหินในแนวแกน โดยการทดสอบอัดน้ำด้วยแรงดันแบบคงที่เท่ากับ 0.3 เมกะปาสกาล การเปลี่ยนแปลงของตัวอย่างหินพรุนถูกวัดจากการเปลี่ยนแปลงปริมาตรของหิน ผลของความซึมผ่านที่ได้จากการทดสอบจะถูกแสดงอยู่ในฟังก์ชันของความดันรอบข้าง และความเค้นที่แตกต่างกัน

ผลจากการทดสอบความซึมผ่านของหินทรายโดยวิธีอัดน้ำด้วยแรงดันแบบคงที่ภายใต้ สภาวะความเค้นที่ต่างกันระบุว่า ก่อนถึงจุดบวมตัวของหินค่าความซึมผ่านจะลดลงเมื่อค่าความเครียดเชิงปริมาตรเพิ่มขึ้น ซึ่งอาจเป็นผลมาจากการยุบตัวของช่องว่างในหิน และในสภาวะนี้ค่าอัตราส่วนการเปลี่ยนแปลงระหว่างความซึมผ่านต่อความเครียดเชิงปริมาตรจะลดลงเมื่อค่าความดันรอบข้างเพิ่มขึ้น เมื่อหินอยู่ในสภาวะผ่านจุดบวมตัวของหินไปแล้ว ค่าความซึมผ่านจะเพิ่มขึ้นตามการบวมตัวของหินเพราะเกิดการขยายตัวของรอยแตกเนื่องมาจากการเพิ่มความเค้นกดในแนวแกนจนกระทั่งเกิดการวิบัติ แบบจำลองแบบไฟไนต์ดิฟเฟอเรนซ์จำนวน 2 แบบ ถูกสร้างขึ้นเพื่อเป็นตัวแทนอุโมงค์เดี่ยวรูปทรงกระบอกในมวลหิน และอุโมงค์รูปวงกลมในแนวนอนที่อยู่ภายใต้สภาวะความเค้นไม่เท่ากัน ผลที่ได้จากแบบจำลองเชิงตัวเลขระบุว่าค่าความซึมผ่านของหินรอบอุโมงค์เดี่ยวเพิ่มขึ้นจาก 107×10^{-9} ถึง 120×10^{-9} เมตรต่อวินาที สำหรับหินทรายชุดพระวิหารและจาก 140×10^{-12} ถึง 300×10^{-12} เมตรต่อวินาที สำหรับหินทรายชุดภูกระดึงเมื่ออัตราส่วนระหว่างค่าความเค้นในแนวแกนต่อแนวแกนลดลงจาก 0.8 ถึง 0.2 ค่าความซึมผ่านของหินรอบอุโมงค์ขนานเพิ่มขึ้นจาก 120×10^{-9} ถึง 180×10^{-9} เมตรต่อวินาที สำหรับหินทราย

ชุดพระวิหาร และจาก 350×10^{-12} ถึง 1350×10^{-12} เมตรต่อวินาที สำหรับหินทรายชุดภูกระดึงเมื่อค่า
ความเค้นในแนวแกนเพิ่มจาก 10 ถึง 40 เมกกะปาสกาล

สาขาวิชา เทคโนโลยีธรณี

ปีการศึกษา 2552

ลายมือชื่อนักศึกษา _____

ลายมือชื่ออาจารย์ที่ปรึกษา _____

NATTHAWAT AKKRACHATTRARAT : PERMEABILITY OF INTACT
SANDSTONES UNDER DEVIATORIC STRESS STATES. THESIS
ADVISOR : ASSOC. PROF. KITTITEP FUENKAJORN, Ph.D., PE. ., 78 PP.

SANDSTONE/PERMEABILITY/DEVIATORIC STRESS/FLOW

The objectives of this research are to experimentally determine the effects of anisotropic stress states on the permeability of porous rocks. Numerical modeling is performed to study the hydraulic conductivity of rock around single opening in infinite plate and of pillars between parallel circular openings under deviatoric stresses. The effort primarily involves conducting constant-head flow test on intact cylindrical sandstone specimens under a variety of confining pressures and deviatoric stresses. The rock specimens are prepared from Phu Phan, Phra Wihan and Phu Kradung formations of Khorat group, representing ones of the aquifers in the north and northeast of Thailand. Hoek cell is used to apply constant confining pressures (ranging from 1, 2 to 3 MPa) to the specimens while the axial stress is increased until failure. During loading the rock permeability in axial direction is monitored by performing constant-head flow test with water injection pressure up to 0.3 MPa. The changes of rock porosity are measured from the volumetric changes of the specimen. The permeability results are presented as a function of confining pressure, deviatoric stress.

The results from the constant head flow tests under deviatoric stress states suggest that before dilation strength the permeability decreases with increasing volumetric strain. This is probably due to the contraction of the pore spaces in the specimen. Within this stage the change of rock hydraulic conductivity to the change of volumetric strain ($\Delta K/\Delta \varepsilon_v$ ratio) decreases as increasing the confining pressures.

After dilation strength the rock permeability increases with specimen dilation probably because of the initiation and propagation of micro-cracks due to the applied axial stress approaching failure. Two finite difference mesh models are constructed to represent single circular opening in infinite plate and parallel circular tunnels under deviatoric stresses. The results suggest that the hydraulic conductivity of rock around single circular tunnel increases from 107×10^{-9} to 120×10^{-9} m/s for PW sandstone, and 140×10^{-12} to 300×10^{-12} m/s for PK sandstone as the horizontal-vertical stress ratio decreases from 0.8 to 0.2. The hydraulic conductivity of rock pillars between parallel circular openings increases from 120×10^{-9} to 180×10^{-9} m/s for PW sandstone, and 350×10^{-12} to 1350×10^{-12} m/s for PK sandstone as the vertical stress increases from 10 to 40 MPa.

School of Geotechnology

Academic Year 2008

Student's Signature _____

Advisor's Signature _____

ACKNOWLEDGEMENTS

The author wishes to acknowledge the support from the Suranaree University of Technology (SUT) who has provided funding for this research.

Grateful thanks and appreciation are given to Assoc. Prof. Dr. Kittitep Fuenkajorn, thesis advisor, who lets the author work independently, but gave a critical review of this research. Many thanks are also extended to Asst. Prof. Thara Lekuthai and Dr. Prachaya Tepnarong, who served on the thesis committee and commented on the manuscript.

Finally, I most gratefully acknowledge my parents and friends for all their supports throughout the period of this research.

Natthawat Akkrachattrarat

TABLE OF CONTENTS

	Page
ABSTRACT (THAI)	I
ABSTRACT (ENGLISH).....	III
ACKNOWLEDGEMENTS.....	V
TABLE OF CONTENTS	VI
LIST OF TABLES.....	IX
LIST OF FIGURES	X
LIST OF SYMBOLS AND ABBREVIATIONS.....	XVII
CHAPTER	
I INTRODUCTION	1
1.1 Background of problems and significance of the study	1
1.2 Research objectives	2
1.3 Research methodology	2
1.3.1 Literature review.....	3
1.3.2 Sample collection and preparation	3
1.3.3 Constant head flow test under various confining pressures	4
1.3.4 Numerical modeling	4
1.3.5 Thesis writing and presentation.....	4

TABLE OF CONTENTS (Continued)

	Page
1.4	Scope and limitations of the study..... 4
1.5	Thesis contents 5
II	LITERATURE REVIEW 6
2.1	Introduction 6
2.2	Permeability of rock mass 6
2.3	Permeability of intact rock 9
2.4	Damage growth and permeability change 11
2.5	The effect of fluids on deformations 13
2.6	Stress dependent permeability 15
2.7	Permeability-porosity relationship 17
2.8	Effect of pore pressure and permeability in deep boreholes 19
III	SAMPLE PREPARATION 22
3.1	Introduction 22
3.2	Samples collection..... 22
3.3	Mineralogical study 25
IV	LABORATORY EXPERIMENT 26
4.1	Introduction 26
4.2	Test method 26
4.3	Test results..... 27
4.4	Discussions 39

TABLE OF CONTENTS (Continued)

	Page
V NUMERICAL MODELING	40
5.1 Objective.....	40
5.2 Rock properties for computer modeling.....	40
5.3 Finite difference simulations	41
5.3.1 Single circular opening in infinite plate under deviatoric stresses	41
5.3.2 Results	45
5.3.2.1 Effect of horizontal-to-vertical stress ratio (k)	46
5.3.2.2 Effect of magnitudes of stress	46
5.3.3 Horizontal parallel circular opening under deviatoric stresses	55
5.3.4 Results	57
V DISCUSSIONS, CONCLUSIONS AND RECOMMENDATIONS FOR FUTURE STUDIES	62
6.1 Discussions and conclusions	62
6.2 Recommendations for future studies	63
REFERENCES	64
APPENDIX A TECHNICAL PUBLICATION	68
BIOGRAPHY	86

LIST OF TABLES

Table	Page
3.1 Mineral compositions of three sandstones determined by X-ray diffraction analysis	25
4.1 Results of flow testing under deviatoric stresses.....	28
5.1 Summary of the basic mechanical properties as obtained from Walsri et al. (2009).	41
5.2 Variables used in FLAC simulations for single circular opening in infinite plate with 4 m radius.....	42
5.3 Initial hydraulic conductivity of sandstone specimens.....	44
5.4 Variables used in FLAC simulations for horizontal parallel opening	55

LIST OF FIGURES

Figure	Page
1.1 Research methodology.....	3
2.1 Fluid flow paths in intact and fractured rock specimens (Indraratna and Ranjith, 2001).....	7
2.2 Application of fracture and matrix permeability in different locations (Indraratna and Ranjith, 2001)	8
2.3 Pressure gradients along a rock specimen (Indraratna and Ranjith, 2001).....	10
2.4 Permeability change of Bandera sandstone under stress conditions (Wilhelmi et al.,1967).	18
2.5 Volumes and permeability dilatancy of Westerly granite (Zoback et al., 1975).....	18
2.6 (a) Notation of stresses around a vertical borehole and (b) graphs showing the distribution of elastic stresses along a horizontal drawn from the borehole axis (Spivak and popov, 1986).....	21
3.1 Laboratory core drilling. The core drilling machine (model SBEL 1150) is used to drill core specimens using diamond impregnated bit with diameter of 54 mm.....	23

LIST OF FIGURES (Continued)

Figure	Page
3.2	A core specimen of PK sandstone is cut to length by a cutting machine 24
3.3	Some sandstone specimens prepared for the constant head flow test under deviatoric stress states 24
4.1	Laboratory arrangement for constant head flow tests of sandstone cylindrical specimen under deviatoric stress 28
4.2	Laboratory arrangement for constant head flow tests of sandstone cylindrical specimen under deviatoric stress 29
4.3	Applied principal stress directions with respect to the bedding planes for all specimens. 29
4.4	Permeability of Phra Wihan sandstone specimen tested under confining pressure of 1 MPa (top) with the corresponding stress-strain curves (bottom) 30
4.5	Permeability of Phra Wihan sandstone specimen tested under confining pressure of 2 MPa (top) with the corresponding stress-strain curves (bottom) 31
4.6	Permeability of Phra Wihan sandstone specimen tested under confining pressure of 3 MPa (top) with the corresponding stress-strain curves (bottom) 32

LIST OF FIGURES (Continued)

Figure	Page
4.7	Permeability of Phu Phan sandstone specimen tested under confining pressure of 1 MPa (top) with the corresponding stress-strain curves (bottom).....33
4.8	Permeability of Phu Phan sandstone specimen tested under confining pressure of 2 MPa (top) with the corresponding stress-strain curves (bottom).....34
4.9	Permeability of Phu Phan sandstone specimen tested under confining pressure of 3 MPa (top) with the corresponding stress-strain curves (bottom).....35
4.10	Permeability of Phu Kradung sandstone specimen tested under confining pressure of 1 MPa (top) with the corresponding stress-strain curves (bottom).....36
4.11	Permeability of Phu Kradung sandstone specimen tested under confining pressure of 2 MPa (top) with the corresponding stress-strain curves (bottom).....37
4.12	Permeability of Phu Kradung sandstone specimen tested under confining pressure of 3 MPa (top) with the corresponding stress-strain curves (bottom).....38
5.1	Finite difference mesh for modeling single circular opening in infinite media (Model A).....44

LIST OF FIGURES (Continued)

Figure	Page
5.2	Constitutive relation assumed in this analysis 45
5.3	Volumetric strain and permeability of Phra Wihan sandstone simulated around single circular opening subjected to $\sigma_1=10$ MPa and $\sigma_3=2$ MPa ($\nu=0.35$, $E=8.66$ GPa)..... 47
5.4	Volumetric strain and permeability of Phra Wihan sandstone simulated around single circular opening subjected to $\sigma_1=10$ MPa and $\sigma_3=4$ MPa ($\nu=0.35$, $E=8.66$ GPa)..... 47
5.5	Volumetric strain and permeability of Phra Wihan sandstone simulated around single circular opening subjected to $\sigma_1=10$ MPa and $\sigma_3=6$ MPa ($\nu=0.35$, $E=8.66$ GPa)..... 48
5.6	Volumetric strain and permeability of Phra Wihan sandstone simulated around single circular opening subjected to $\sigma_1=10$ MPa and $\sigma_3=8$ MPa ($\nu=0.35$, $E=8.66$ GPa)..... 48
5.7	Volumetric strain and permeability of Phu Kradung sandstone simulated around single circular opening subjected to $\sigma_1=10$ MPa and $\sigma_3=2$ MPa ($\nu=0.30$, $E=7.70$ GPa)..... 49
5.8	Volumetric strain and permeability of Phu Kradung sandstone simulated around single circular opening subjected to $\sigma_1=10$ MPa and $\sigma_3=4$ MPa ($\nu=0.30$, $E=7.70$ GPa)..... 49

LIST OF FIGURES (Continued)

Figure	Page
5.9 Volumetric strain and permeability of Phu Kradung sandstone simulated around single circular opening subjected to $\sigma_1=10$ MPa and $\sigma_3=6$ MPa ($\nu=0.30$, $E=7.70$ GPa).....	50
5.10 Volumetric strain and permeability of Phu Kradung sandstone simulated around single circular opening subjected to $\sigma_1=10$ MPa and $\sigma_3=8$ MPa ($\nu=0.30$, $E=7.70$ GPa).....	50
5.11 Volumetric strain and permeability of Phra Wihan sandstone simulated around single circular opening subjected to $\sigma_1=10$ MPa and $\sigma_3=5$ MPa ($\nu=0.30$, $E=7.70$ GPa).....	51
5.12 Volumetric strain and permeability of Phra Wihan sandstone simulated around single circular opening subjected to $\sigma_1=20$ MPa and $\sigma_3=10$ MPa ($\nu=0.30$, $E=7.70$ GPa).....	51
5.13 Volumetric strain and permeability of Phra Wihan sandstone simulated around single circular opening subjected to $\sigma_1=30$ MPa and $\sigma_3=15$ MPa ($\nu=0.30$, $E=7.70$ GPa).....	52
5.14 Volumetric strain and permeability of Phra Wihan sandstone simulated around single circular opening subjected to $\sigma_1=40$ MPa and $\sigma_3=20$ MPa ($\nu=0.30$, $E=7.70$ GPa).....	52

LIST OF FIGURES (Continued)

Figure	Page
5.15 Volumetric strain and permeability of Phu Kradung sandstone simulated around single circular opening subjected to $\sigma_1=10$ MPa and $\sigma_3=5$ MPa ($\nu=0.30$, $E=7.70$ GPa).....	53
5.16 Volumetric strain and permeability of Phu Kradung sandstone simulated around single circular opening subjected to $\sigma_1=20$ MPa and $\sigma_3=10$ MPa ($\nu=0.30$, $E=7.70$ GPa).....	53
5.17 Volumetric strain and permeability of Phu Kradung sandstone simulated around single circular opening subjected to $\sigma_1=30$ MPa and $\sigma_3=15$ MPa ($\nu=0.30$, $E=7.70$ GPa).....	54
5.18 Volumetric strain and permeability of Phu Kradung sandstone simulated around single circular opening subjected to $\sigma_1=40$ MPa and $\sigma_3=20$ MPa ($\nu=0.30$, $E=7.70$ GPa).....	54
5.19 Finite difference mesh for modeling parallel circular opening (Model B).....	56
5.20 Volumetric strain and permeability of Phra Wihan sandstone simulated around horizontal parallel tunnel subjected to $\sigma_v=10$ MPa ($\nu=0.35$, $E=8.66$ GPa)	58
5.21 Volumetric strain and permeability of Phra Wihan sandstone simulated around horizontal parallel tunnel subjected to $\sigma_v=20$ MPa ($\nu=0.35$, $E=8.66$ GPa)	58

LIST OF FIGURES (Continued)

Figure	Page
5.22 Volumetric strain and permeability of Phra Wihan sandstone simulated around horizontal parallel tunnel subjected to $\sigma_v=30$ MPa ($\nu=0.35$, $E=8.66$ GPa)	59
5.23 Volumetric strain and permeability of Phra Wihan sandstone simulated around horizontal parallel tunnel subjected to $\sigma_1=40$ MPa ($\nu=0.35$, $E=8.66$ GPa)	59
5.24 Volumetric strain and permeability of Phu Kradung sandstone simulated around horizontal parallel tunnel subjected to $\sigma_1=10$ MPa ($\nu=0.30$, $E=7.70$ GPa)	60
5.25 Volumetric strain and permeability of Phu Kradung sandstone simulated around horizontal parallel tunnel subjected to $\sigma_1=20$ MPa ($\nu=0.30$, $E=7.70$ GPa)	60
5.26 Volumetric strain and permeability of Phu Kradung sandstone simulated around horizontal parallel tunnel subjected to $\sigma_1=30$ MPa ($\nu=0.30$, $E=7.70$ GPa)	61
5.27 Volumetric strain and permeability of Phu Kradung sandstone simulated around horizontal parallel tunnel subjected to $\sigma_1=40$ MPa ($\nu=0.30$, $E=7.70$ GPa)	61

LIST OF SYMBOLS AND ABBREVIATIONS

A	=	Cross section area
C^*	=	Shear-enhance compaction
D	=	Diameter
dp	=	Pressure gradient
dx	=	Length of the specimen
g	=	Acceleration of gravity
k	=	Coefficient of permeability
K	=	Hydraulic conductivity
k_1	=	Maximum principal permeability tensor
k_3	=	Minimum principal permeability tensor
k_f	=	Fracture permeability
k_m	=	Matrix permeability
K_0	=	Initial hydraulic conductivity
L	=	Length
m/s	=	Meter/Second
p_0	=	Initial pressure
p_e	=	Exit pressure
P_{geo}	=	Magnitude of the lithostatic
p_i	=	Inlet pressure

LIST OF ABBREVIATIONS (Continued)

psi	=	Pound/inch ²
p_t	=	Final pressure
q	=	Fluid flow rate
R_{bh}	=	Borehole radius
V_o	=	Oil volume
V_R	=	Rock volume
V_s	=	Volume of oil displaced by loading platen
ε_1	=	Axial strain
ε_2	=	Lateral strain
ε_3	=	Lateral strain
ε_D	=	Dilation strain
ε_v	=	Volumetric strain
μ	=	Viscosity of the fluid
ρ	=	Density of the fluid
σ_1	=	Maximum principal stress
σ_2	=	Intermediate principal stress
σ_3	=	Minimum principal stress
σ_r	=	Radial stress
σ_θ	=	Tangential stress
β	=	Isothermal compressibility
λ	=	Coefficient of the lateral outward thrust
ν	=	Poisson ratio

CHAPTER I

INTRODUCTION

1.1 Background of problems and significance of the study

Hydraulic properties of porous rocks are one of the important parameters in determining the potential yields of groundwater aquifers and the recovery of oil and gas reservoirs. It has been commonly found that the confining pressure can notably reduce the effective porosity of rocks, and subsequently decrease their permeability. The sensitivity of the rock hydraulic properties to the magnitude of confinement primarily depends on rock types and their packing density. This finding has been concluded from many flow tests conducted in the laboratory under controlled-hydrostatic pressures. In the actual field conditions, however, rocks around groundwater pumping wells and petroleum production wells are subjected to anisotropic stress states where the tangential and axial stresses are normally higher than the radial stress. The difference becomes even greater for a deeper borehole. In principle the rock deformation and the change of pore spaces under anisotropic stress state are different from those under isotropic condition. Knowledge and experimental evidences on how the rock permeability changes under anisotropic stress conditions have been rare.

It has been experimentally found that permeability of intact rocks is affected by the confining pressures (Iskan et al., 2006; Shangxian and Shangxu, 2006) and by deviatoric stresses (Ferfera et al., 1997; Oda et al., 2002; Pusch and Weber, 1998;

Heiland, 2003; Zhou and Shao, 2006). The rock permeability generally decreases logarithmically with increasing the confining pressures. Under deviatoric stresses the rock permeability first decreases due to a reduction of pore spaces, and starts to increase due to the damage growth after the rock is dilated under differential stresses.

1.2 Research objectives

The objectives of this research are to experimentally determine the effects of anisotropic stress states on the permeability of porous rocks, and numerical modeling in this research aims at studying the behavior and hydraulic conductivity of rock around single and parallel circular tunnel in infinite plate under deviatoric stresses. The effort primarily involves conducting constant-head flow test on intact cylindrical sandstone specimens under a variety of confining pressures and deviatoric stresses. The permeability results will be presented as a function of confining pressure, deviatoric stress, and effective porosity. The research findings will improve our understanding of hydraulic properties of porous rocks as affected by the magnitudes and directions of the applied stress. A true understanding of the hydro-mechanical responses of the porous rocks to the complex stress conditions is necessary for predicting the rates of production of groundwater from aquifer, or oil and gas from reservoir.

1.3 Research methodology

The research methodology (Figure 1) comprises 5 steps; literature review, sample collection and preparation, laboratory testing, computer modeling, and thesis writing and presentation.

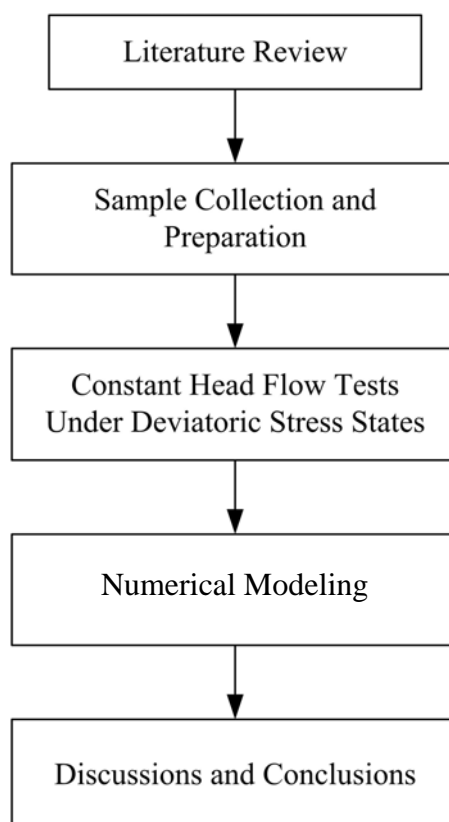


Figure 1.1 Research methodology.

1.3.1 Literature review

Literature review is carried out to study the genesis and classification of fractures, permeability of rock mass, apertures, and stress effects on fracture void geometry. The sources of information are from text books, journals, technical reports and conference papers. A summary of the literature review is given in the thesis.

1.3.2 Sample collection and preparation

Sandstone samples are collected from the site. A minimum of 3 sandstone types is tested. Sample preparation is carried out in the laboratory at the Suranaree University of Technology. Samples prepared for the constant head test are 5 cm in diameter and 10 cm long.

1.3.3 Constant head flow test under various confining pressures.

A constant diameter water pump is used to inject water pressure to one end of the specimen. The specimen is placed in triaxial cell which is used to applied constant confining pressures to the rock. The applied confining pressures vary from 1 to 3 MPa. The injected water pressure is about 0.3 MPa which is controlled by using a regulating valve at the top of nitrogen gas tank. A high precision pipette is use to collect outflow of water at the other end of the specimen. The measured flow rates at each confining pressure are measured to calculate the rock permeability.

1.3.4 Numerical modeling

A 2-dimensional finite difference mesh is constructed to graphically represent the rock formation. The computations use the linear finite element code “FLAC”. The algorithm of this computer code is designed to calculate the stress and displacement. It is used to determine elastic zone, plastic zone and volumetric strain.

Results from laboratory measurements in terms of rock permeability and stress states will be used to construct computer models to simulate or predict the hydraulic conductivity of the rock around the tunnels during operation.

1.3.5 Thesis writing and presentation

All research activities, methods and results are documented and complied in the thesis.

1.4 Scope and limitations of the study

The scope and limitations of the research include as follows.

1. Laboratory experiments are conducted on specimens from three formations of sandstone, including Phu Kra-dueng, Pra Wihan and Phu Phan sandstones.

2. Hoek cell will be used to apply constant confining pressures (ranging from 1, 2 to 3 MPa) to the specimens while the axial stress is increased until failure.
3. The changes of rock porosity are measured from the volumetric changes of the specimen.
4. All tests are conducted under ambient temperature.
5. Up to 3 samples are tested for each rock type.
6. The minimum size of specimens is 5 cm in diameter and 10 cm long.
7. Water is used as flow medium.
8. No field testing is conducted.

1.5 Thesis contents

Chapter I introduces the thesis by briefly describing the background of problems and significance of the study. The research objectives, methodology, scope and limitations are identified. **Chapter II** summarizes results of the literature review. **Chapter III** describes the sample collection and preparation. **Chapter IV** presents the results obtained from the constant head flow test under deviatoric stresses. **Chapter V** describes the numerical modeling to predict the hydraulic conductivity of rock around openings. **Chapter VI** concludes the research results, and provides recommendations for future research studies. **Appendix A** provides detailed of technical publication.

CHAPTER II

LITERATURE REVIEW

2.1 Introduction

Relevant topics and previous research results are reviewed to improve an understanding of fluid flow through porous rock. These include (1) permeability of intact rock, (2) permeability of intact rock, (3) damage growth and permeability change, (4) effect of fluids on deformations, (5) stress dependent permeability, (6) permeability-porosity relationship and (7) effect of pore pressure and permeability on well stability in deep boreholes

2.2 Permeability of rock mass

Indraratna and Ranjith (2001) state that permeability is simply the ability to conduct fluids, such as water, gas or multi-phase flows (e.g. water + gas, water + gas + oil) through porous media, such as soil or rocks. The permeability of discontinuities is referred to as the fracture permeability or the intrinsic permeability, whereas intact permeability is referred to as the matrix permeability. Therefore, the combined permeability of rock mass is given by

$$k = k_f + k_m \tag{2.1}$$

where k is the combined permeability of rock mass, and k_f and k_m are the individual fracture permeability and matrix permeability, respectively.

For crystalline rocks, fluid flow through rock matrix is much less than that through fractures, because the extent of interconnected pores and the pore sizes in hard rocks is generally small. Permeability can greatly influence the mechanical behavior of rocks, thereby increasing or decreasing the stability of rock structures. As shown in Figure 2.1, fluid flow within a rock specimen can take place through either the rock matrix or interconnected discontinuities or combination of both. Under single-phase fluid flow, permeability can be divided into three main categories: (1) Matrix permeability, (2) Fracture permeability and (3) Dual permeability. Application of fractured and matrix permeability in different locations is shown in Figure 2.2 and the calculation of permeability is as follows (Indraratna and Ranjith, 2001).

$$K = \frac{\rho g k}{\mu} \quad (2.2)$$

where K is hydraulic conductivity, ρ is density of the fluid, g is acceleration of gravity, k is the coefficient of permeability and μ is the dynamic viscosity of the fluid

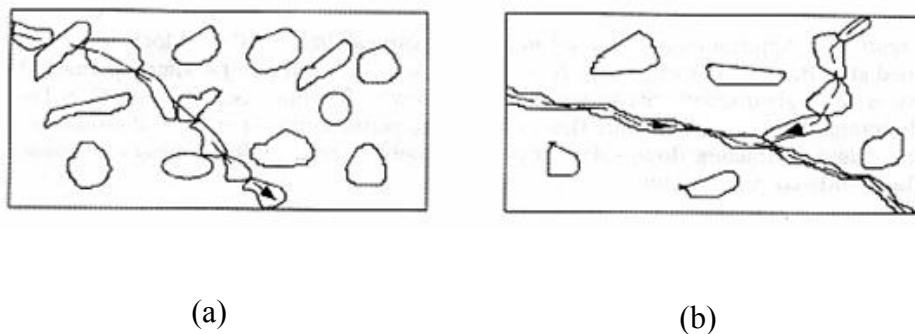


Figure 2.1 (a) Intact rock with voids, where possible flow occurs through interconnected voids. (b) Specimen with a major discontinuity, where flow occurs through discontinuity and any interconnected voids (Indraratna and Ranjith, 2001).

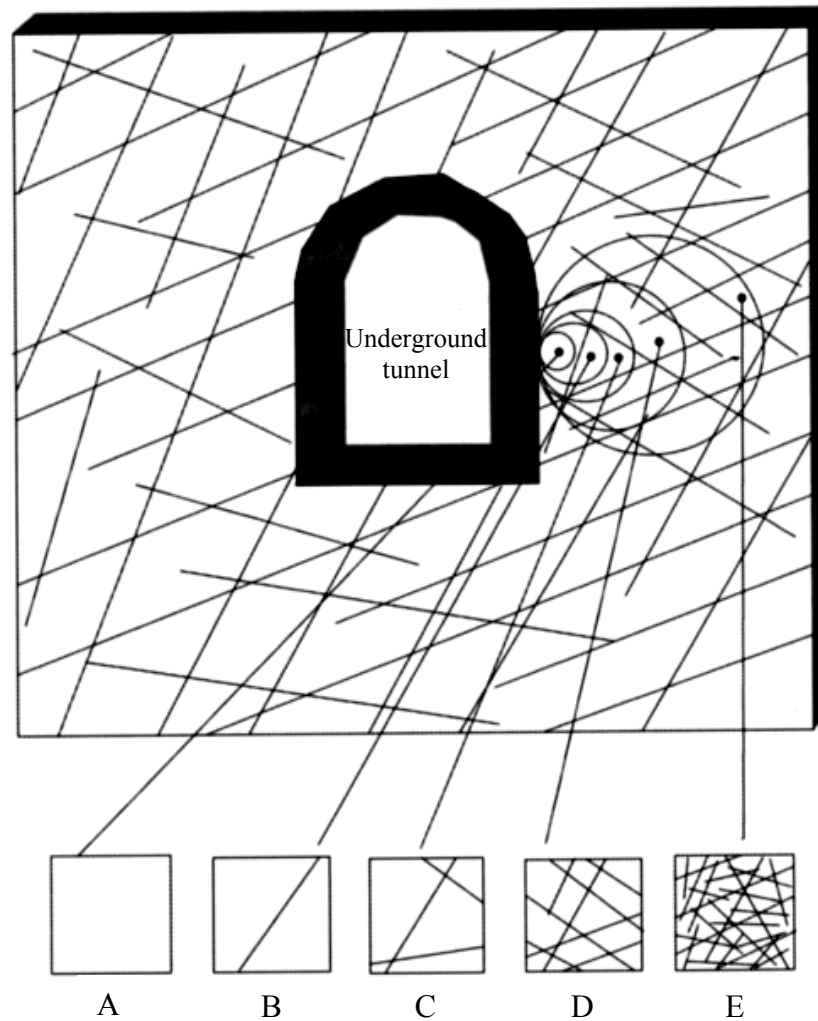


Figure 2.2 Application of fracture and matrix permeability in different locations (Indraratna and Ranjith, 2001).

A = Intact rock (continuum flow) – Matrix permeability,

B = Single discontinuity – Fractured permeability,

C = Two discontinuities – Fractured permeability,

D = Several discontinuities – Fractured permeability,

E = Rock mass – Matrix permeability.

2.3 Permeability of intact rock

Indraratna and Ranjith (2001) state that under steady-state flow rate approach, for a cylindrical rock specimen, the coefficient of matrix/intact rock permeability (k_m) can be written using Darcy's law:

$$k_m = \frac{4q\mu}{\pi D^2 (dp/dx)} \quad (2.3)$$

where q is fluid flow rate through the specimen, dp/dx is the pressure gradient along the length (dx) of the specimen (Figure 2.3), μ is the dynamic viscosity of the fluid and D is the diameter of the specimen.

Apart from the hydraulic gradient and surrounding stresses applied on the specimen, the matrix permeability depends on the properties of the matrix, characterized by the pore size (voids), shapes and the interconnectivity of voids. If the fluid traveling through the porous rock is gas, then the component of the matrix coefficient of air permeability (k_m) is estimated according to the following equation:

$$k_m = \frac{2qp_e\mu L}{(p_i^2 - p_e^2)A} \quad (2.4)$$

where q = gas flow rate, μ = dynamic viscosity of gas, L = length of the specimen, A = cross-section area of specimen, p_i = inlet pressure of gas and p_e = exit pressure of gas.

If the permeability measurement is based on the transient method, the following expressions are used to calculate the matrix permeability coefficient. The pressure pulse decays with time according to the expression given below:

$$p_t = p_0 e^{-\alpha t} \quad (2.5)$$

where p_t and p_0 are final and initial pressure, respectively, t is the decay time and α is an empirical constant. The matrix permeability coefficient for transient method is given by Kranz et al. (1979):

$$k_m = \frac{\alpha \beta \mu L V_1 V_2}{A(V_1 + V_2)} \quad (2.6)$$

where β = isothermal compressibility of fluid, A = cross-sectional area, V_1 and V_2 = volume of pore fluid at the top and the bottom of the sample, respectively, L = length of the specimen and α is calculated using Eqn. 4 for given initial pressure, and for the time period, t .

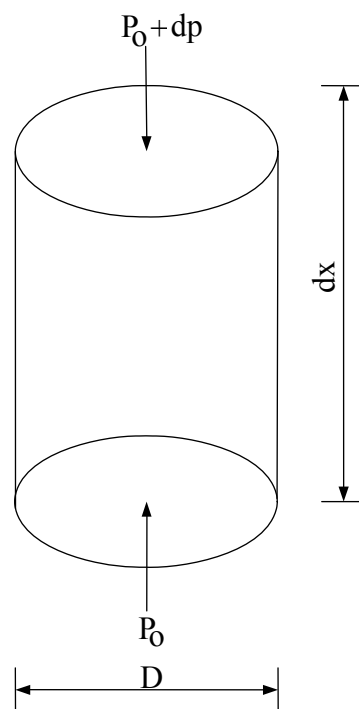


Figure 2.3 Pressure gradients along a rock specimen (Indraratna and Ranjith, 2001).

2.4 Damage growth and permeability change

Oda et al. (2002) study micro cracking (crack growth), along with accumulation of inelastic strain, taking place in crystalline rock, such as granite, when it is subjected to differential stress. As a result, growing cracks become interconnected, completely altering permeability. Therefore, coupling between crack growth and permeability change must be determined to fully understand the hydro-mechanical response of rocks subjected to non-hydrostatic stress. Rocks under stress in the field can be regarded as isotropic porous media, in spite of the fact that cracks grow preferentially parallel to the major stress.

Trimmer (1982) and Kiyama et al. (1996) carried out transient pulse tests in a triaxial vessel to clarify permeability change under increasing stress up to failure. Their tests seemed ideal for that purpose. It should be noted, however, that such tests might result in serious underestimation of permeability coefficients because dead zones, where no microcracking occurs, commonly develop at the top and bottom ends of a triaxially deformed sample (Oda et al., 2002). More importantly, it is not easy to obtain quantitative data concerning damage growth in such tests.

Risnes et al. (2003) stated that hydrostatic loading is the conventional test procedure to determine the stress dependence of permeability. However, hydrostatic tests do not truly reflect the deviatoric stress state that exists in most reservoirs. The main objective of the present project was to study permeability changes under deviatoric stresses, like encountered in standard triaxial tests. However in measuring permeability in a triaxial cell, end effects may be important. The friction between the axial steel pistons and the sample may cause stress concentrations and thereby a non-homogeneous strain pattern towards the sample ends. To overcome this problem, the

cell was modified to have pressure outlets from the mid-section of the sample, with the pressure tubes connected to the outside of the cell for pressure recording. The cell was designed for 1.5 in plugs with plug lengths of about 80 mm. Tests were performed on two types of high porosity outcrop chalk: Liège chalk with porosity around 40 percent and permeability 1-2 millidarcy, and Aalborg chalk with porosity around 45 percent and permeability in the range 3-5 millidarcy. Methanol was used as saturating fluid for the chinks. In addition some sandstone samples from core material were included. The porosity values were rather high, around 30 %, and the permeability ranged from around 50 millidarcy to over one darcy. Synthetic oil was used as saturating fluid for the sandstone samples, to avoid any reactions with clay minerals. The results so far can be summarized as follows : (1) In almost all the tests, the permeability calculated by the overall pressure drop is smaller than the mid-section permeability. The reduction could typically be around 20 %. This means that end-effects play an important role. (2) The permeability generally decreases with increasing hydrostatic stresses. This is in agreement with observations from other sources. (3) During deviatoric phases the average stress level is increasing, but the changes in permeability are rather small, even if the tests are run beyond the yield stress. The mid-section permeability seems to show a small increasing trend with increasing deviatoric stresses after yield. But the yield point does not seem to have any drastic effect on the permeability. (4) The overall permeability seems in general to show a decreasing trend under deviatoric stresses. The results indicate that permeability changes with pressure depletion under reservoir conditions may be much less than expected from hydrostatic tests or tests uncorrected for end-effects.

Zhou and Shao (2006) present a coupled model for anisotropic damage and permeability evolution by using a micro-macro approach. The damage state is represented by a space distribution of microcrack density. The evolution of damage is directly linked to the propagation condition of microcracks. The macroscopic free enthalpy function of cracked material is obtained by using micromechanical considerations. It is assumed that the microcracks exhibit normal aperture which is associated with the crack growth due to the asperity of crack faces. By using Darcy's law for macroscopic fluid flow and assuming laminar flow in microcracks, the overall permeability of the representative volume element is obtained by an averaging procedure taking into account the contribution of crack aperture in each orientation.

2.5 The effect of fluids on deformations

Zhu et al. (2002) investigate the influence of stress on permeability anisotropy during mechanical compaction, a series of triaxial compression experiments with a new loading configuration called hybrid compression were conducted on three porous sandstones. The effective mean and differential stresses in hybrid compression tests were identical to those in conventional triaxial extension tests. Permeability was measured along the axial direction in both hybrid compression and conventional extension tests, which corresponds to flow along the maximum principal stress direction in the former case and the minimum principal stress direction in the latter case. Since their loading paths coincide, the comparison of permeability values from the two types of tests provides quantitative estimates of the development of permeability anisotropy as a function of effective mean and differential stresses. Our data show that the permeability evolution is primarily controlled by stress. Before the

onset of shear-enhanced compaction (C^*), permeability and porosity reduction are solely controlled by the effective mean stress, with negligible stress-induced anisotropy. With the onset of shear-enhanced compaction and initiation of cataclastic flow, the deviatoric stress induces enhanced permeability and porosity reduction. The permeability tensor may show significant anisotropy. Their data indicate that the maximum principal component of permeability tensor (k_1) is parallel to the maximum principal stress (σ_1), and the minimum principal component (k_3) is parallel to the minimum principal stress (σ_3). During the initiation and development of shear-enhanced compaction, k_1 can exceed k_3 by as much as two orders of magnitude. With the progressive development of cataclastic flow, changes of permeability and porosity become gradual again, and the stress-induced permeability anisotropy diminishes as k_1 and k_3 gradually converge. Their data imply that permeability can be highly anisotropic in tectonic settings undergoing cataclastic flow, inducing the fluid to flow preferentially along conduits subparallel to the maximum compression direction. However, this development of permeability anisotropy is transient in nature, becoming negligible with an accumulation of strain of about 10%. The anisotropic development of permeability in a lithified rock is dominantly controlled by microcracking and pore collapse. This is fundamentally different from the mechanisms active in unconsolidated materials such as sediments and fault gouges, in which the permeability evolution is primarily controlled by the development of fabric and shear localization via the accumulation of shear strain.

2.6 Stress dependent permeability

Dautriat et al. (2007) state that mechanical effects are of great importance during reservoir production and induce sensible changes of the transport properties. This work focuses on the forecast of the change of porosity and permeabilities of reservoir rocks submitted to hydrostatic and deviatoric stress states representative of the field conditions. To predict these evolutions, they need to perform flow experiments with representative stress conditions. Their triaxial cell was designed to achieve this purpose and allows the measurement of permeabilities in the directions along and transverse to the principal direction of stresses. A good knowledge of the rock microstructures is also fundamental to choose the correct set of parameters for the simulation tools, and the input from our micro scanner facility is therefore of great importance. Using their directional permeability triaxial apparatus, They applied different stress paths to sandstones and carbonates samples and the evolutions of porosity and permeabilities were monitored during loading. They performed a microstructural analysis of these rocks using Mercury Porosimetry and Computed Micro Tomography imaging. From the 3D reconstructions, they extracted the poral network skeletons and the associated pore and throat size distributions. Then they performed two kinds of pore network modeling, one based on the real pore geometry and another based on a statistical description, to calculate the macroscopic transport properties. They included a model of pressure dependence of pore and throat sizes, based on deformation of porous inclusions in the framework of elasticity theory, to simulate the evolution of the transport properties with pressure. This model requires the knowledge of the elastic moduli of the rocks which were determined experimentally from the compression experiments. They show that the experimental

determination of the evolution of directional permeabilities under hydrostatic and deviatoric stress conditions is feasible. The pressure dependences can be of valuable importance and therefore influence of mechanical effects should be investigated in experimental transport studies. Finally, they show that pore network modeling associated with CMT imaging can be used to forecast the pressure evolution of transport properties and therefore to understand the reservoir response to production.

Pusch and Weber (1998) state that the conversion of rock properties like porosity and permeability to downhole or in-situ conditions is routinely based on compressive stress-strain relationships. In a stress field, which is free from sinks and sources, isostatic stress conditions can be assumed in underground porous formations. This situation however changes in the vicinity of shafts, wells, storage caverns, tunnels and underground galleries, where the tangential and radial stress are different at the wall of the cavity. As a consequence the deformation of the rock leads to embrittlement, microfracturing, fracture and disintegration of rock zones and transportation of rock fragments (sand production). The whole spectrum of phenomena from dislocation to fracturing is controlled by the continuum-mechanics principle. For a variety of materials – unconsolidated and consolidated sands, crystalline rocks, clay, rock salt etc. – the stress-strain relationship is well defined from elastic to viscous behavior, comprising all intermediate stages of elastoplastic to viscoplastic state. The most complicated material behavior of salt rocks even includes time dependent effects, like creeping, which has to be taken into account in rock mechanical models.

The deformation of porous media is mathematically characterized by the superposition of elastic and non-elastic strain components. If the deviatoric stress

ratio that is the ratio of the maximum and the minimum normal stress is low, the compression-state of pore space deformation dominates. If a critical stress ratio is exceeded, the increasing shear tension leads to an extension of the pore volume (dilatancy). The mathematical algorithms for the correlation of stress – strain – permeability relations are based on power law functions and the cubic root law for the permeability of fissure-networks. Walsh (1981) and Witherspoon (1980) have described such functions for crystalline rocks, Ali (1987) and Wilhelmi and Somerton (1967) for sedimentary rocks. An example is shown in Figure 2.4.

For increasing deviatoric stress ratios, Holt (1989) describes a pronounced permeability reduction for North Sea reservoir rocks (sandstones), if the elastic deformation boundary of roughly 70 MPa is exceeded. This may lead to plastic deformation of the near wellbore zone and to sand production. In compression experiments with Dalquhandy-sandstone Smart (1992) observes a permeability and corresponding strain minimum, which leads to disintegration of the rock. Zoback and Byerlee (1975) have performed experiments with Westerly-granite and correlates a pore volume and permeability dilatancy with the deviator stress after exceeding the critical stress ratio σ_1 / σ_3 , as it is shown in Figure 2.5.

2.7 Permeability-porosity relationship

Ghabezloo et al. (2008) presented the evaluation of the permeability-porosity relationship in a low permeability porous material using the results of a single transient test. This method accounts for both elastic and non-elastic deformations of the sample during the test and is applied to a hardened class G oil well cement paste. An initial hydrostatic undrained loading is applied to the sample. The generated

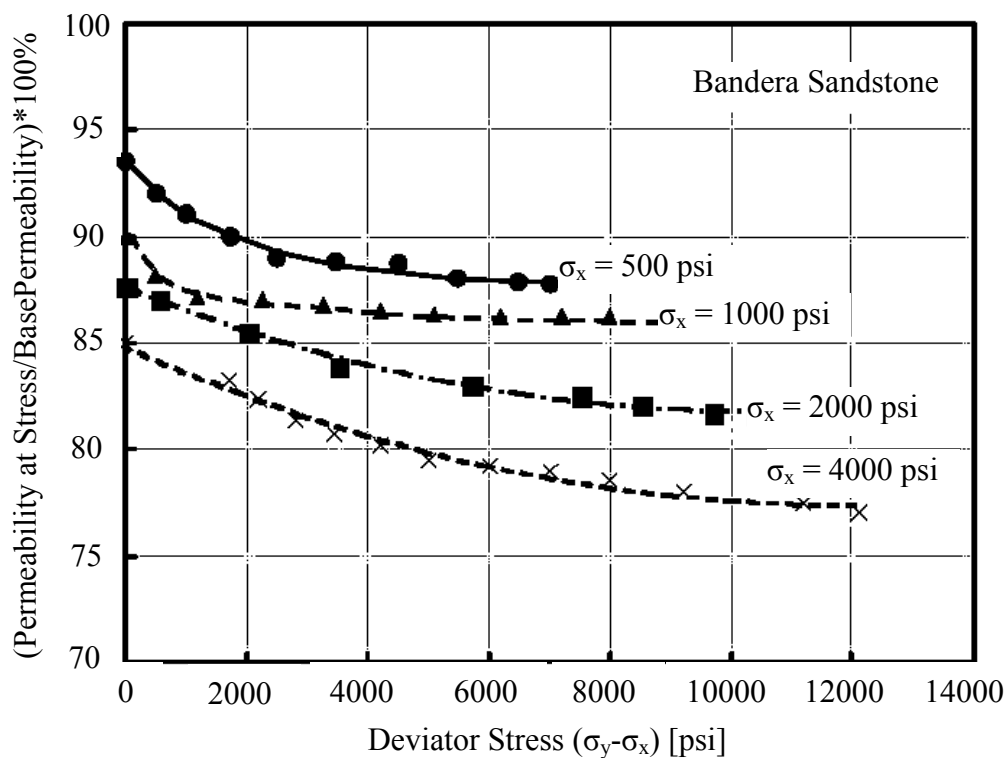


Figure 2.4 Permeability change of Bandera sandstone under stress conditions (Wilhelmi et al., 1967).

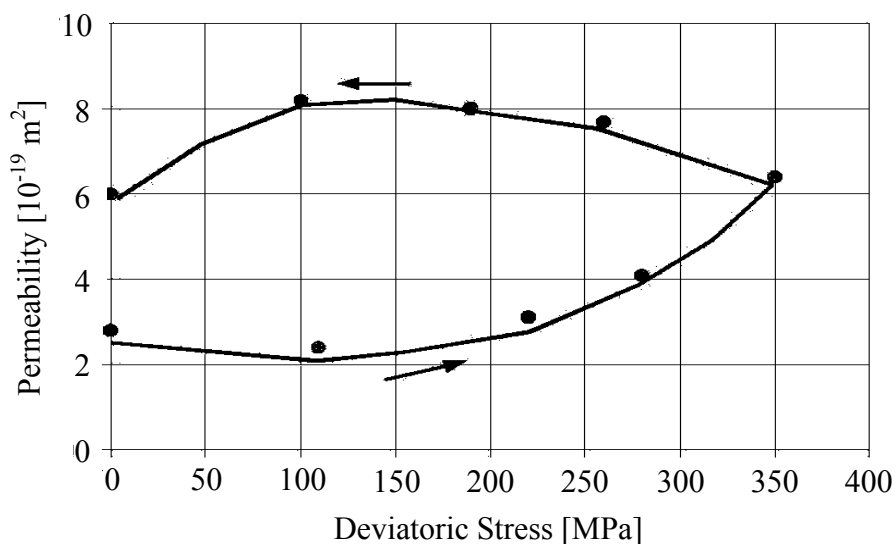


Figure 2.5 Volumes and permeability dilatancy of Westerly granite (Zoback et al., 1975).

excess pore pressure is then released at one end of the sample while monitoring the pore pressure at the other end and the radial strain in the middle of the sample during the dissipation of the pore pressure. These measurements are back analyzed to evaluate the permeability and its evolution with porosity change. The effect of creep of the sample during the test on the measured pore pressure and volume change is taken into account in the analysis. This approach permits to calibrate a power law permeability-porosity relationship for the tested hardened cement paste. The porosity sensitivity exponent of the power-law is evaluated equal to 11 and is shown to be mostly independent of the stress level and of the creep strains.

2.8 Effect of pore pressure and permeability in deep boreholes

Stavrogin and Tarasov (2001) state that boreholes which penetrate a zone of high-level compressive stress change the stress state in the rock mass surrounding the borehole. This stress state is defined by the principal stresses: $\sigma_1 > \sigma_2 > \sigma_3$. Values of the principal compressive stresses around a borehole can be determined, for example, by the equations formulated are as follow (Spivak and Popov, 1986):

$$\sigma_1 = \sigma_\theta = -(\lambda P_{\text{geo}} - P_{\text{bh}}) R_{\text{bh}}^2 / R^2 - P_{\text{geo}} \quad (2.6)$$

$$\sigma_2 = \sigma_z = -P_{\text{geo}} \quad (2.7)$$

$$\sigma_3 = \sigma_r = (\lambda P_{\text{geo}} - P_{\text{bh}}) R_{\text{bh}}^2 / R^2 - \lambda P_{\text{geo}} \quad (2.8)$$

where P_{geo} is the magnitude of the lithostatic or geostatic pressure; P_{bh} is the hydrostatic pressure of the column of drilling fluid exerted on the borehole wall; λ is

the coefficient of lateral outward thrust; R_{bh} is the borehole radius; R is the distance from borehole axis to the point under study in the rock mass.

The various stresses and graphic indicating the stress distribution around a borehole are shown in Figure 2.6. Graphs were plotted for the case $\lambda = 1$ and $\rho_{df} = 0.5\rho_{rock}$, where ρ_{df} and ρ_{rock} are the specific gravity of the drilling fluid and rock respectively. In this computation scheme, Archimedian forces are not taken into account since they are not of major significance in the investigations.

The rock immediately adjacent to the borehole wall is subjected to the most extreme conditions since tangential stresses σ_{θ} reach their maximum value here, while the radial stress σ_r , which determines the magnitude of triaxial confining pressure on the rock and hence its strengths are minimum. The latter assertion follows from the results of studies in which it was experimentally established that under conditions of non-uniform triaxial (volumetric) compression of the type $\sigma_1 > \sigma_2 > \sigma_3$, the resistance of rock to loading is determined by the value of the minimum principal stress σ_3 and depends only slightly on the intermediate stress σ_2 . Where pressure is not exerted by a drilling mud on the borehole wall, however, i.e., under $P_{bh}=0$, the radial stresses $\sigma_r=0$, the rock in the borehole wall is subjected to conditions of plane stress and the rock strength is close to the uniaxial compressive strength. One function of the drilling mud is to increase the stability of the borehole wall. The pressure exerted by the mud on the borehole wall acts, on the one hand, to increase the value of σ_r to a value determined by the weight of the overlying fluid column and, on the other, to reduce the value of σ_{θ} . Experience in drilling deep boreholes has shown that drilling mud does not always fulfill this stabilization role. Increase in the

specific gravity of the fluid (or mud weight) very often produces the opposite effect, i.e., a reduced stability of the borehole wall.

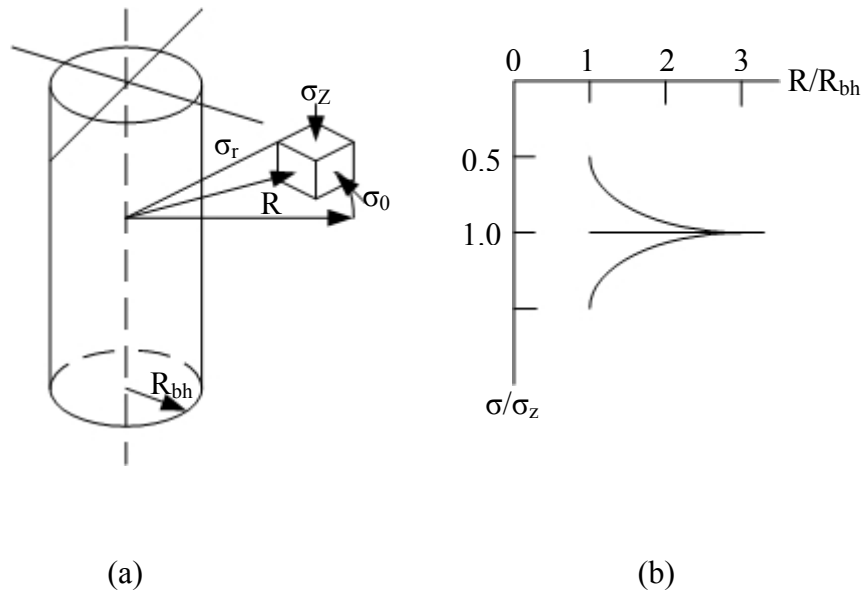


Figure 2.6 (a) Notation of stresses around a vertical borehole and (b) graphs showing the distribution of elastic stresses along a horizontal drawn from the borehole axis (Spivak and popov, 1986).

CHAPTER III

SAMPLE PREPARATION

3.1 Introduction

Sandstone specimens selected for this research are from three sources: Phu Phan, Phra Wihan and Phu Kradung formations (hereafter designated as PP, PW and PK sandstones). They belong to the Khorat group and widely expose in the north and northeast of Thailand. They also have significant impacts on long-term stability of many engineering structured in the region (e.g., embankments and foundations of highways, railways and reservoirs, dam abutments and tunnels).

3.2 Samples collection

The selection criteria are that the rock should be homogeneous as much as possible. This is to minimize the intrinsic variability of the test results. Sample preparation has been carried out for a series for constant head flow testing. It is conducted in the laboratory facility at the Suranaree University of Technology. The process includes coring, cutting and grinding (Figures 3.1 through 3.3). Preparation of these samples follows the ASTM standards (ASTM D4543-08) with a nominal dimension of 5 cm in diameter and 10 cm long. A minimum of six specimens are prepared for each rock type.



Figure 3.1 Laboratory core drilling. The core drilling machine (model SBEL 1150) is used to drill core specimens using diamond impregnated bit with diameter of 54 mm.



Figure 3.2 A core specimen of PK sandstone is cut to length by a cutting machine.

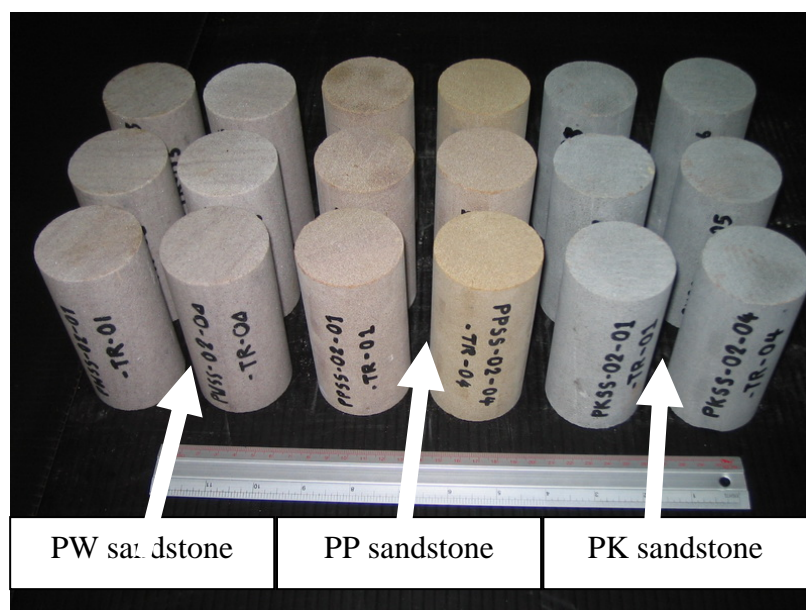


Figure 3.3 Some sandstone specimens prepared for the constant head flow test under deviatoric stress states.

3.3 Mineralogical study

The mineral compositions of the rock samples are determined by using X-ray diffraction method. Table 3.1 gives the results of the X-ray diffraction analysis. The mineral compositions determined will be used as data basis to explain the pore space of rock that affects to the hydraulic conductivity.

Table 3.1 Mineral compositions of three sandstones determined by X-ray diffraction analysis.

Rocks	γ (g/cc)	Grain Size (mm)	Sorting	Mineral Compositions				
				Quartz (%)	Albite (%)	Kaolinite (%)	Feldspar (%)	Mica (%)
PW	2.35	1.5-2.0	well	99.47	-	0.53	-	-
PP	2.45	1.5-2.0	well	98.40	-	-	-	1.60
PK	2.63	0.1-1.5	moderate	48.80	46.10	5.10	-	-

CHAPTER IV

LABORATORY EXPERIMENT

4.1 Introduction

The objectives of laboratory experiment is to determine the effects of anisotropic stress states on the permeability of sandstone specimens, and to develop a mathematical relationship between the hydraulic properties with the deviatoric stress and strain conditions. The effort primarily involves conducting constant-head flow tests on intact cylindrical sandstone specimens under a variety of confining pressures and deviatoric stresses. The permeability results are presented as a function of deviatoric stresses and induced volumetric strain.

4.2 Test method

Constant head flow tests have been performed to assess the effects of deviatoric stresses on the intact sandstone permeability. Figures 4.1 and 4.2 shows the laboratory arrangement of the constant head flow test under deviatoric stresses. After the constant confining pressure is applied using a Hoek cell, the axial stress is increased until failure occurs. The constant confining pressures varied from 1, 2 to 3 MPa. The flow is measured every 6.9 MPa axial stress increment. The injected water pressure is maintained at 0.27 MPa (40 psi) using constant diameter water pump connected to a nitrogen gas tank via a regulating valve. A high precision pipette is used to collect the excess oil released from the triaxial cell by the specimen dilation.

All specimens have the core axis normal to the bedding planes (Figure 4.3). A total of 3 specimens are tested for each sandstone.

The hydraulic conductivity of the specimen (K) is calculated by assuming that the Darcy's law is valid (Indraratna and Ranjith, 2001):

$$K = 4q\mu / [\pi D^2(dp/dx)] \quad (4.1)$$

where q is water flow rate through the specimen (cm^2/s), μ is the dynamic viscosity of the water ($\text{N}\cdot\text{s}/\text{cm}^2$), D is the specimen diameter (cm^2), and dp/dx is the pressure gradient along the length of the specimen.

The excess oil released from the triaxial cell by the specimen dilation is used to calculate the volumetric strain (ε_V) of the specimen during loading:

$$\varepsilon_V = (V_O - V_S) / V_R \quad (4.2)$$

where V_O is the excess oil volume, V_S is the volume of oil displaced by loading platen, and V_R is the volume of rock specimen.

4.3 Test results

Figures 4.4 through 4.12 give the permeability results for PW, PP and PK sandstone specimens as a function of volumetric strain (ε_V). They are compared with their corresponding stress-strain curves obtained under various confining pressures (σ_3). The hydraulic conductivity is calculated by using equation (4.1). Before dilation the permeability of PW, PP and PK sandstone decreases with increasing the deviatoric stress. This agrees with the experimental by Ferfera et al. (1997), Pusch

and Weber (1998), Oda et al. (2002) and Heiland (2003). Table 4.1 summarizes the flow test result under deviatoric stresses.

Table 4.1 Results of flow testing under deviatoric stresses.

Sample No.	P_c (MPa)	E (GPa)	ν	Dilation Strength (MPa)	Ultimate Strength (MPa)	Pre-failure	Post-failure
						$\Delta k/\Delta \epsilon_v$ ($\times 10^{-6}$ m/s)	$\Delta k/\Delta \epsilon_D$ ($\times 10^{-6}$ m/s)
PWSS-01	1	9.66	0.33	42	65	-23.00	-3.15
PWSS-02	2	8.66	0.35	37	55	-19.13	-3.82
PWSS-03	3	8.52	0.33	55	88	-15.02	-4.41
Standard deviation				45 \pm 10	69 \pm 19		
PPSS-01	1	11.58	0.27	60	78	-0.042	-1.31
PPSS-02	2	12.77	0.27	61	79	-0.023	-1.31
PPSS-03	3	13.0	0.26	92	106	-0.002	-0.13
Standard deviation				76 \pm 16	88 \pm 18		
PKSS-01	1	7.47	0.27	58	70	-0.013	-0.61
PKSS-02	2	7.70	0.30	60	75	-0.008	-0.91
PKSS-03	3	7.39	0.31	55	71	-0.007	-0.41
Standard deviation				58 \pm 3	73 \pm 3		

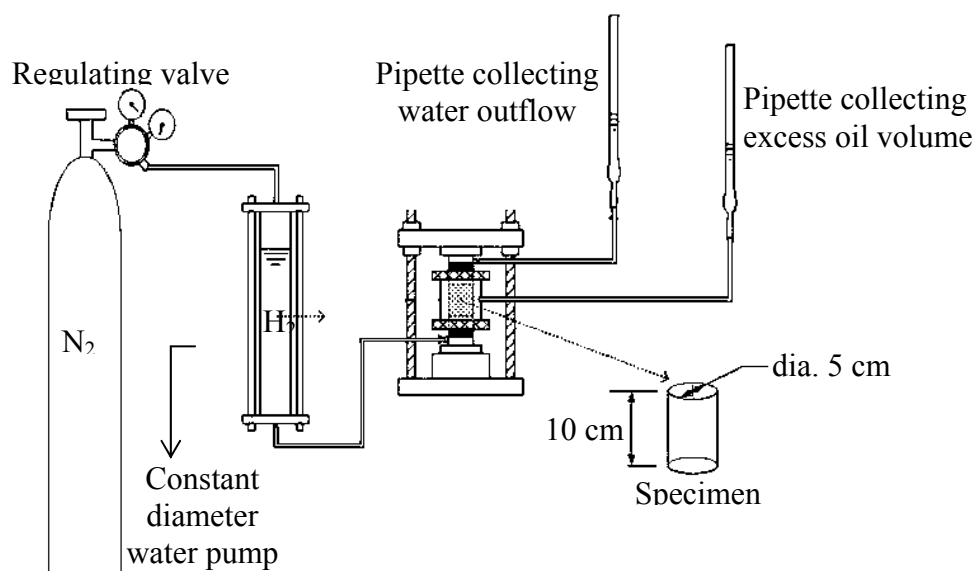


Figure 4.1 Laboratory arrangement for constant head flow tests of sandstone cylindrical specimen under deviatoric stress.

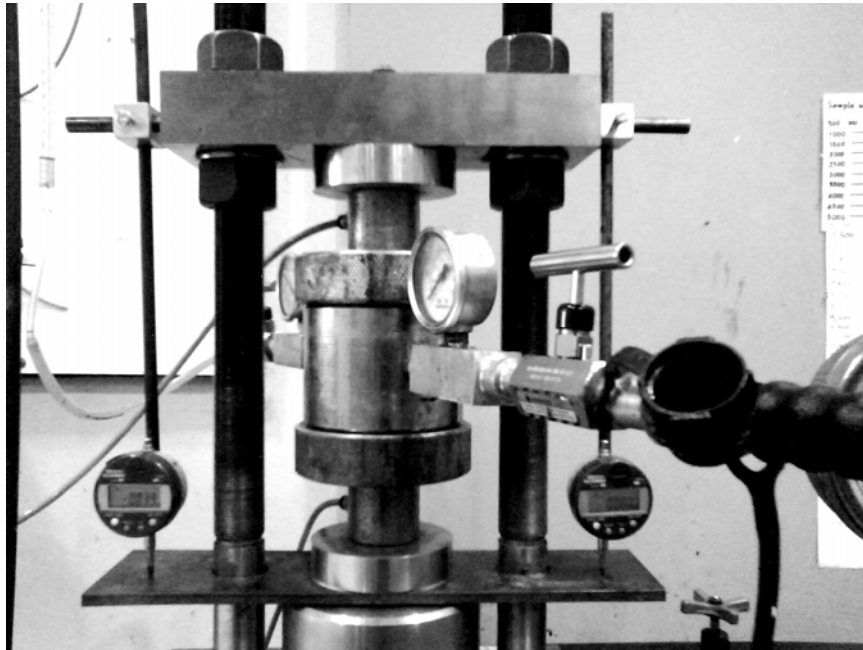


Figure 4.2 Laboratory arrangement for constant head flow tests of sandstone cylindrical specimen under deviatoric stress.

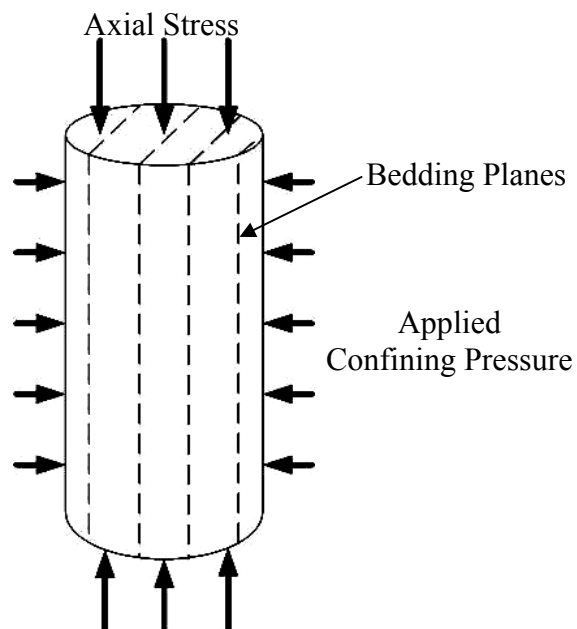


Figure 4.3 Applied principal stress directions with respect to the bedding planes for all specimens.

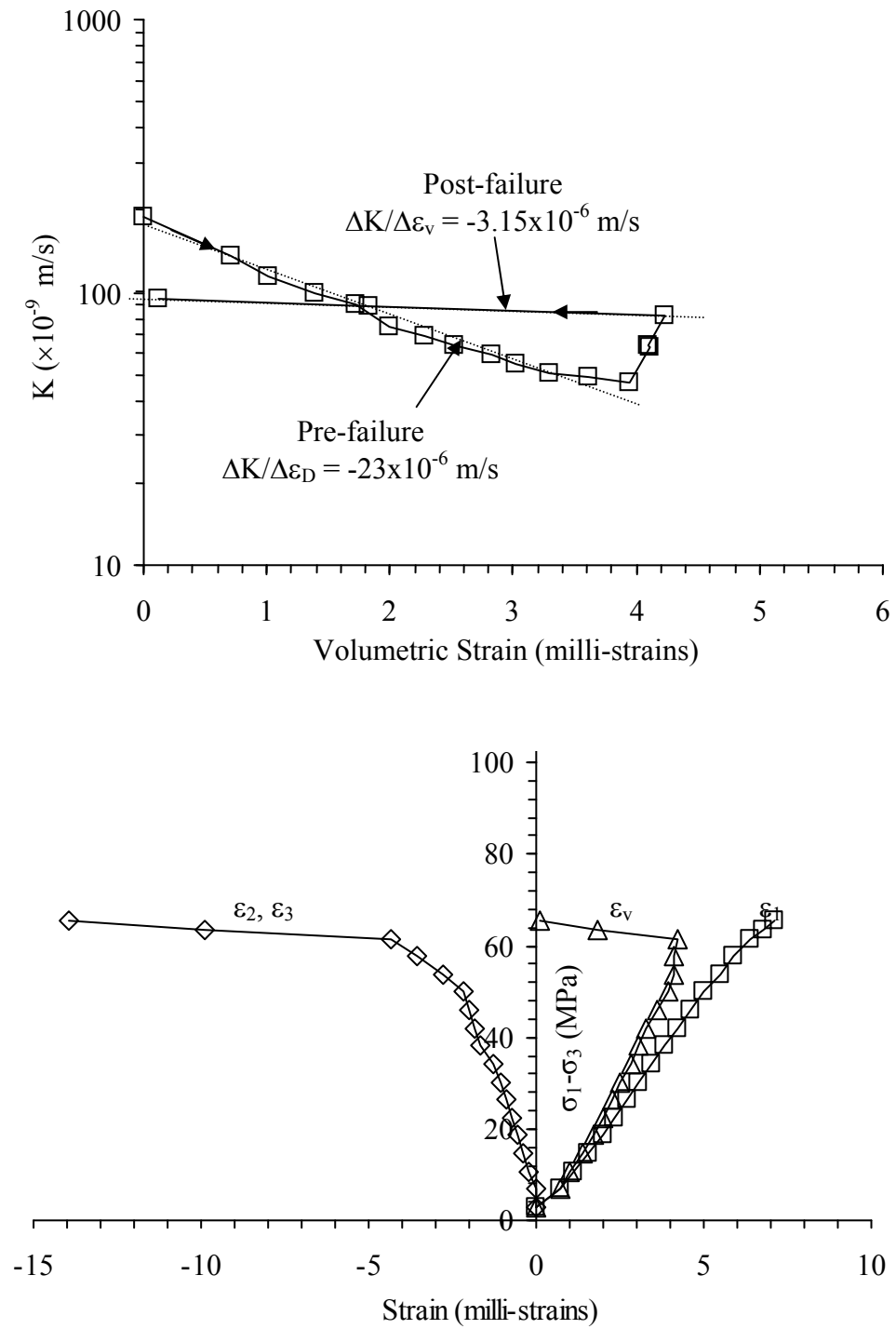


Figure 4.4 Permeability of Phra Wihan sandstone specimen tested under confining pressure of 1 MPa (top) with the corresponding stress-strain curves (bottom).

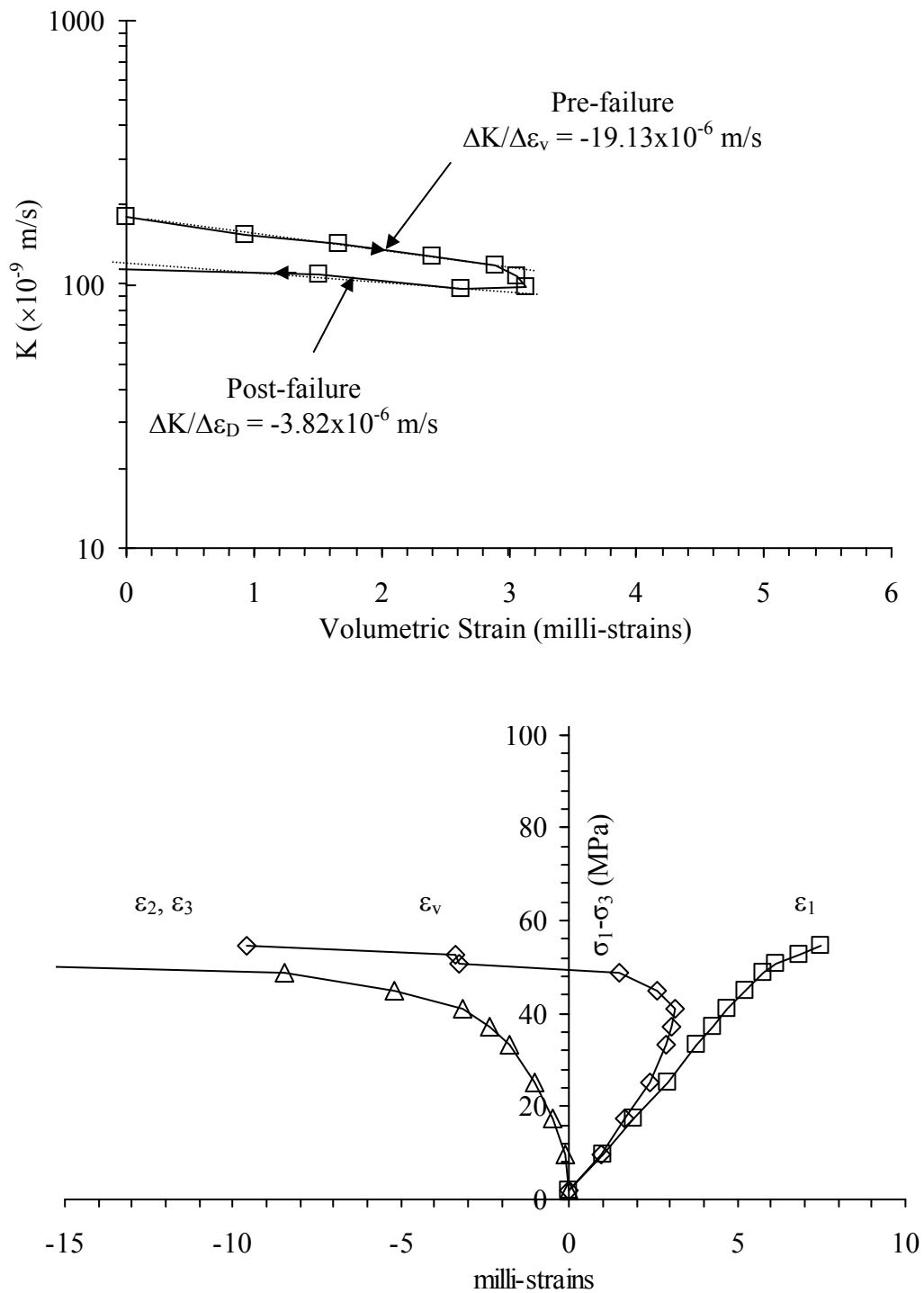


Figure 4.5 Permeability of Phra Wihan sandstone specimen tested under confining pressure of 2 MPa (top) with the corresponding stress-strain curves (bottom).

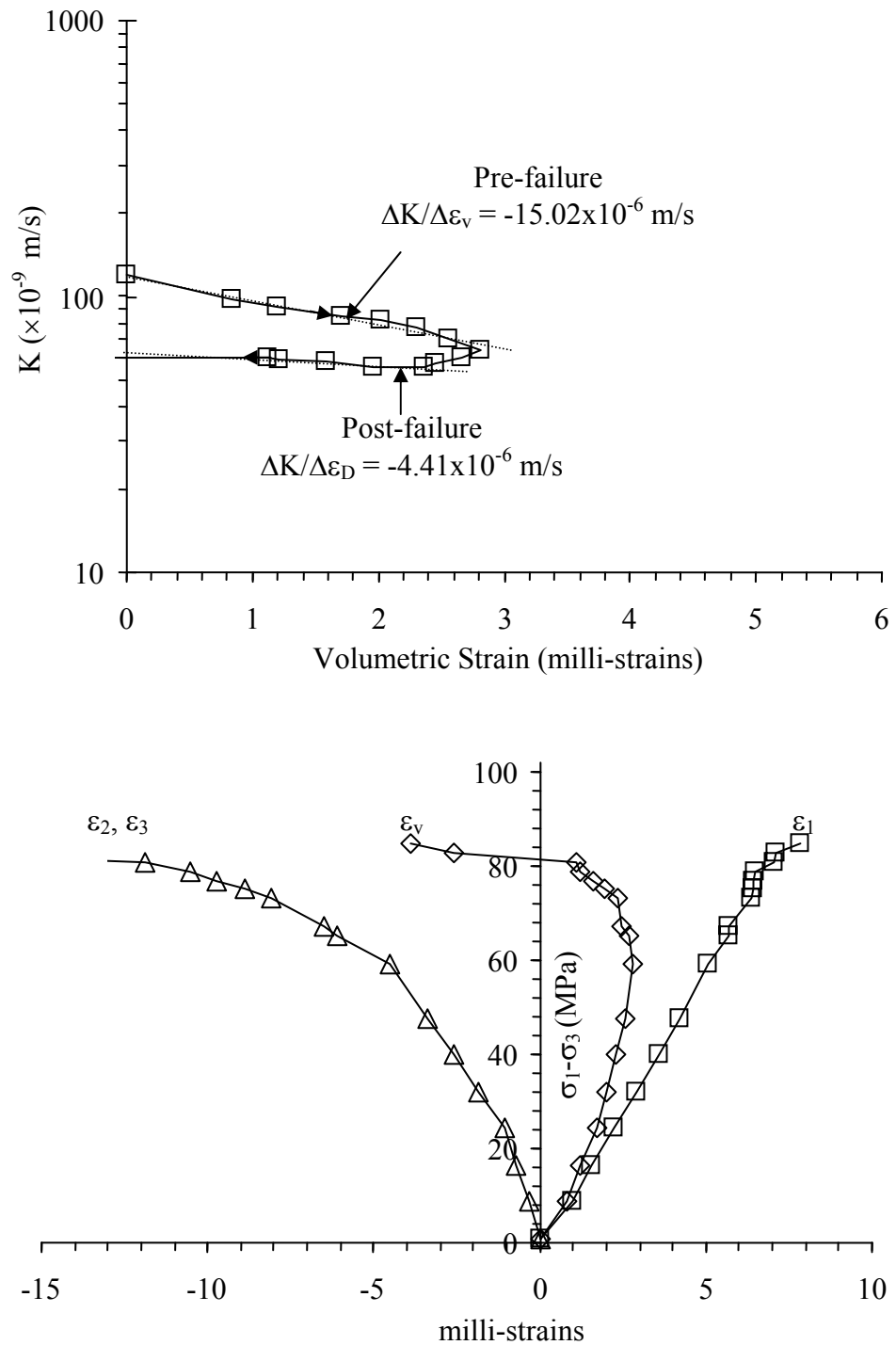


Figure 4.6 Permeability of Phra Wihan sandstone specimen tested under confining pressure of 3 MPa (top) with the corresponding stress-strain curves (bottom).

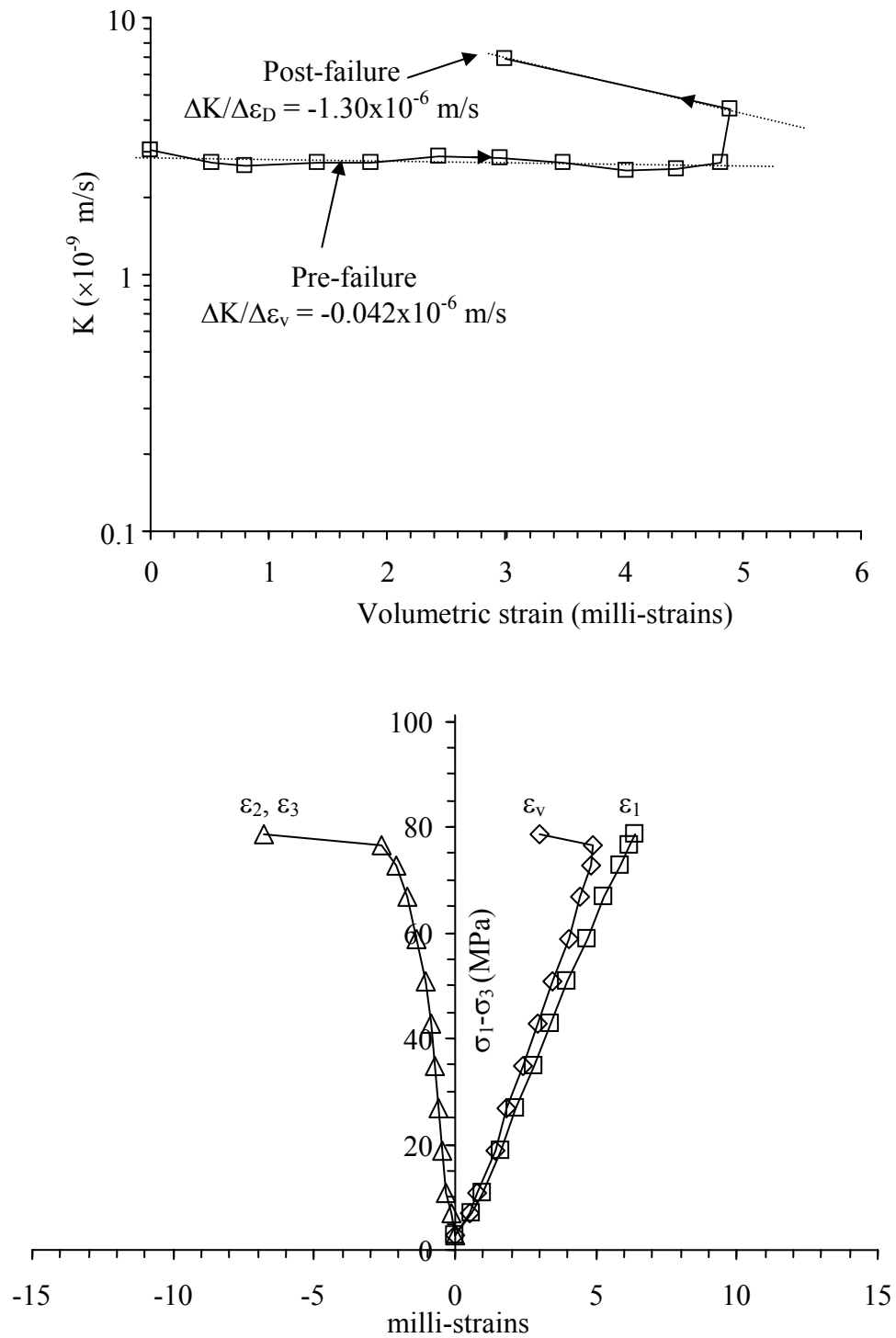


Figure 4.7 Permeability of Phu Phan sandstone specimen tested under confining pressure of 1 MPa (top) with the corresponding stress-strain curves (bottom).

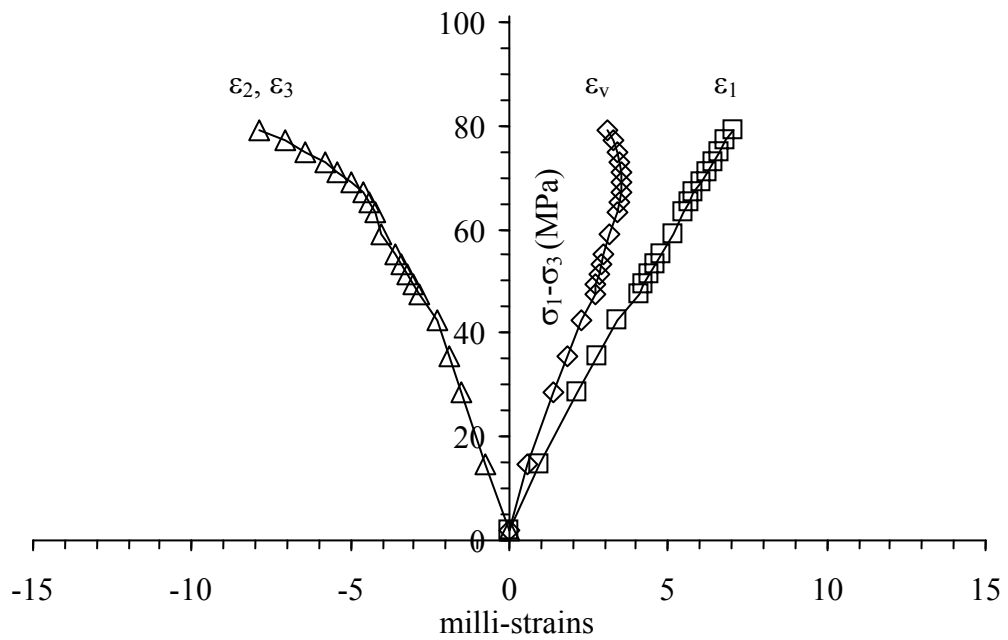
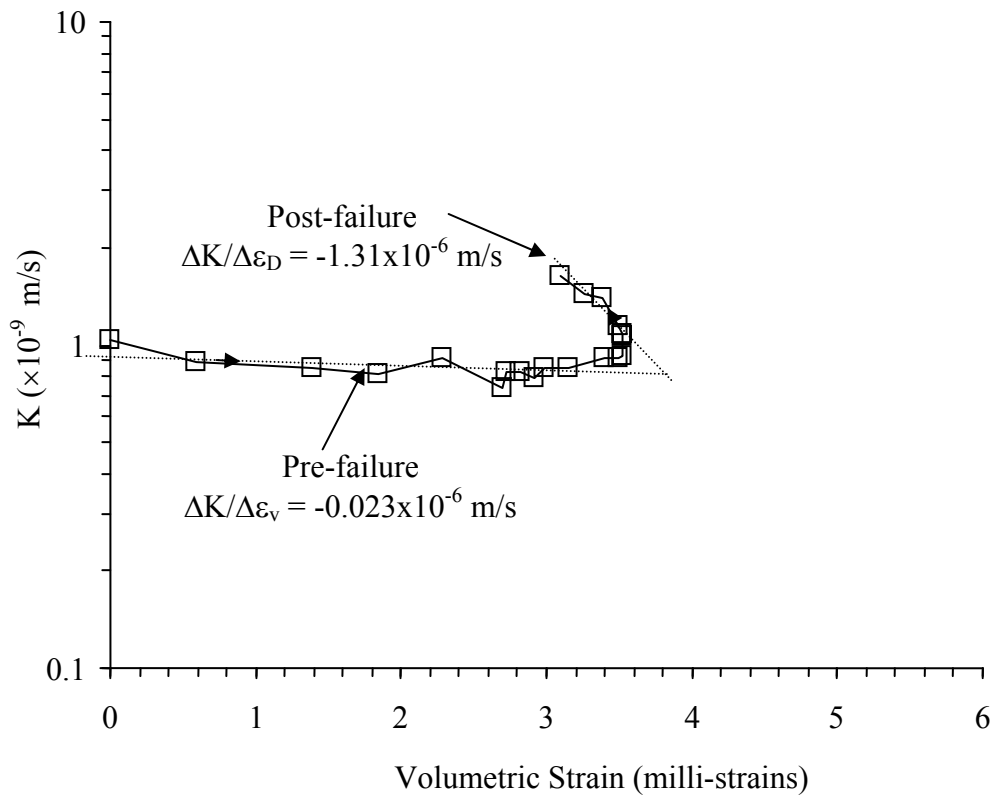


Figure 4.8 Permeability of Phu Phan sandstone specimen tested under confining pressure of 2 MPa (top) with the corresponding stress-strain curves (bottom).

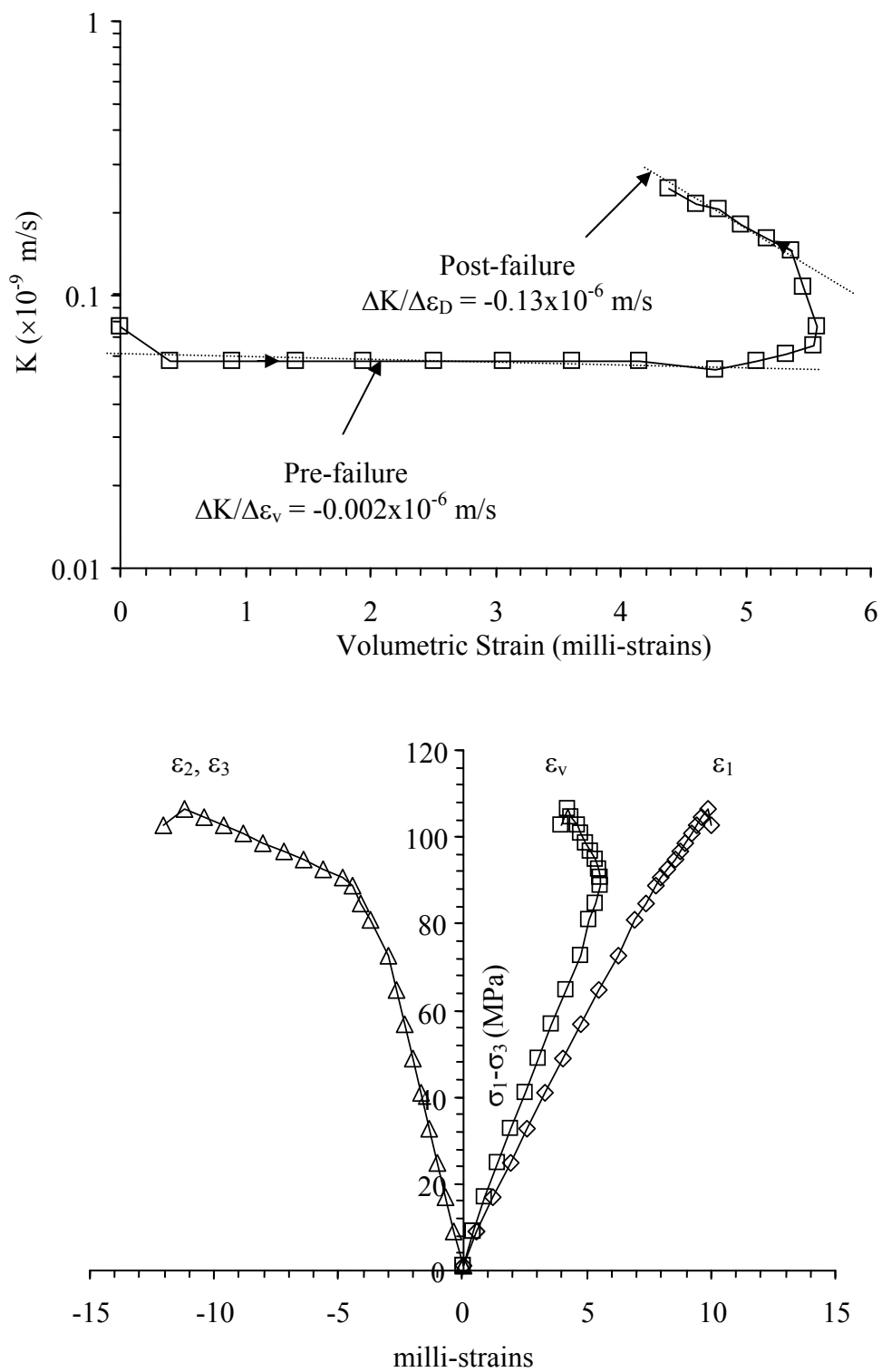


Figure 4.9 Permeability of Phu Phan sandstone specimen tested under confining pressure of 3 MPa (top) with the corresponding stress-strain curves (bottom).

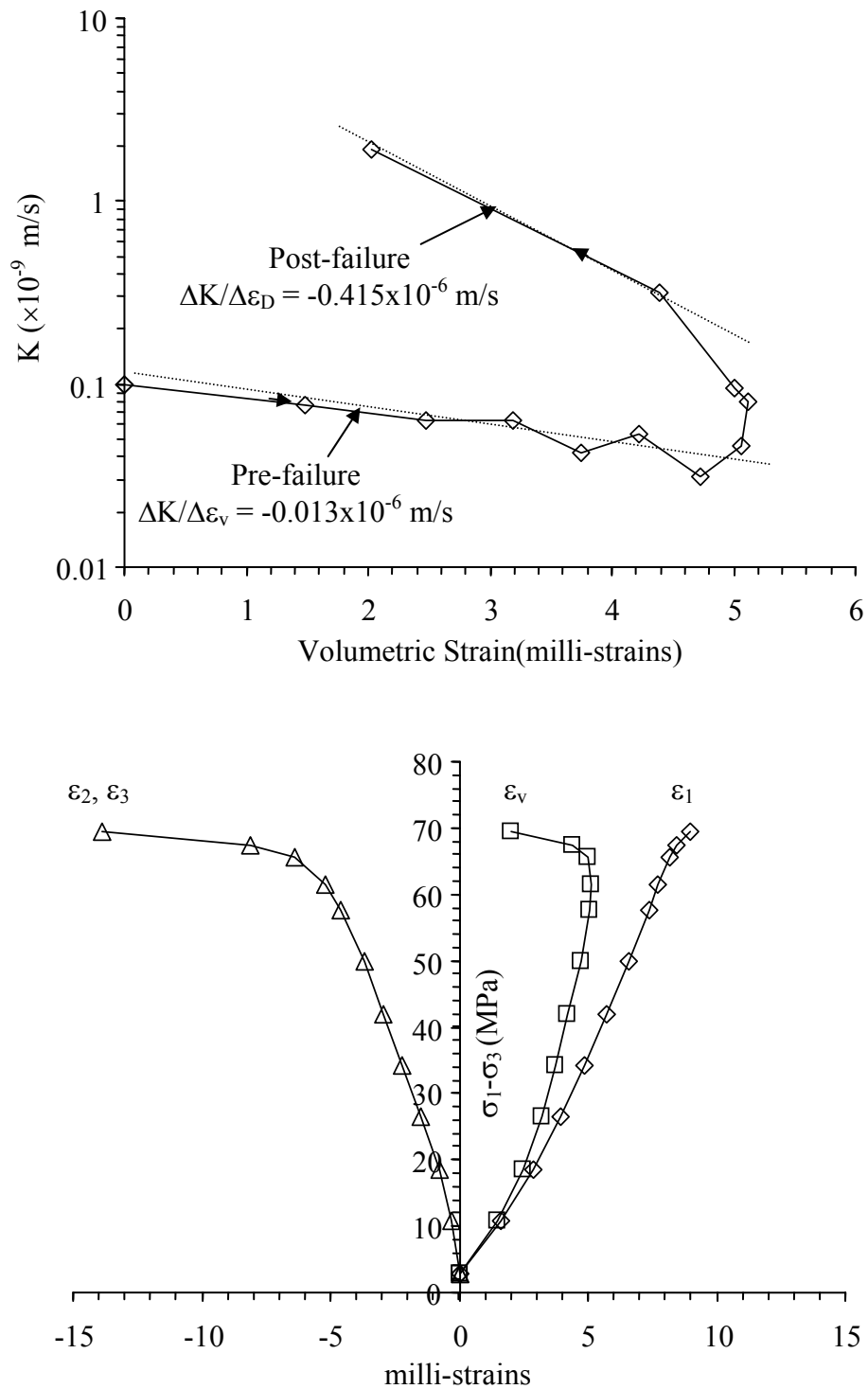


Figure 4.10 Permeability of Phu Kradung sandstone specimen tested under confining pressure of 1 MPa (top) with the corresponding stress-strain curves (bottom).

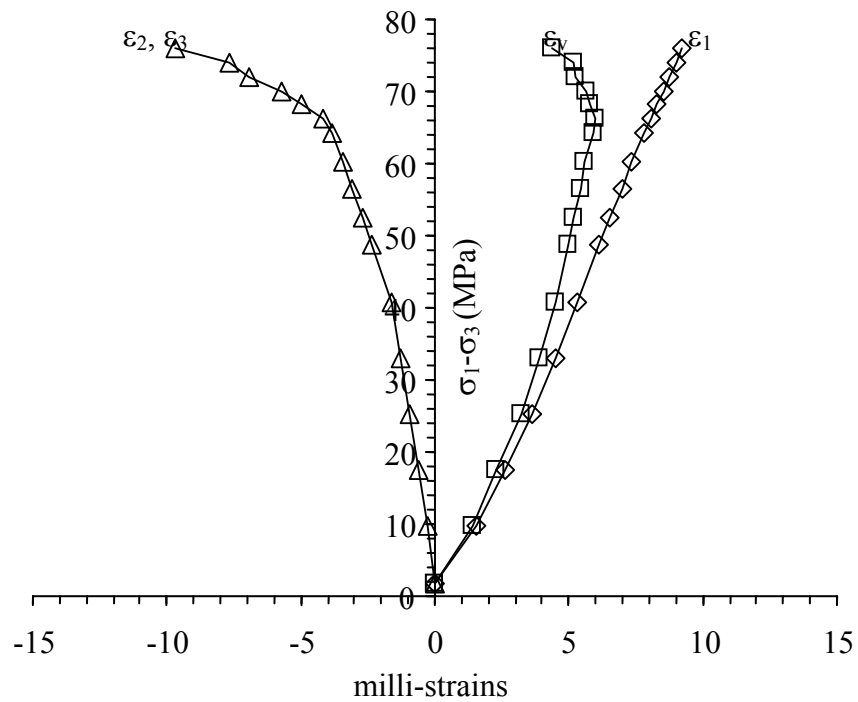
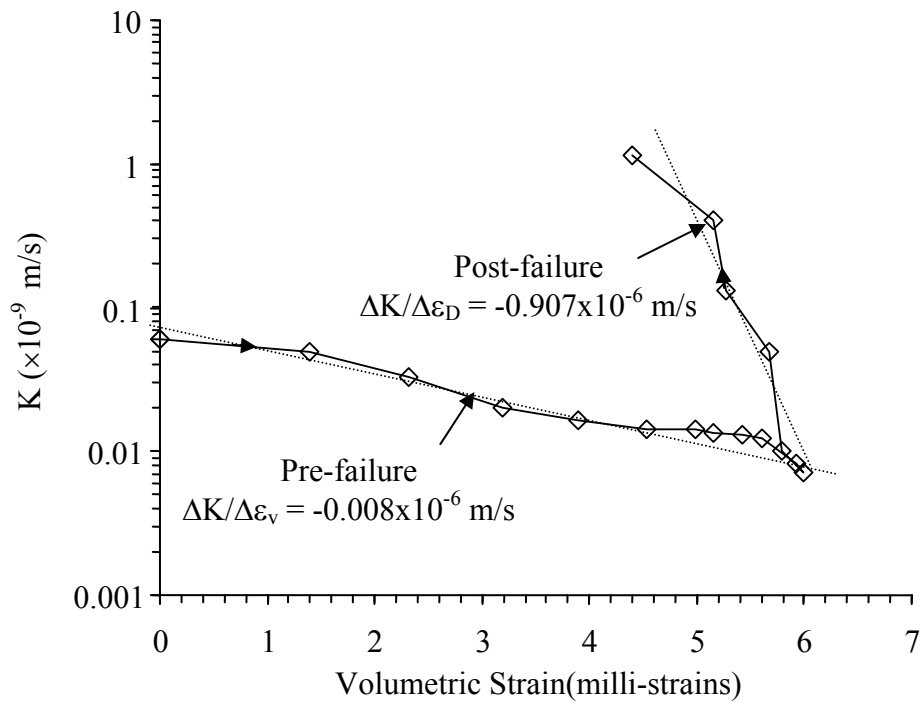


Figure 4.11 Permeability of Phu Kradung sandstone specimen tested under confining pressure of 2 MPa (top) with the corresponding stress-strain curves (bottom).

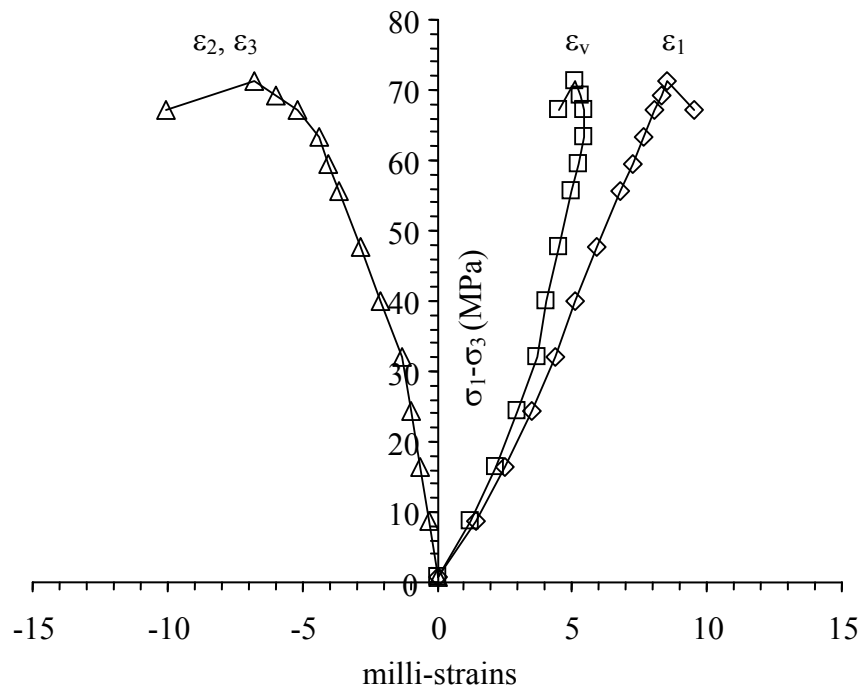
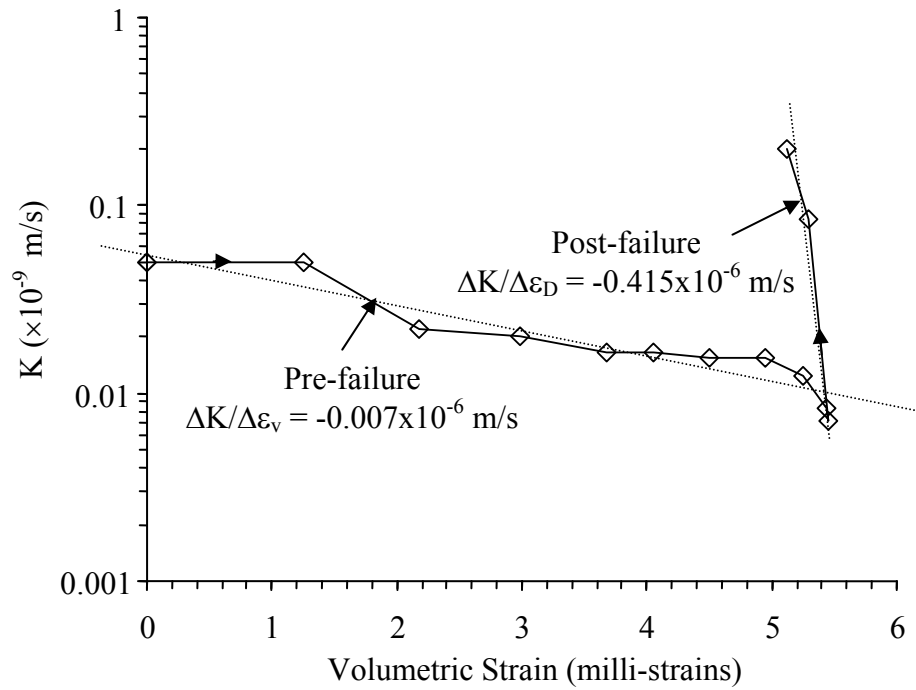


Figure 4.12 Permeability of Phu Kradung sandstone specimen tested under confining pressure of 3 MPa (top) with the corresponding stress-strain curves (bottom).

4.4 Discussions

The permeability-to-volumetric strain ratio ($\Delta K/\Delta\varepsilon_V$) before dilation strength, and the permeability-to-dilation strain ($\Delta K/\Delta\varepsilon_D$) ratio after dilation strength are calculated. Before dilation strength the permeability decreases with increasing volumetric strain. This is probably due to the contraction of the pore spaces in the specimen. Within this stage the $\Delta K/\Delta\varepsilon_V$ ratio decreases as increasing confining pressure. After dilation strength the rock permeability increases with specimen dilation probably because of the initiation and propagation of micro-cracks due to the applied axial stress approaching failure.

CHAPTER V

NUMERICAL MODELING

5.1 Objective

The numerical modeling in this research aims at studying the deformation and failure behavior and hydraulic conductivity of two hypothetical cases: (1) rock around single opening in infinite plate and (2) parallel circular opening under deviatoric stresses. The analysis determines the increase of rock hydraulic conductivity in elastic and plastic zones under deviatoric stresses. Results from the mechanical deformation analysis are used in the evaluation of the changes of rock permeability as affected by the applied stresses. Properties from PW and PK sandstones are used in the numerical modeling.

5.2 Rock properties for computer modeling

Before performing the computer analysis, physical and mechanical properties of sandstone rock are specified in the calculation. FLAC program (Itasca, 1992) is employed for this research. The major and significant constants in the models are elastic modulus and Poisson's ratio of the rock. They are obtained from the constant head flow test in the triaxial compressive strength test. Cohesion, tensile strength, and basic friction angle of PW and PK sandstones are taken from Walsri et al. (2008). Table 5.1 summarizes the basic mechanical properties as obtained from the laboratory. The maximum (σ_1) and minimum (σ_3) principal stresses have been varied from 0.2, 0.4, 0.5, 0.6 to 0.8.

Table 5.1 Summary of the basic mechanical properties as obtained from Walsri et al. (2009).

Basic Mechanical Properties	PW Sandstone	PK Sandstone
Elastic Modulus (measured from loading curves) (GPa)	8.66	7.70
Poisson's Ratio	0.35	0.30
Cohesion (MPa)	10	19
Tension (MPa)	6.7	8.7
Internal Friction Angle (degrees)	58	50
Dilation Angle (degrees)	29	25

5.3 Finite difference simulations

Two finite difference mesh models are constructed to represent the single circular opening in infinite plate and the parallel circular openings under deviatoric stresses. The first model (Model A) represents a single circular opening in infinite plate, and the second model (Model B) analyzes the parallel circular opening under deviatoric stress states. They are analyzed in axis symmetry and plain strain by assuming strain in z-axis is zero.

5.3.1 Single circular opening in infinite plate under deviatoric stresses

In the modeling of the opening, two-dimensional finite difference mesh is created in x-y axis. The third dimensional with z-axis is omitted because this analysis is a plane strain analysis by assuming strain in z-axis to be zero. For the best efficiency, finite difference mesh represents only one-fourth of the domain due to the symmetry. The opening model is under deviatoric stresses of σ_3/σ_1 of 0.2, 0.4, 0.5, 0.6 and 0.8. The variables used in FLAC simulations are shown in Table 5.2.

Figure 5.1 illustrates the model A created from a quarter of circular cross-section with a radius of 4 m. Distance from the right and upper boundaries to the center is 20 m, or equals 5 times of the opening radius. The stresses applied on the top and the right sides are different. The upper and the right boundaries are allowed to freely displace in both x- and y-directions. The left boundary which is a symmetric axis separates the opening in two parts. The y-axis can move in y-direction but not in x-direction. The lower boundary is a symmetrical axis that separates the opening into two parts and the x-axis is fixed in y-direction. In order to clearly illustrate the boundary of the opening in finite difference mesh, elements in the opening are not shown in the figure.

An assumption used in this study is that the opening is a single opening which locates far from any other underground structure, at least 5 times of its radius. This is to prevent the mechanical effect that may be caused by the adjacent structures.

Table 5.2 Variables used in FLAC simulations for single circular opening in infinite plate with 4 m radius.

Series	Maximum Principal Stress (σ_1) (MPa)	Minimum Principal Stress (σ_3) (MPa)	$k=\sigma_3/\sigma_1$
1	20	4	0.2
	20	8	0.4
	20	12	0.6
	20	16	0.8
2	10	5	0.5
	20	10	0.5
	30	15	0.5
	40	20	0.5

For the elastic-plastic materials assumed here, the algorithm in FLAC defines that the plastic deformation will occur after the induced deviatoric stresses exceed the rock strength. The rock strength is defined here using the Coulomb criterion with the parameters given in Table 5.1. As a result in the elastic zone the deviatoric and volumetric strains are calculated from the rock elastic parameters. In the plastic zone (where the deviatoric stress exceeds rock strength) the deviatoric and volumetric strains are determined based on an assumption that the material behaves as perfectly plastic after failure occurs, as shown in Figure 5.2.

The volumetric strains calculated for the elastic zone and plastic zone are independently used to determine the increase of the rock permeability, i.e. by the following relation:

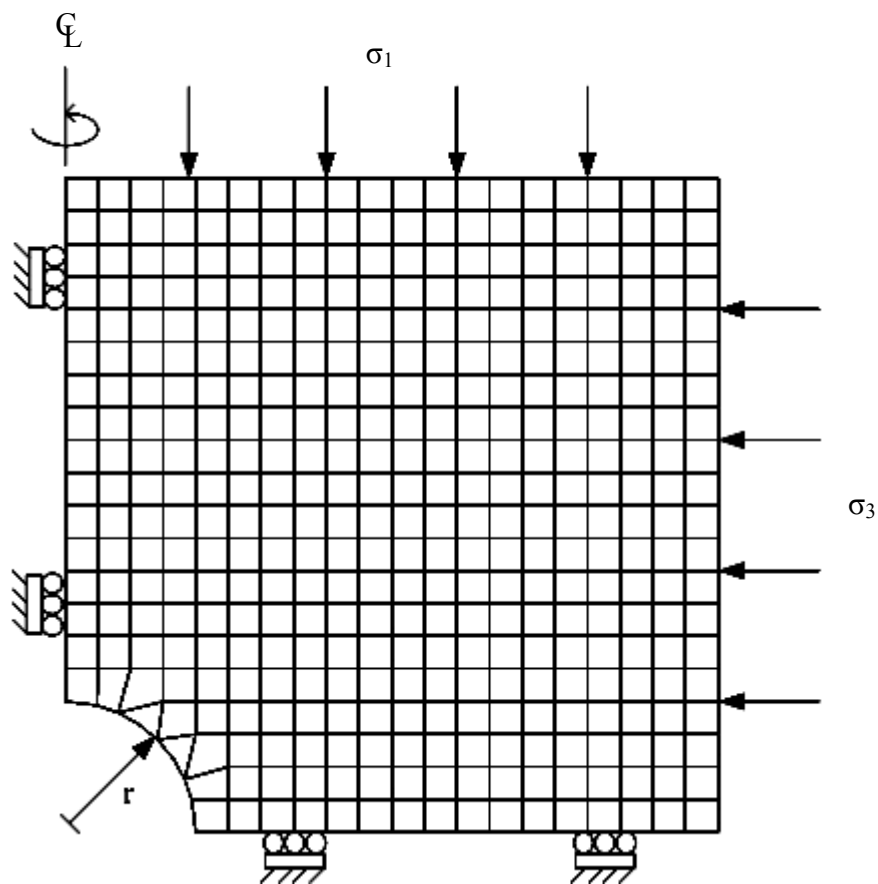
$$\Delta K = A \cdot \Delta \varepsilon_v \quad (5.1)$$

where A is empirical constant ($\Delta K / \Delta \varepsilon_v$) obtained from chapter IV, which depends on rock material.

Once the distribution of the volumetric strain is obtained from the FLAC computation, the increase of the rock hydraulic conductivity (ΔK) can be calculated. By point-by-point summation of the permeability increase (ΔK) with the initial permeability (K_0) of the rock, the absolute increase of the rock hydraulic conductivity can be obtained. Table 5.3 summarizes the initial hydraulic conductivity of the tested sandstone

Table 5.3 Initial hydraulic conductivity of sandstone specimens.

Rocks	K_o (m/s)
Phra Wihan Sandstone	100×10^{-9}
Phu Phan Sandstone	1×10^{-9}
Phu Kradung Sandstone	50×10^{-12}

**Figure 5.1** Finite difference mesh for modeling single circular opening in infinite media (Model A).

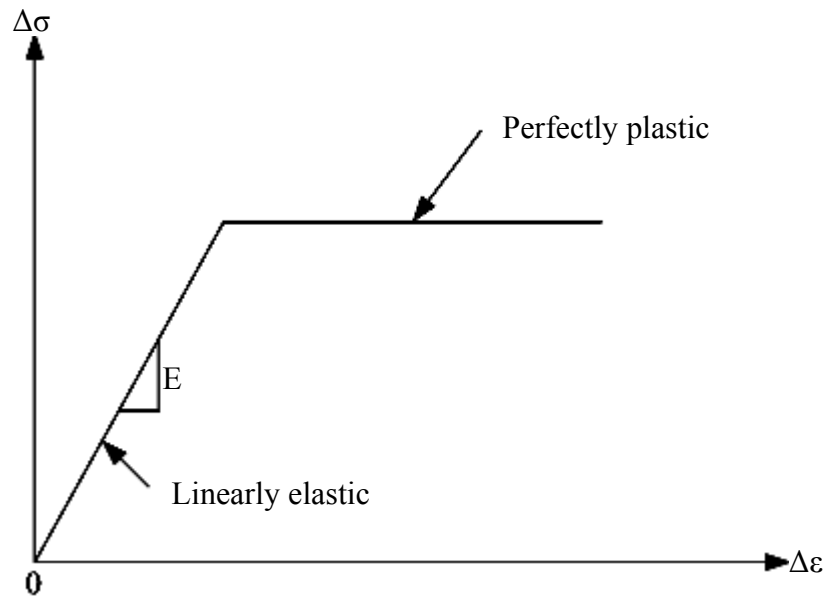


Figure 5.2 Constitutive relation assumed in this analysis.

5.3.2 Results

The finite difference results indicate that the maximum volumetric strain of horizontal-to-vertical stress ratio (k) of 0.2, 0.4, 0.6 and 0.8 are 0.2×10^{-3} , 0.14×10^{-3} , 0.1×10^{-3} and 0.07×10^{-3} for Phra Wihan sandstone and 0.25×10^{-3} , 0.2×10^{-3} , 0.16×10^{-3} and 0.1×10^{-3} for Phu Kradung sandstone. The vertical stress is constant at 10 MPa and the horizontal stress varied from 2, 4, 6 to 8 MPa. Due to the distribution of volumetric strain the hydraulic conductivity is increased. The maximum hydraulic conductivity of horizontal-to-vertical stress ratio of 0.2, 0.4, 0.6 and 0.8 are 120×10^{-9} , 116×10^{-9} , 112×10^{-9} and 107×10^{-9} m/s for Phra Wihan sandstone and 300×10^{-12} , 250×10^{-12} , 190×10^{-12} and 140×10^{-12} for Phu Kradung sandstone.

From the modeling of horizontal-to-vertical stress ratio of 0.5 it is found that the maximum volumetric strains for vertical stress of 10, 20, 30 and 40 MPa are 0.12×10^{-3} , 0.2×10^{-3} , 0.3×10^{-3} and 0.4×10^{-3} for Phra Wihan sandstone and

0.15×10^{-3} , 0.3×10^{-3} , 0.4×10^{-3} and 0.6×10^{-3} for Phu Kradung sandstone. The maximum hydraulic conductivity for the vertical stresses of 10, 20, 30 and 40 MPa are 114×10^{-9} , 124×10^{-9} , 140×10^{-9} and 150×10^{-9} m/s for Phra Wihan sandstone and 123×10^{-12} , 380×10^{-12} , 550×10^{-12} and 650×10^{-12} m/s for Phu Kradung sandstone.

5.3.2.1 Effect of horizontal-to-vertical stress ratio (k)

Comparison of hydraulic conductivity of rock around opening as affected by the difference between the horizontal-to-vertical stress ratio reveals that the hydraulic conductivity is higher for the opening with lower k. The maximum hydraulic conductivity increased from 107×10^{-9} to 120×10^{-9} m/s for PW sandstone and 140×10^{-12} to 300×10^{-12} m/s for PK sandstone as the horizontal-to-vertical stress ratio decreases from 0.8 to 0.2. Figures 5.2 to 5.9 show the comparison of the hydraulic conductivity around the opening wall, in x- and y-directions for 4 different horizontal-to-vertical stress ratios.

5.3.2.2 Effect of magnitudes of stress

Comparison of the hydraulic conductivity of rock around the opening with $k = 0.5$, shows that the maximum hydraulic conductivity increased from 120×10^{-9} to 150×10^{-9} m/s for PW sandstone and 123×10^{-12} to 650×10^{-12} m/s for PK sandstone as the vertical stress increases from 10 to 40 MPa. Figures 5.10 to 5.17 show the comparison of the hydraulic conductivity at the opening wall with horizontal-vertical stress ratio of 0.5.

The comparison of the plastic zone of rock around the opening reveals that the plastic zone is small for the opening under low stresses. The plastic zone increases as the stresses increases.

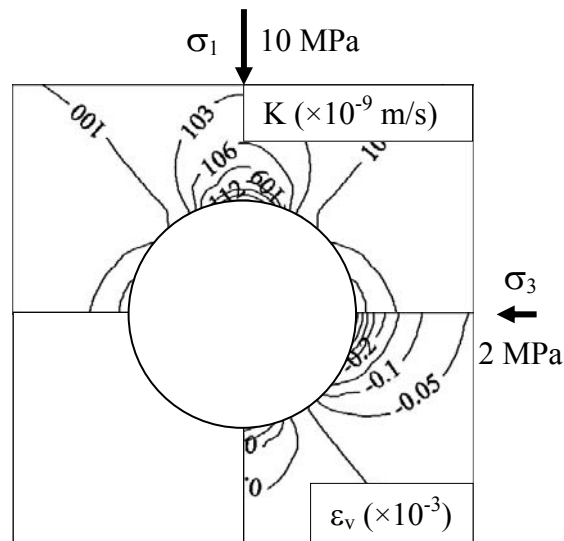


Figure 5.3 Volumetric strain and permeability of Phra Wihan sandstone simulated around single circular opening subjected to $\sigma_1=10$ MPa and $\sigma_3=2$ MPa ($\nu=0.35$, $E=8.66$ GPa).

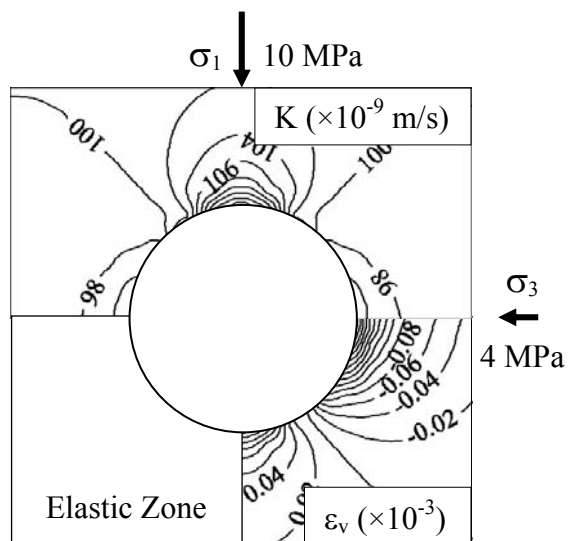


Figure 5.4 Volumetric strain and permeability of Phra Wihan sandstone simulated around single circular opening subjected to $\sigma_1=10$ MPa and $\sigma_3=4$ MPa ($\nu=0.35$, $E=8.66$ GPa).

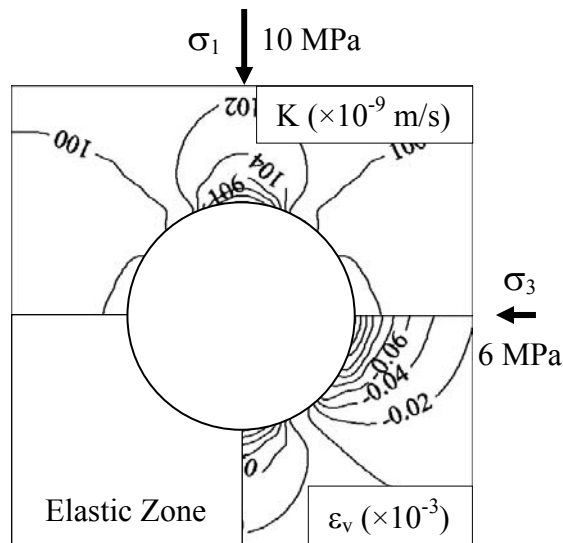


Figure 5.5 Volumetric strain and permeability of Phra Wihan sandstone simulated around single circular opening subjected to $\sigma_1=10$ MPa and $\sigma_3=6$ MPa ($\nu=0.35$, $E=8.66$ GPa).

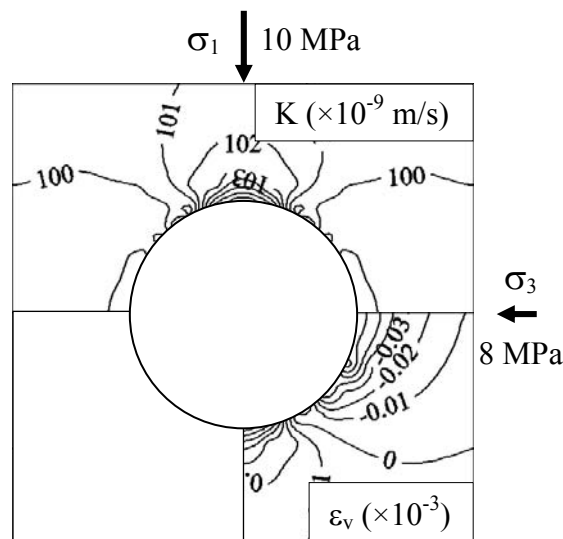


Figure 5.6 Volumetric strain and permeability of Phra Wihan sandstone simulated around single circular opening subjected to $\sigma_1=10$ MPa and $\sigma_3=8$ MPa ($\nu=0.35$, $E=8.66$ GPa).

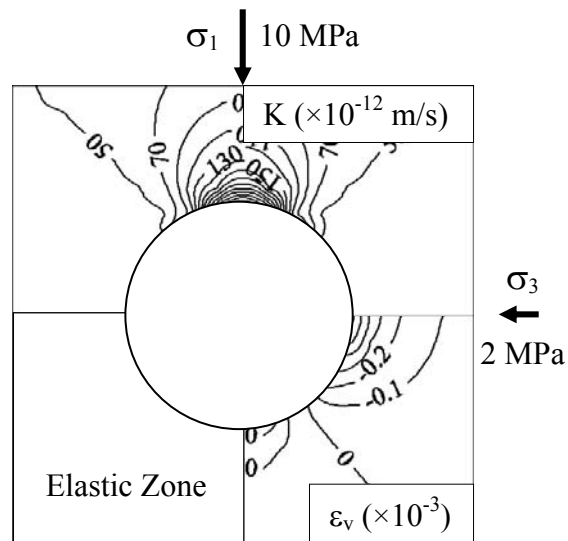


Figure 5.7 Volumetric strain and permeability of Phu Kradung sandstone simulated around single circular opening subjected to $\sigma_1=10$ MPa and $\sigma_3=2$ MPa ($\nu=0.30$, $E=7.70$ GPa).

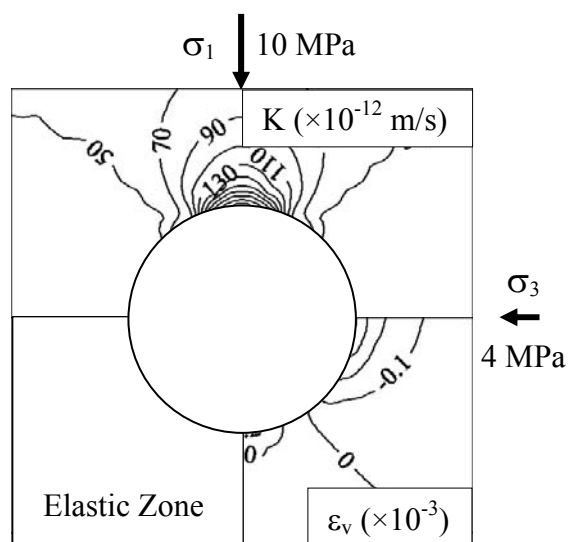


Figure 5.8 Volumetric strain and permeability of Phu Kradung sandstone simulated around single circular opening subjected to $\sigma_1=10$ MPa and $\sigma_3=4$ MPa ($\nu=0.30$, $E=7.70$ GPa).

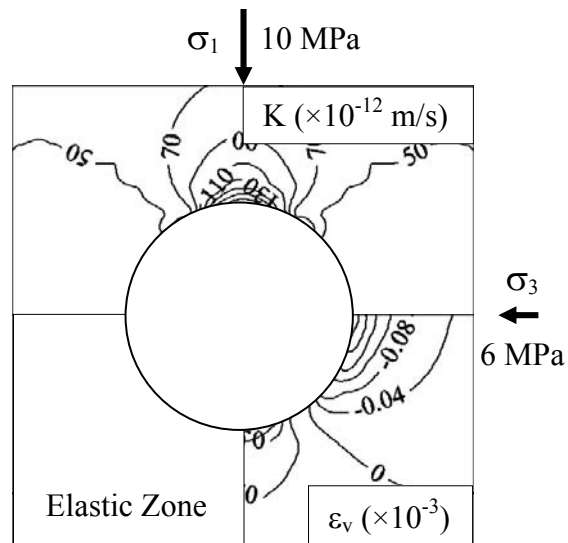


Figure 5.9 Volumetric strain and permeability of Phu Kradung sandstone simulated around single circular opening subjected to $\sigma_1=10$ MPa and $\sigma_3=6$ MPa ($\nu=0.30$, $E=7.70$ GPa).

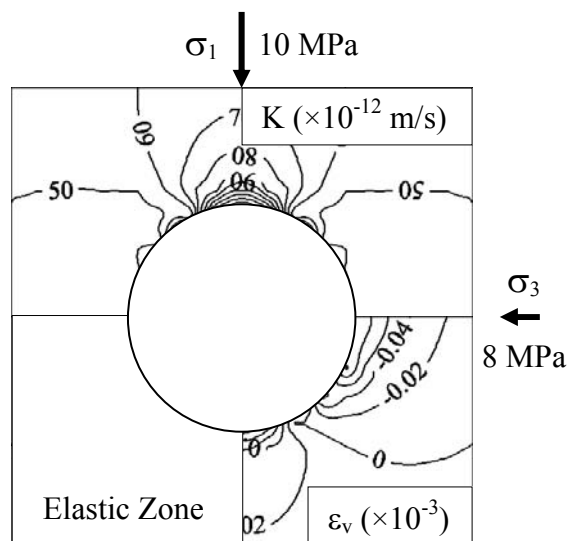


Figure 5.10 Volumetric strain and permeability of Phu Kradung sandstone simulated around single circular opening subjected to $\sigma_1=10$ MPa and $\sigma_3=8$ MPa ($\nu=0.30$, $E=7.70$ GPa).

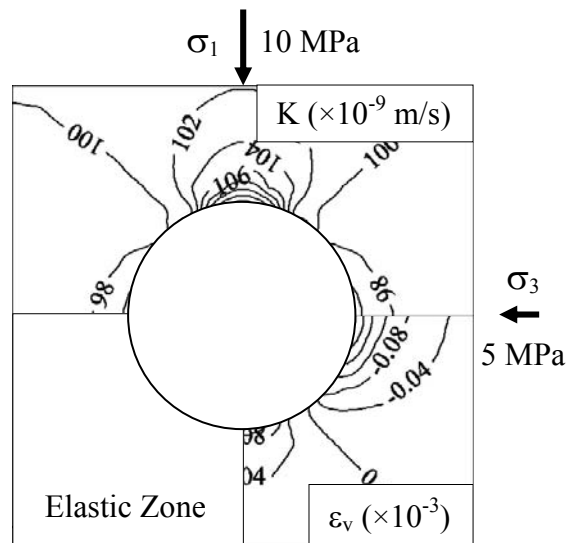


Figure 5.11 Volumetric strain and permeability of Phra Wihan sandstone simulated around single circular opening subjected to $\sigma_1=10$ MPa and $\sigma_3=5$ MPa ($\nu=0.30$, $E=7.70$ GPa).

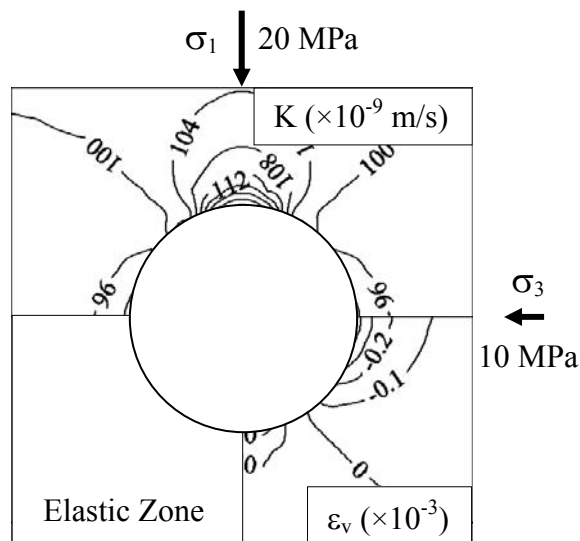


Figure 5.12 Volumetric strain and permeability of Phra Wihan sandstone simulated around single circular opening subjected to $\sigma_1=20$ MPa and $\sigma_3=10$ MPa ($\nu=0.30$, $E=7.70$ GPa).

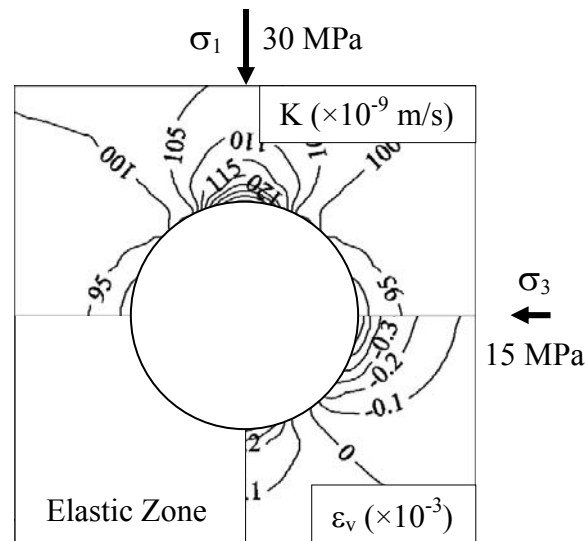


Figure 5.13 Volumetric strain and permeability of Phra Wihan sandstone simulated around single circular opening subjected to $\sigma_1=30$ MPa and $\sigma_3=15$ MPa ($\nu=0.30$, $E=7.70$ GPa).

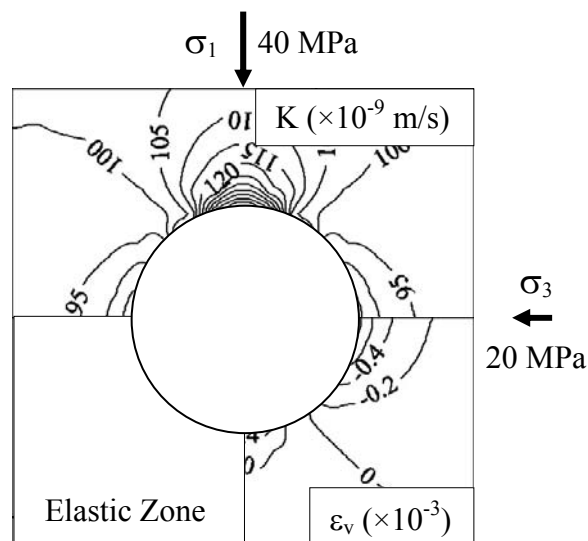


Figure 5.14 Volumetric strain and permeability of Phra Wihan sandstone simulated around single circular opening subjected to $\sigma_1=40$ MPa and $\sigma_3=20$ MPa ($\nu=0.30$, $E=7.70$ GPa).

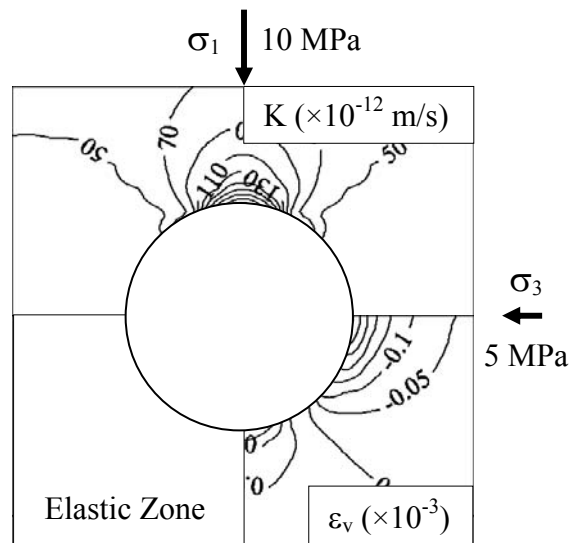


Figure 5.15 Volumetric strain and permeability of Phu Kradung sandstone simulated around single circular opening subjected to $\sigma_1=10$ MPa and $\sigma_3=5$ MPa ($\nu=0.30$, $E=7.70$ GPa).

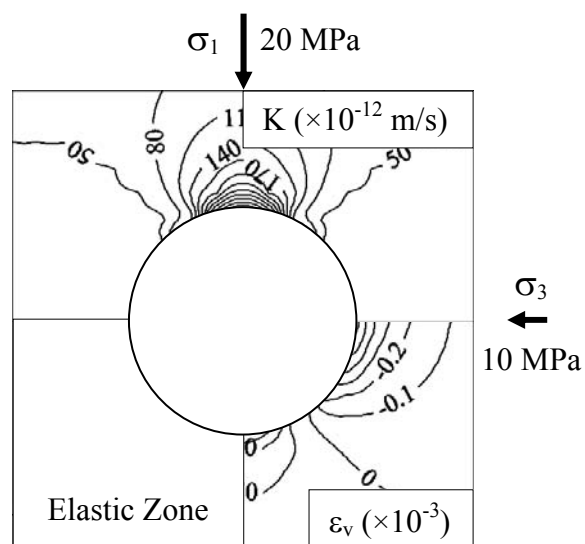


Figure 5.16 Volumetric strain and permeability of Phu Kradung sandstone simulated around single circular opening subjected to $\sigma_1=20$ MPa and $\sigma_3=10$ MPa ($\nu=0.30$, $E=7.70$ GPa).

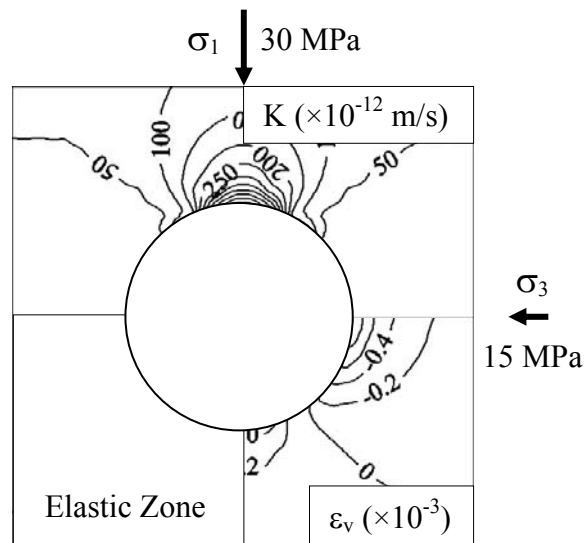


Figure 5.17 Volumetric strain and permeability of Phu Kradung sandstone simulated around single circular opening subjected to $\sigma_1=30$ MPa and $\sigma_3=15$ MPa ($\nu=0.30$, $E=7.70$ GPa).

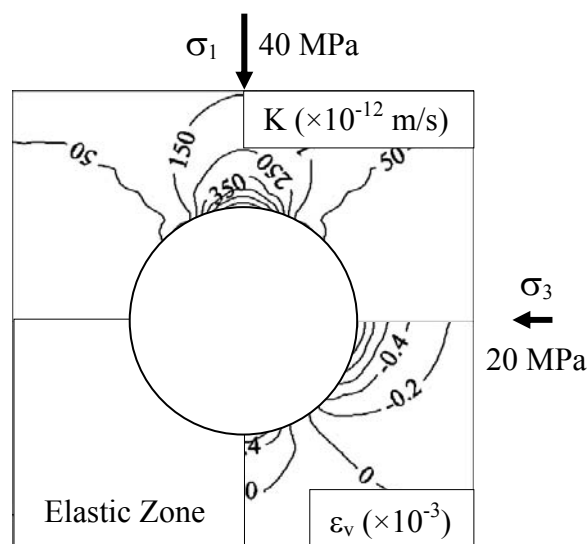


Figure 5.18 Volumetric strain and permeability of Phu Kradung sandstone simulated around single circular opening subjected to $\sigma_1=40$ MPa and $\sigma_3=20$ MPa ($\nu=0.30$, $E=7.70$ GPa).

5.3.3 Horizontal parallel circular opening under deviatoric stresses

For this modeling, two-dimensional finite difference mesh is created in x-y axis. The third dimensional with z-axis is omitted because this analysis is a plane strain analysis by assuming strain in z-axis to be zero. For the best efficiency, finite difference mesh represents a half of the domain due to the symmetry. The opening model is under vertical stresses varied from 10 to 40 MPa. The variables used in FLAC simulations are shown in Table 5.4.

Table 5.4 Variables used in FLAC simulations for horizontal parallel opening.

Rocks	Opening depth (m)	Opening radius (m)	Vertical Stress (MPa)
Phra Wihan Sandstone	16	4	10
			20
			30
			40
Phu Kradung Sandstone	16	4	10
			20
			30
			40

Figure 5.18 illustrates the model B created from a half of circular cross section with a radius of 4 m. Distance from the center-to-center of the opening is 16 m. The stress applied on the top is vertical stress. The upper boundary is allowed to freely displace in both x- and y-directions. The left boundary which is a symmetric axis separates the opening in two parts. The y-axis can move in y-direction but not in x-direction. The lower and right boundaries are symmetrical axis that separates the

opening into many parts, the x-axis is fixed in y-direction and y-axis is fixed in x-direction. In order to clearly illustrate the boundary of the opening in finite difference mesh, elements in the opening are not shown in the figure.

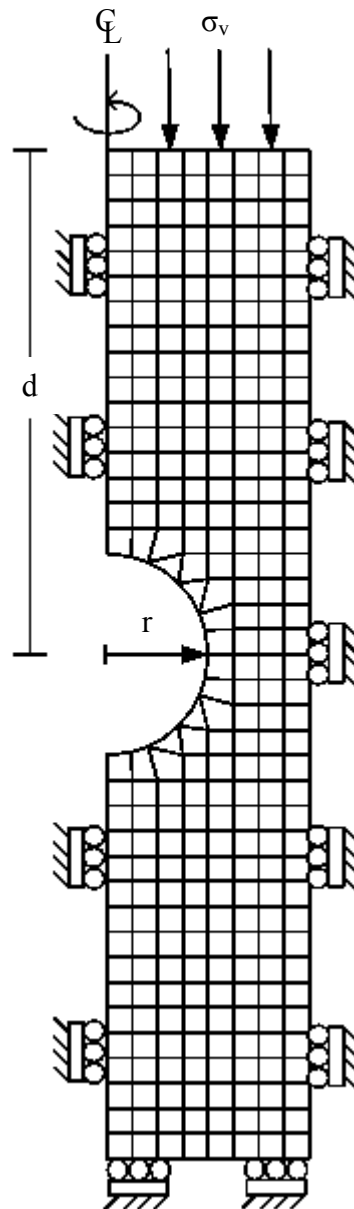


Figure 5.19 Finite difference mesh for modeling parallel circular opening (Model B).

5.3.4 Results

From the modeling of parallel circular openings under the vertical stress of 10, 20, 30 and 40 MPa it is found that the maximum volumetric strains are 0.2×10^{-3} , 0.4×10^{-3} , 0.6×10^{-3} and 0.8×10^{-3} for Phra Wihan sandstone, and 0.3×10^{-3} , 0.6×10^{-3} , 0.9×10^{-3} and 1.2×10^{-3} for Phu Kradung sandstone. Due to the induced volumetric strain the hydraulic conductivity is increased. The maximum hydraulic conductivity for the vertical stresses of 10, 20, 30 and 40 are 120×10^{-9} , 135×10^{-9} , 155×10^{-9} and 180×10^{-9} m/s for Phra Wihan sandstone, and are 350×10^{-12} , 650×10^{-12} , 950×10^{-12} and 1350×10^{-12} m/s for Phu Kradung sandstone.

Comparison of the maximum hydraulic conductivity with the vertical stresses of 10, 20, 30 and 40 MPa indicate that the hydraulic conductivity of rock pillar between parallel circular openings increased from 120×10^{-9} to 180×10^{-9} m/s for Phra Wihan sandstone, and from 350×10^{-12} to 1350×10^{-12} m/s for Phu Kradung sandstone as the vertical stress increases from 10 to 40 MPa. Figures 5.19 to 5.26 show the comparison of the hydraulic conductivity in the pillars.

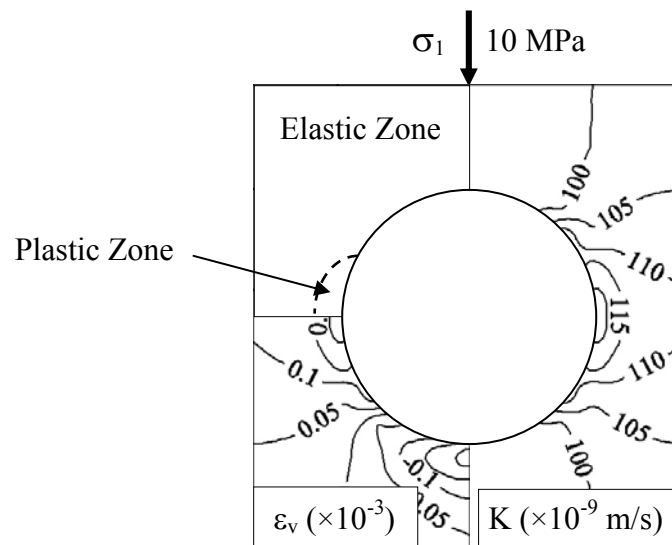


Figure 5.20 Volumetric strain and permeability of Phra Wihan sandstone simulated around horizontal parallel tunnel subjected to $\sigma_v=10$ MPa ($\nu=0.35$, $E=8.66$ GPa).

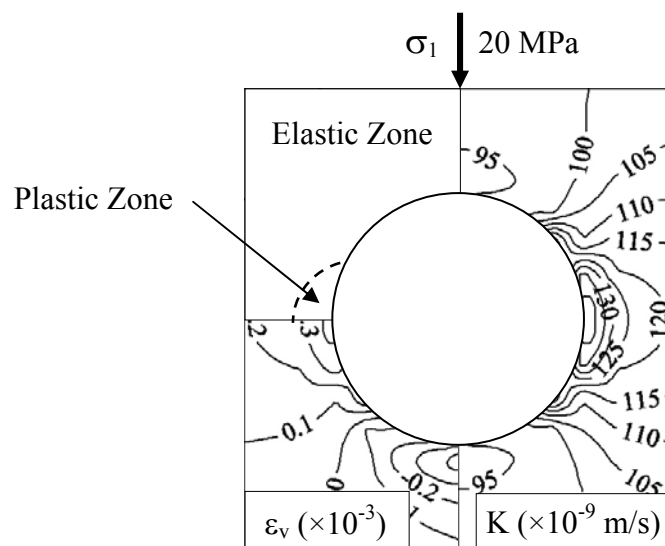


Figure 5.21 Volumetric strain and permeability of Phra Wihan sandstone simulated around horizontal parallel tunnel subjected to $\sigma_v=20$ MPa ($\nu=0.35$, $E=8.66$ GPa).

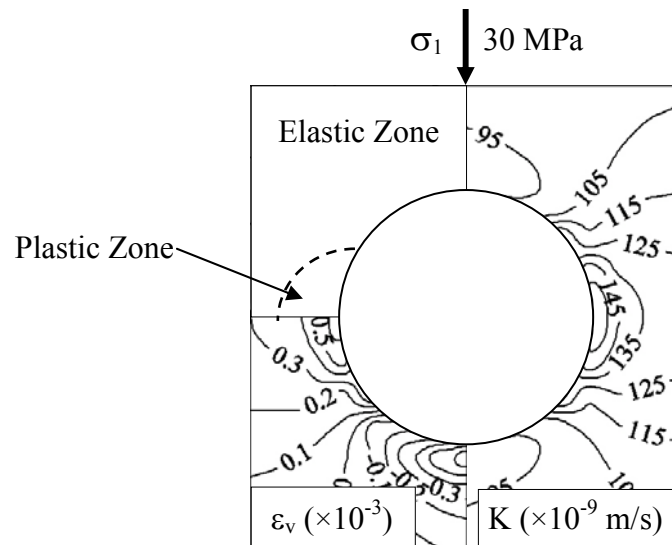


Figure 5.22 Volumetric strain and permeability of Phra Wihan sandstone simulated around horizontal parallel tunnel subjected to $\sigma_v=30$ MPa ($\nu=0.35$, $E=8.66$ GPa).

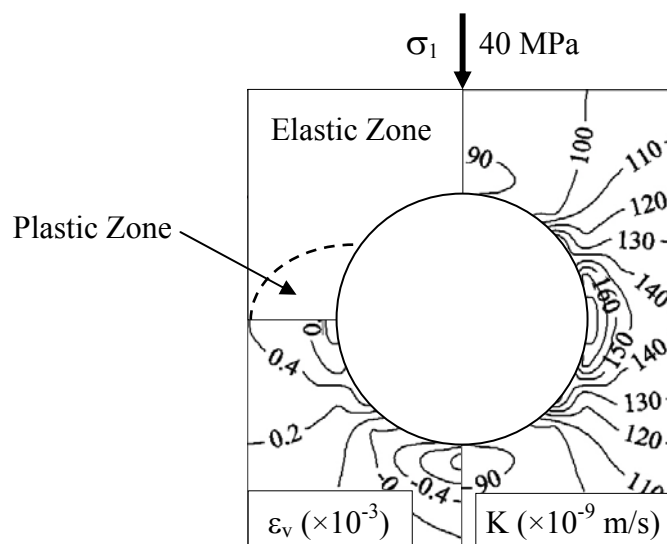


Figure 5.23 Volumetric strain and permeability of Phra Wihan sandstone simulated around horizontal parallel tunnel subjected to $\sigma_1=40$ MPa ($\nu=0.35$, $E=8.66$ GPa).

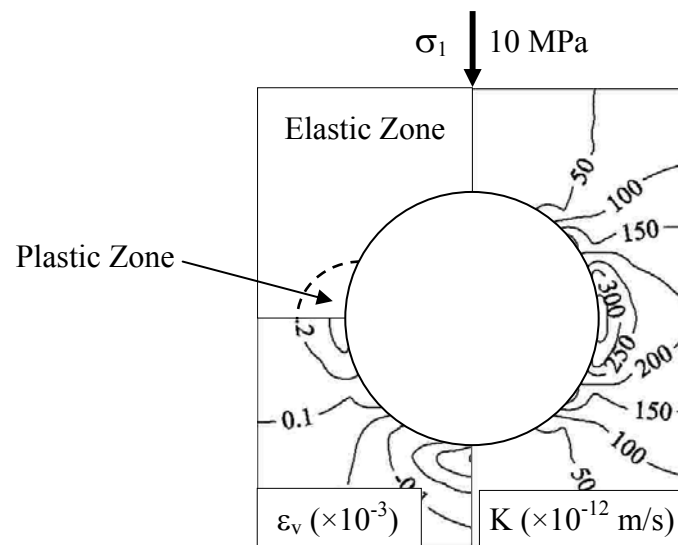


Figure 5.24 Volumetric strain and permeability of Phu Kradung sandstone simulated around horizontal parallel tunnel subjected to $\sigma_1=10$ MPa ($\nu=0.30$, $E=7.70$ GPa).

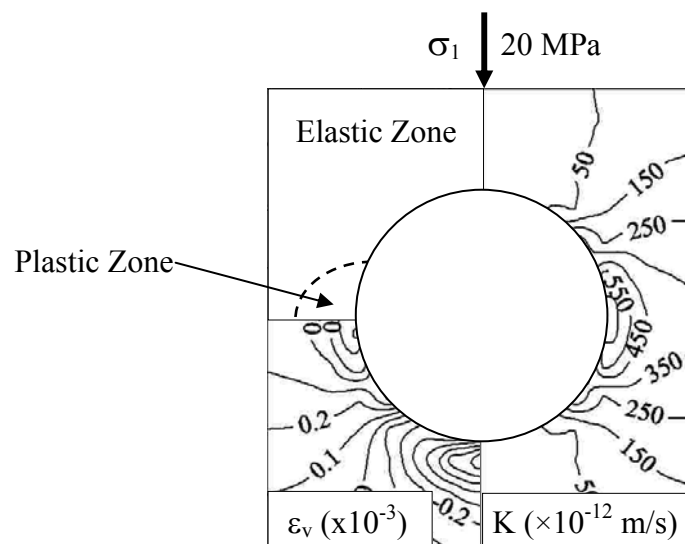


Figure 5.25 Volumetric strain and permeability of Phu Kradung sandstone simulated around horizontal parallel tunnel subjected to $\sigma_1=20$ MPa ($\nu=0.30$, $E=7.70$ GPa).

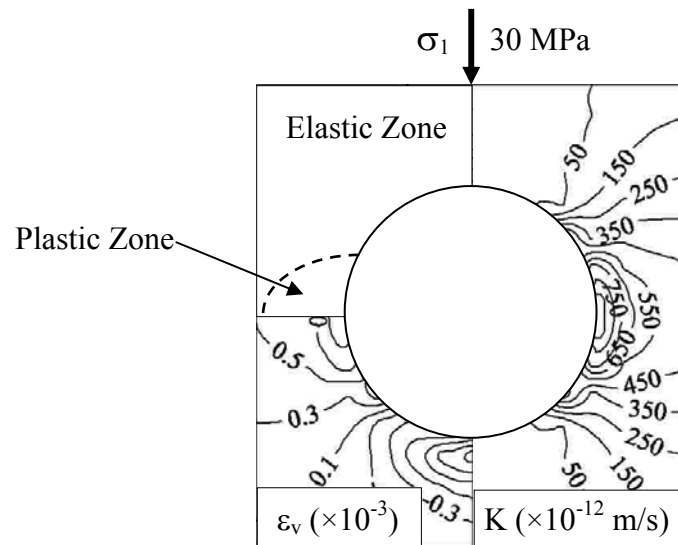


Figure 5.26 Volumetric strain and permeability of Phu Kradung sandstone simulated around horizontal parallel tunnel subjected to $\sigma_1=30$ MPa ($\nu=0.30$, $E=7.70$ GPa).

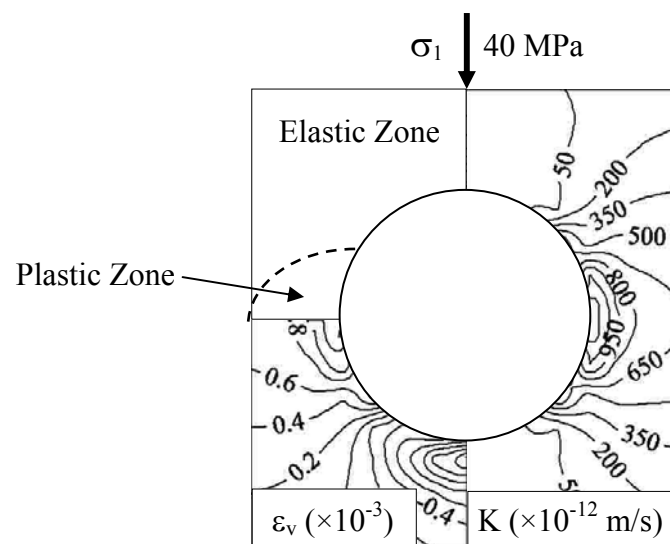


Figure 5.27 Volumetric strain and permeability of Phu Kradung sandstone simulated around horizontal parallel tunnel subjected to $\sigma_1=40$ MPa ($\nu=0.30$, $E=7.70$ GPa).

CHAPTER VI

DISCUSSIONS, CONCLUSIONS AND RECOMMENDATIONS FOR FUTURE STUDIES

6.1 Discussions and conclusions

The results from the constant head flow tests under deviatoric stress states indicate that before dilation strength the rock permeability of PW, PP and PK sandstones decreases with increasing volumetric strain due to the contraction of the pore spaces in the specimen. Within this stage the $\Delta K/\Delta \epsilon_V$ ratio decreases as increasing the confining pressure. After dilation strength the rock permeability increases with specimen dilation because of the initiation and propagation of micro-cracks due to the applied axial stress approaching failure. This agrees with the experimental results by Ferfera et al. (1997), Pusch and Weber (1998), Oda et al. (2002) and Heiland (2003).

Analytical work that supported the laboratory testing is the numerical analysis to study the displacement and hydraulic conductivity of the sandstone under deviatoric stress states around the opening. Evaluation from the hydraulic conductivity of rock around the opening can be concluded that the hydraulic conductivity of rock around single circular opening increases as the horizontal-to-vertical stress ratio decreases, and increases with the mean stress increases. The hydraulic conductivity of rock pillars between the parallel circular openings increases as the vertical stress increases.

The findings from this research have improved our understanding of the hydraulic properties of porous rocks as affected by the magnitudes and directions of the applied stress. A true understanding of the hydro-mechanical responses of the porous rocks to the complex stress conditions is necessary for predicting the rates of production of groundwater from aquifer, or oil and gas from reservoir. The $\Delta K/\Delta \epsilon_v$ ratio apparently depends on rock type. For rock with large dilation a high ratio is expected. A higher $\Delta K/\Delta \epsilon_v$ ratio will result in a large increase of the rock permeability under dilation stage. The results from this research probably under estimate the in-situ rock permeability in dilation zone because the post-failure of the brittle rocks is likely to yield system of fracturing, and hence leading to a much higher hydraulic conductivity.

The data interpretation and analysis performed here assume that the rock permeability under deviatoric stresses is isotropic and can be represented by a scalar form. The actual rock permeability beyond the dilation strength may not be isotropic due to the orientation of the induced microcracks within the specimen.

6.2 Recommendations for future studies

The study in this research can be taken as a preliminary guideline and process of study and design. More laboratory testing should be performed using the higher confining pressures with larger specimens. The higher water injection pressures are needed to accelerate the test duration. The rock permeability as affected by the bedding plane should also be studied. The rock permeability under deviatoric stresses of maximum, intermediate and minimum principal stresses should be evaluated.

REFERENCES

- ASTM D4543-08. Standard Practices for Preparing Rock Core as Cylindrical Test Specimens and Verifying Conformance to Dimensional and Shape Tolerances. **Annual Book of ASTM Standards** (Vol. 04.08). Philadelphia: American Society for Testing and Materials.
- Akkrachattrarat, N., Suanprom, Buaboocha P., and Fuenkajorn, K. (2009). Flow Testing of Sandstone Fracture under Normal and Shear Stresses. In **Proceedings of the Second Thailand Symposium on Rock Mechanics**, Thailand, pp 319-334., Suranaree University of Technology.
- Ali, H.S. (1987). The Effect of Overburden Pressure, SPE-Paper 15730 5. **SPE Middle-East Oil Show Proc.** Manama, Bahrain, pp 7-10.
- Dautriat, J., Gland, N., Youssef, S., Rosenberg, E., and Bekri, S. (2007). Stress dependent permeabilities of sandstones and carbonates: Compression experiments and pore network modeling. **2007 SPE Annual Technical Conference and Exhibition**. Anaheim, California, U.S.A. 11–14 November 2007.
- Ferfera, F.M.R., Sarda, J.P., Bouteica, M., and Vincke, O. (1997). Experimental study of monophasic permeability changes under various stress paths. **International Journal of Rock Mechanics and Mining Sciences**. 34: 3-4.
- Ghabezloo, S., Sulem, J., and Saint-Marc, J. (2008). Evaluation of a permeability-porosity relationship in a low permeability creeping material using a single transient test. **International Journal of Rock Mechanics and Mining Sciences**. DOI 10.1016/j.ijrmms.2008.10.003.

- Heiland, J. (2003). Permeability of triaxially compressed sandstone: Influence of deformation and strain-rate on permeability. **Pure Applied Geophysics**. 160: 889-908.
- Holt, R.M. (1989). Permeability Reduction Induced Nonhydrostatic Stress Field, **SPE-Paper 19595 Annual Technical Conference.**, San Antonio, Oct. 8-11.
- Indraratna, B. and Ranjith, P.G. (2001). Laboratory measurement of two-phase flow parameters in rock joints based on high pressure triaxial testing. **Journal of Geotechnical and Geoenvironmental Engineering**. 127(6): 530-542.
- Indraratna, B. and Ranjith, P. (2001). **Hydromechanical Aspects and Unsaturated Flow in Joints Rock.**, Lisse: A.A. Balkema.
- Iscan, A.G., Kok, M.V., and Bagci, A.S. (2006). Estimation of permeability and rock mechanical properties of limestone reservoir rocks under stress conditions by strain gauge. **Journal of Petroleum Science and Engineering**. 53: 13-24.
- Itasca (1992a). **FLAC–Fast Lagrangian Analysis of Continua, Version 4.0**, User Manual. Itasca Consulting Group Inc., Minneapolis, MN, USA.
- Itasca (1992b). User **Manual for FLAC–Fast Lagrangian Analysis of Continua, Version 4.0**, Itasca Consulting Group Inc., Minneapolis, MN.
- Kiyama, T., Kita, H., Ishijima, Y., Yanagidani, T., Aoki, K., and Sato, T. (1996). Permeability in anisotropic granite under hydrostatic compression and triaxial compression including post-failure region. In: Aubertin, M., Hassani, F., Mii, H. (Eds.), **Rock Mechanics**. Balkema, Rotterdam, pp. 1643–1650.
- Kranz, R.L., Frankel, A.D., Engelder, T., and Scholz, C.H. (1979). The permeability of whole and jointed granite. **International Journal of Rock Mechanics and Mining Sciences Geomechanics Abstract**. 16: 225-334.

- Oda, M., Takemura, T., and Aoki, T. (2002). Damage growth and permeability change in triaxial compression tests of Inada granite. **Mechanics of Materials**. 34: 313–331.
- Pusch, G. and Weber, J.R. (1998). Correlation of rock permeability and anisotropic stress conditions for the integration of rock mechanical and hydraulic flow models. In **Proceedings of the International Symposium of the Society of Core Analysts**. September 14-16, den Haag, Netherlands.
- Risnes, R., Faldaas, I., Korsnes, R.I., and Norland, T. (2003). Measurements on Stress Dependent Permeability. **Geophysical Research Abstracts**. 5: 03507.
- Shangxian, Y. and Shangxu W. (2006). Effect and mechanism of stresses on rock permeability at different scales. **Science in China: Series D Earth Sciences** 2006. 49(7): 714-723.
- Smart, B.G. (1992). The Effects of Combined Changes in Pore Fluid Chemistry and Stress State on Reservoir Permeability. **PSTI-Technical Bulletin No. 1**. pp 14-17.
- Spivak, A.I. and Popov, A.M. (1986). **Breaking Rocks During Drilling [in Russian]**, Nedra, Moscow.
- Stavrogin, A.N. and Tarasov, B.G. (2001). **Experimental Physics and Rock Mechanics**. Lisse: A.A. Balkema.
- Trimmer, D. (1982). Laboratory measurements of ultralowpermeability of geological materials. **Revised Sciences Instruments**. 53(8).
- Walsh, J.B. (1981). Effect of Pore Pressure and Confining Pressure on Fracture Permeability, **International Journal of Rock Mechanics, Mining Sciences and Geomechanics**. 18: 429-435.

- Walsri, C., Poonprakon, P., Thosuwan, R., and Fuenkajorn, K. (2009). Compressive and tensile strengths of sandstones under true triaxial stresses. In **Proceedings of the Second Thailand Symposium on Rock Mechanics**, Thailand, pp 199-218., Suranaree University of Technology.
- Wilhelmi, B. and Somerton, W.H. (1967). Simultaneous Measurement of Pore and Elastic Properties of Rocks under Triaxial Stress Conditions, **SPE-Journal**. 9: 283 – 294.
- Witherspoon, P.A. (1980). Validity of the Cubic Law for Fluid Flow in a Deformable Rock Fracture. **Water Resources Research**. 16(6): 1016-1024.
- Zeigler, B. (1976). **Theory of Modelling and Simulation**. New York: John Wiley and Sons.
- Zhou, J.J. and Shao, J.F. (2006). micromechanical study of damage growth and permeability variation in brittle rocks. **Studia Geotechnica et Mechanica**. 28(1): 62-73.
- Zhu, W., Montési, Laurent G.J., and Wong, T.F. (2002). Effects of stress on the anisotropic development of permeability during mechanical compaction of porous sandstones. **Geological Society, London, Special Publications**. 200: 119-136.
- Zoback, M.D. and Byerlee, J.D. (1975). The effect of microcrack dilatancy on permeability of westerly granite. **Journal of Geophysicss Research**. 80(5): 52–755.

APPENDIX A

TECHNICAL PUBLICATION

TECHNICAL PUBLICATION

Akkrachattrarat, N., Suanprom, Buaboocha P., and Fuenkajorn, K. (2009). **Flow Testing of Sandstone Fracture under Normal and Shear Stresses.** In Proceeding 2nd Thailand Symposium on Rock Mechanics. Chonburi, Thailand. 12 - 13 March 2009.

Flow testing of sandstone fractures under normal and shear stresses

N. Akkrachattrarat, P. Suanprom, J. Buaboocha & K. Fuenkajorn
Geomechanics Research Unit, Suranaree University of Technology, Thailand

Keywords: Permeability, fracture, aperture, shear stress, deviatoric stress

ABSTRACTS: Flow tests have been performed to determine hydraulic conductivity of intact sandstone specimens under confining pressures and deviatoric stresses, and of tension-induced fractures under normal and shear stresses. The results indicate that the intact sandstone permeability decreases with increasing volumetric strain before dilation strength probably due to the closure of voids and micro-cracks, and increases with the specimen dilation after the dilation strength probably due to the initiation and propagation of cracks and fractures. The physical aperture e_p and hydraulic aperture e_h increase with shearing displacement, particularly under high normal stresses. The magnitudes of fracture permeability under no shear and under peak shear stress are similar. The K_p is about an order of magnitude greater than K_b , particularly in the residual shear region. Both tend to decrease exponentially with increasing normal stress. The difference between the permeability under residual shear stress and that under peak stress becomes larger under higher normal stresses. The fracture hydraulic conductivities exponentially decrease from 10000×10^{-6} m/s to 100×10^{-6} m/s as the normal stresses are increased from 0.35 MPa to 2.06 MPa. Under normal stress alone a permanent fracture closure is usually observed after unloading as evidenced by the permanent reduction of the measured flow rates.

1 INTRODUCTION

Groundwater in rock mass is one of the key factors governing the mechanical stability of slope embankments, underground mines and tunnels. The lack of proper understanding of the water pressure and flow characteristics in rock mass makes it difficult to predict the water inflow for underground mines and tunnels under complex hydro-geological environments. Unlike those in the soil mass, permeability of rock mass is path dependent, controlling mainly by the system of fracture as the permeability of the intact rocks is normally low. For undisturbed rock mass (before excavation) the joint characteristics (e.g., roughness, aperture, spacing and orientation) that dictate the amount and direction of water flow, can be adequately determined by means of in-situ measurements, and are sometimes assisted by numerical modeling. Slope or underground excavations disturb the surrounding rock, alter the stress states on the fracture planes, and often cause relative displacements of the rock fractures. In most cases the excavations usually increase the surrounding rock mass permeability, sometimes by several orders of magnitude.

It has been experimentally found that permeability of intact rocks is affected by the confining pressures (Iscaan et al., 2006; Shangxian & Shangxu, 2006) and by deviatoric stresses (Ferfera et al., 1997; Oda, 2002; Pusch & Weber, 1998; Heiland, 2003; Zhou & Shao, 2006). The rock permeability generally decreases logarithmically with increasing the confining pressures. Under deviatoric stresses the rock permeability first decreases due to a reduction of pore spaces, and starts to increase due to the damage growth after the rock is dilated under differential stresses.

Fracture apertures and hydraulic conductivity are the main factors governing the rock mass permeability. Xiao et al. (1999), Pyrak-Noltea & Morrisa (2000), Niemi et al. (1997), Indraratna & Ranjith (2001) and Baghbanan & Jing (2008) conclude from their experimental results that fracture permeability exponentially decreases with increasing normal stresses. The apertures and permeability of rock fractures are also affected by the shearing displacement (Auradou et al., 2006). The flow testing results on fractures in granite and marble by Lee & Cho (2002) indicate that the fracture permeability increases by up to two orders of magnitude as the shearing displacement increases. This finding is supported by the results of numerical simulations by Son et al. (2004).

The objective of this study is to experimentally determine the hydraulic conductivity of fractures in sandstone specimens under normal and shear stresses. Constant head flow tests are conducted to obtain data basis on the permeability of intact sandstones under hydrostatic pressures and deviatoric stresses. The rock permeability is correlated with the volumetric strain before failure and with the volumetric dilation after failure. Falling head tests are performed to determine the permeability of tension-induced fractures under normal and shear stresses. The flow rates are monitored from before peak shear strength through residual shear strength. The fracture hydraulic conductivities calculated from the physical, mechanical and hydraulic apertures are compared. The joint normal and shear stiffness parameters are determined.

2 ROCK SAMPLES

The tested sandstones are from four sources: Phu Phan, Phra Wihan, Phu Kradung and Sao Kua formations (hereafter designated as PP, PW, PK and SK sandstones). They belong to the Khorat group and widely expose in the north and northeast of Thailand. X-ray diffraction analyses have been performed to determine their mineral compositions. Table 1 summarizes the results. These fine-grained quartz sandstones are selected for this study primarily because they have highly uniform texture, grain size and density.

3 FLOW TESTING ON INTACT SANDSTONES

3.1 *Permeability of Intact Sandstones under Confining Pressures*

Constant head flow tests have been performed to assess the effects of hydrostatic pressures and deviatoric stresses on the intact sandstone permeability. Figure 1 shows the laboratory arrangement of the constant head flow test under various confining pressures. The sandstone specimens have a nominal dimension of 5 cm in diameter and 10 cm long. A constant diameter water pump is used to inject water pressure of 0.14 MPa (20 psi) to bottom end of the specimen while the specimen is confined in a triaxial cell. The injected water pressure is controlled by using a regulating valve at the top of nitrogen gas tank. The constant confining pressures vary from 3.45 (500 psi), 6.90, 10.34, 13.79, 17.24 to 20.69 MPa (3000 psi). A

Table 1. Mineral compositions of tested sandstones obtained from X-ray diffraction.

Rocks	Density (g/cc)	Grain Size (mm)	Sorting	Mineral Compositions				
				Quartz (%)	Albite (%)	Kaolinite (%)	Feldspar (%)	Mica (%)
PW	2.35	1.5-2.0	well	99.47	-	0.53	-	-
PP	2.45	1.5-2.0	well	98.40	-	-	-	1.60
PK	2.63	0.1-1.5	moderate	48.80	46.10	5.10	-	-
SK	2.37	0.1-1.0	poorly	57.00	39.50	-	2.90	0.60

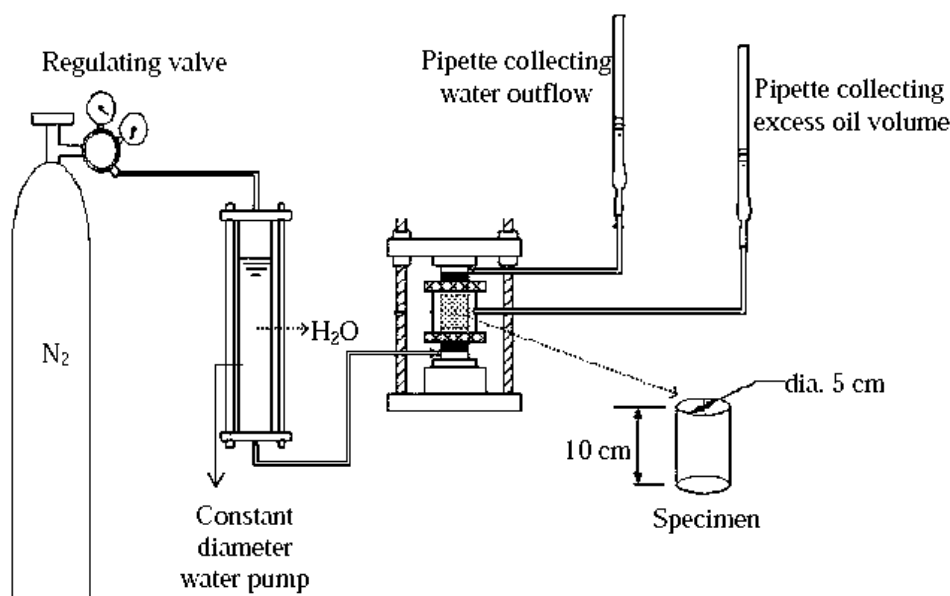


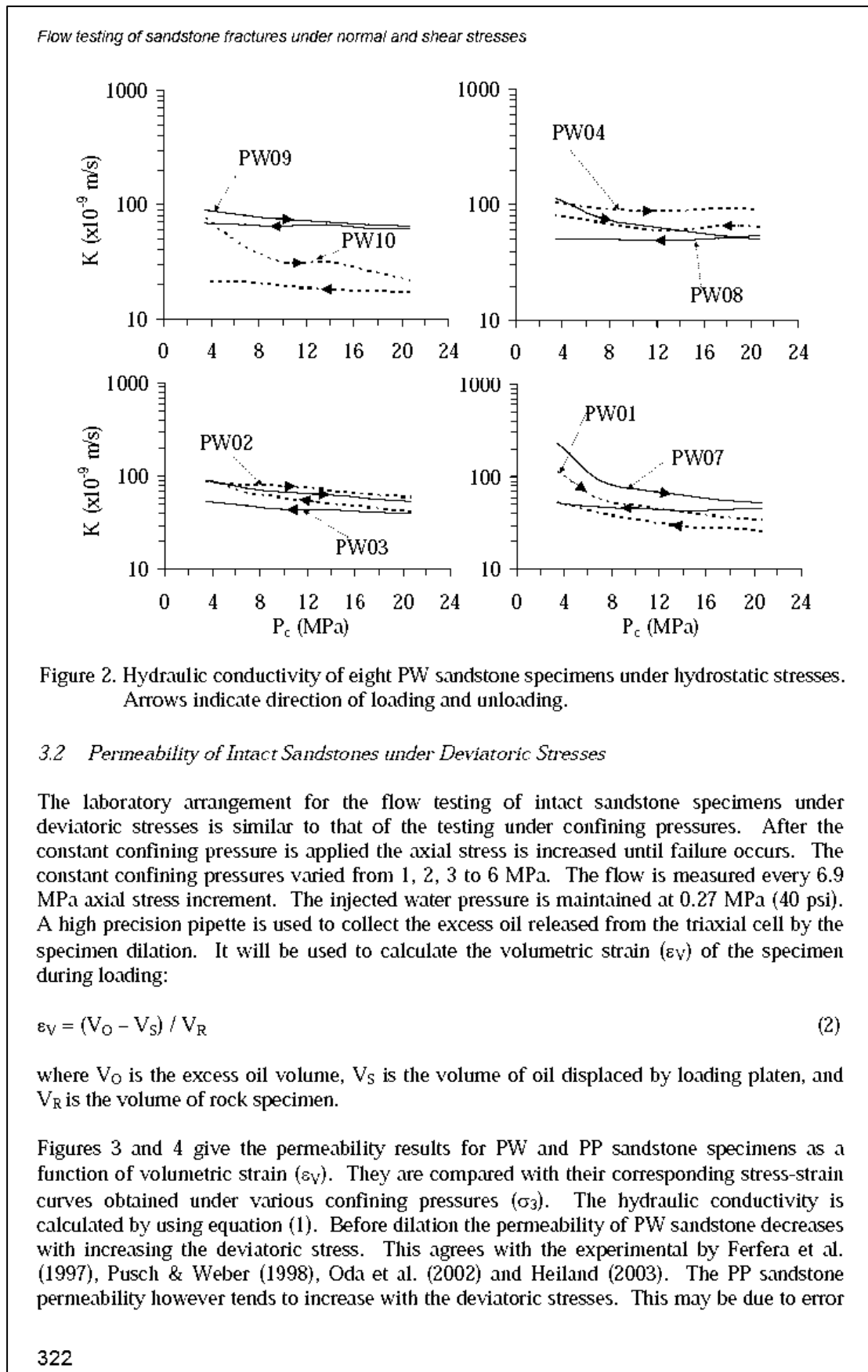
Figure 1. Laboratory arrangement for constant head flow tests.

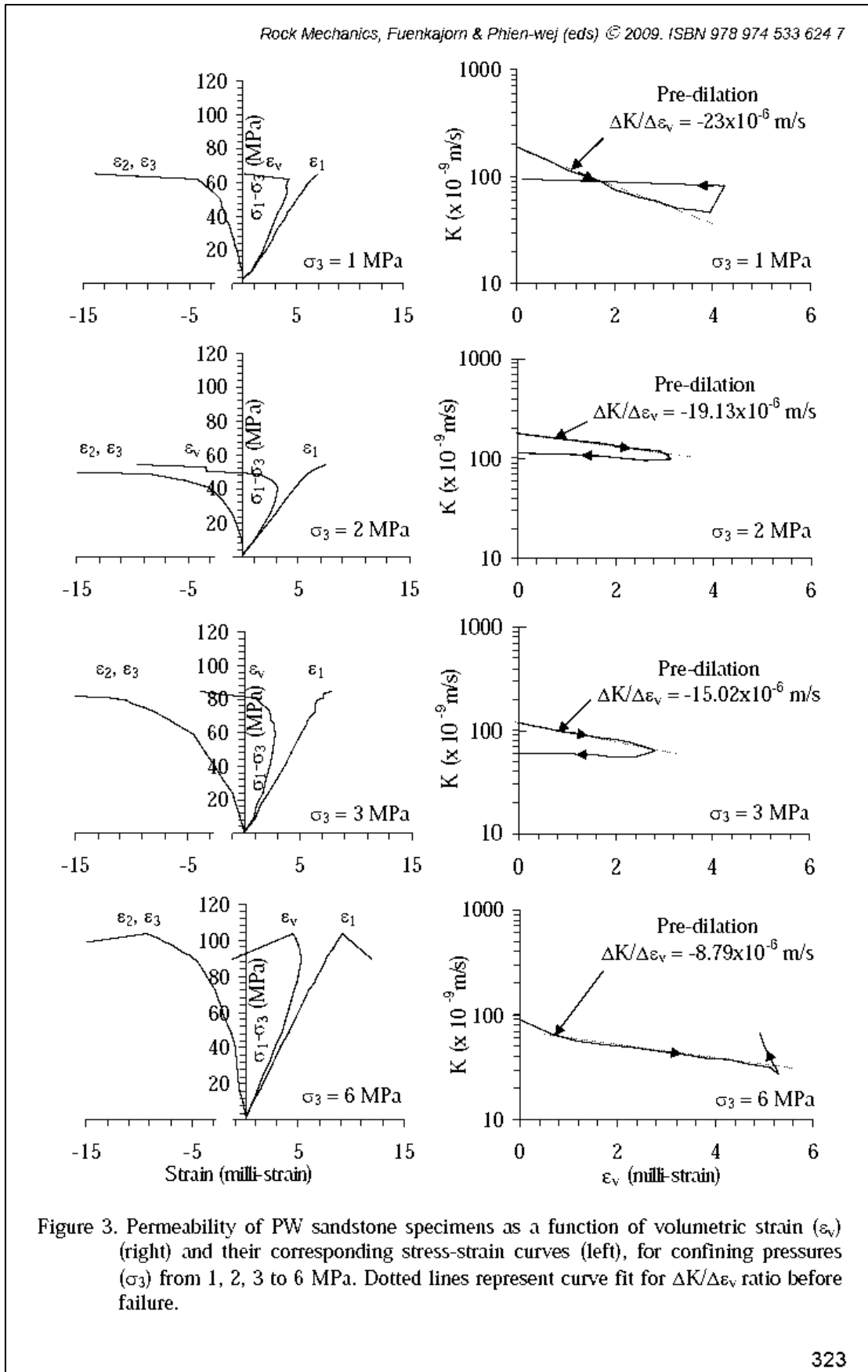
high precision pipette collects the outflow of water at the top end of the specimen. The measured flow rates under each confining pressure are used to calculate the specimen permeability. The hydraulic conductivity (K) is calculated by assuming that the Darcy's law is valid (Indraratna & Ranjith, 2001):

$$K = 4q\mu / [\pi D^2(dp/dx)] \quad (1)$$

where q is water flow rate through the specimen (cm^2/s), μ is the dynamic viscosity of the water ($\text{N}\cdot\text{s}/\text{cm}^2$), D is the specimen diameter (cm^2), and dp/dx is the pressure gradient along the length of the specimen.

Figure 2 plots the hydraulic conductivity for eight PW sandstone specimens under confining pressures between 3.45 MPa and 20.7 MPa. The permeability decreases from about 100×10^{-9} m/s to about 50×10^{-9} m/s as the confining pressures increase from 3.45 MPa to 20.7 MPa. The flow rates measured during unloading show a permanent reduction of the rock permeability, suggesting that a permanent closure of the pore spaces has occurred.





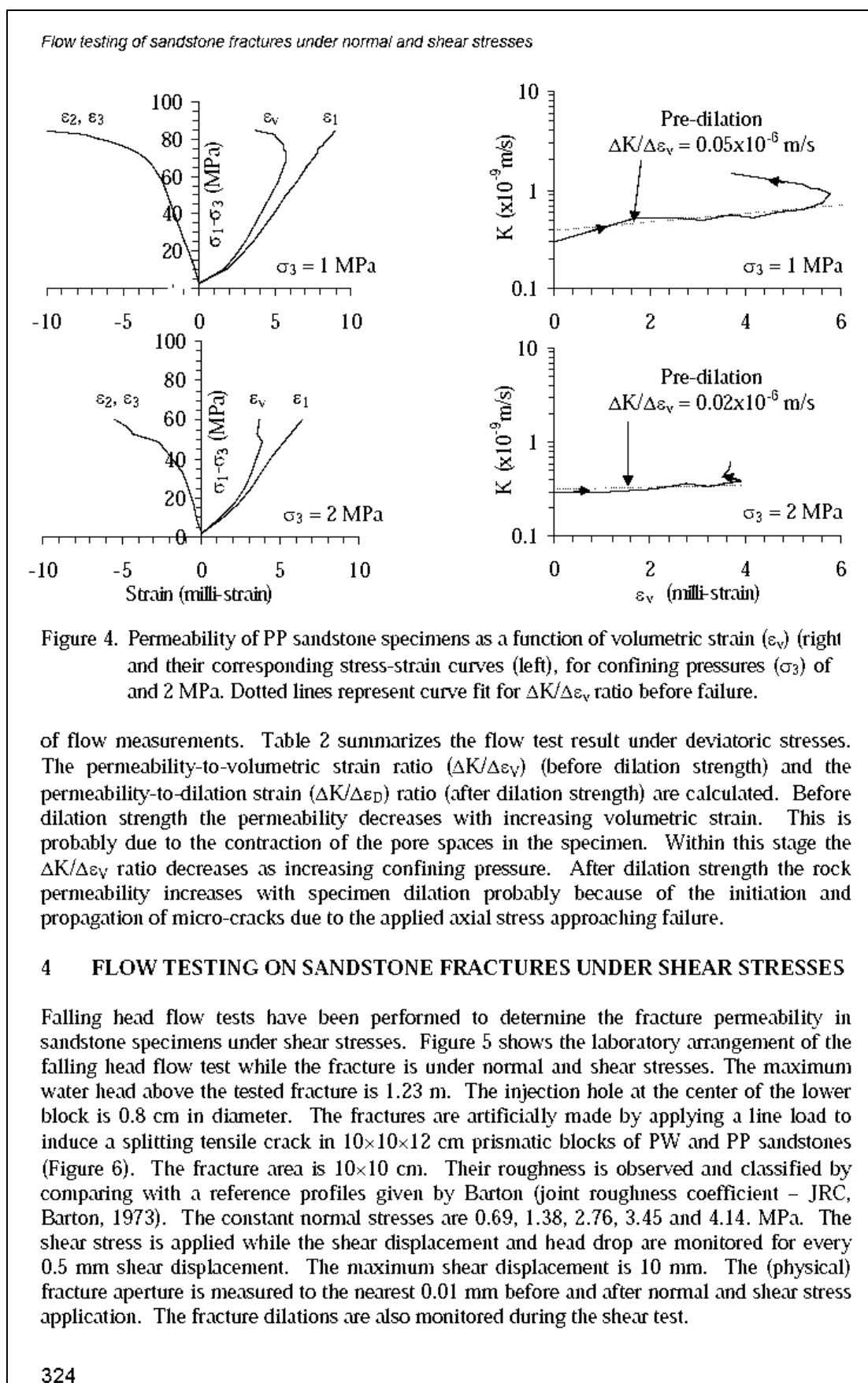


Table 2. Results of flow testing under deviatoric stresses.

	Sample No.	P_c (MPa)	E (GPa)	ν	Dilation Strength (MPa)	Ultimate Strength (MPa)	Pre-failure	Post-failure
							$\Delta k/\Delta \varepsilon_v$ ($\times 10^{-6}$ m/s)	$\Delta k/\Delta \varepsilon_d$ ($\times 10^{-6}$ m/s)
PW	PWSS-01	1	9.31	0.23	42	65	-23.00	-3.15
	PWSS-02	2	9.14	0.25	37	55	-19.13	-3.82
	PWSS-03	3	8.52	0.33	55	88	-15.02	-4.41
	PWSS-04	6	11.98	0.29	64	103	-8.79	-100
Mean \pm SD					49 \pm 12	78 \pm 25		
PP	PPSS-01	1	7.89	0.31	69	85	0.05	-0.21
	PPSS-02	2	8.66	0.31	49	60	0.02	-0.21
Mean \pm SD					59 \pm 10	72 \pm 13		

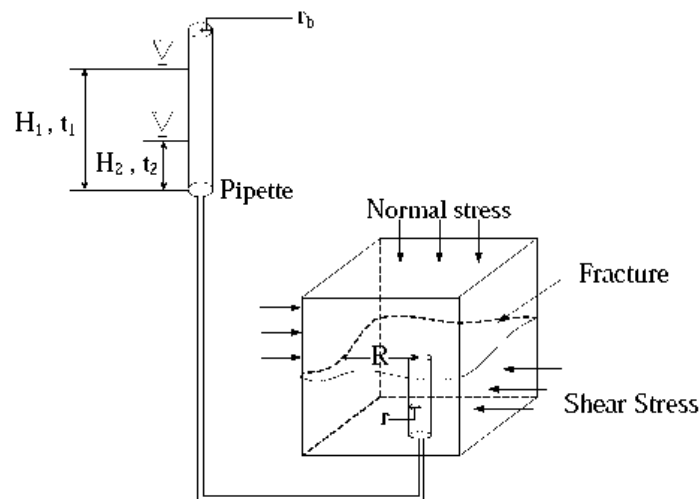


Figure 5. Laboratory arrangement for falling head test under normal and shear stresses.

The physical, mechanical and hydraulic apertures are used to calculate the hydraulic conductivity of the tested fractures. The physical aperture (e_p) is obtained from the actual measurements of the fractures before and during normal and shear stress applications. The measurement points are at the four corners of the shear box. The physical aperture at each shear displacement is an average from the four measurements. The mechanical aperture (e_m) in mm is calculated by (Barton & Bakhtar, 1983 and Bandis et al., 1983, 1985):

$$e_m = [JRC/5] / [0.2(\sigma_c/JCS) - 0.1] \quad (3)$$

where σ_c and JCS are the uniaxial compressive strength and joint compressive strength of the rock in MPa. Here σ_c and JCS are assumed to be equal.

The equivalent hydraulic aperture (e_h) for radial flow is calculated by (Maini, 1971):

$$e_h = [[\ln(H_1/H_2)r_b^2 \ln(R/r)6\mu] / [(t_2 - t_1)\gamma]]^{1/3} \quad (4)$$

Flow testing of sandstone fractures under normal and shear stresses

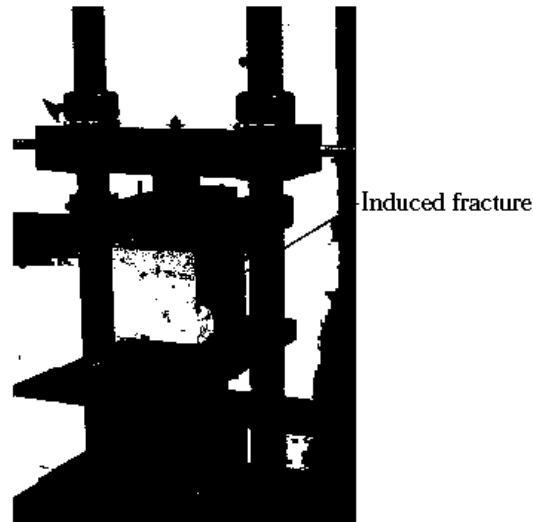


Figure 6. A 10×10×12 cm block of PW sandstone is line-loaded to induce tensile fracture in the mid-length of the block.

where γ is the unit weight of water (N/m^3), μ is the dynamic viscosity ($\text{N}\cdot\text{s}/\text{m}^2$), H_1 and H_2 are the water heads at t_1 and t_2 , r_b is the pipette radius (m), R is the radius of flow path (m), and r is the radius of the radius injection hole (m).

The fracture permeability is calculated by (Zeigler, 1976):

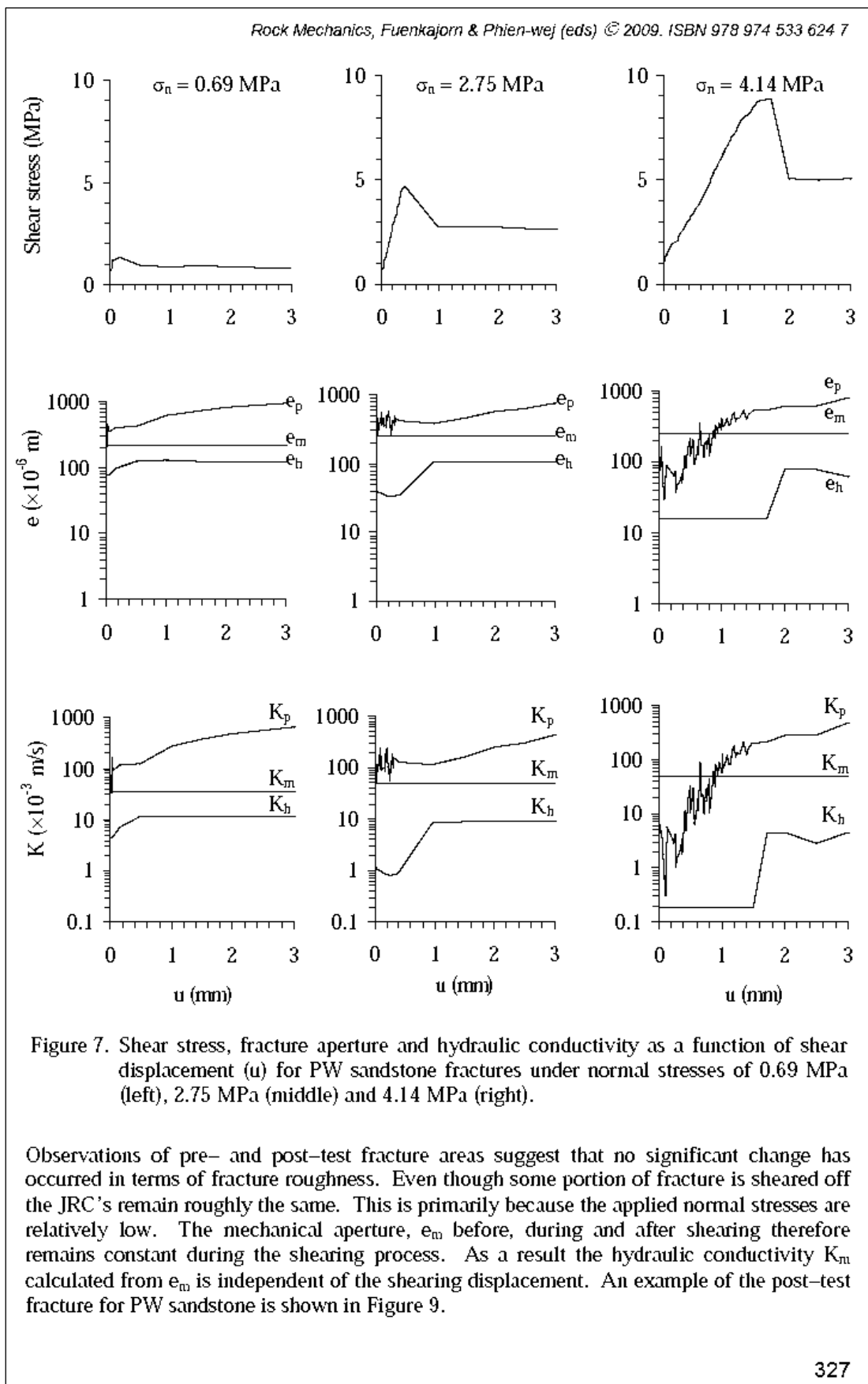
$$K = \gamma e^2 / 12\mu \quad (5)$$

where K represents hydraulic conductivity between smooth and parallel plates and e is the parallel plate aperture. It is assumed here that the flow is isotropic across the fracture plane, and that the intact rock is impermeable. From section 3 the intact PW sandstone permeability is about 0.1×10^{-6} m/s which is very low compared to the fracture permeability. The other sandstone permeability is less than 0.0001×10^{-6} m/s (measurement limit).

Here the fracture conductivity is calculated for three types of fracture apertures: e_p , e_m and e_h , and differentiated by different symbols as K_p – physical, K_m – mechanical, and K_h – hydraulic conductivities.

The measured JRC values range from 11, 13 to 15, which are classified as rough and undulating; bedding and tectonic joints; and relief joints, respectively. From equation (3) the equivalent mechanical apertures for the above JRC values are 220, 260 and 300 micrometers.

The fracture hydraulic conductivities are calculated for the three aperture measurements and plotted as a function of shear displacement (u) for normal stresses of 0.69, 2.75 and 4.14 MPa in Figures 7 and 8 for PW and PP sandstones. They are also compared with their corresponding shear stress-shear displacement diagram. Since the shear stresses after the peak value remain relatively consistent through 10 mm of displacement, up to 3 mm shear displacement is plotted in the figures.



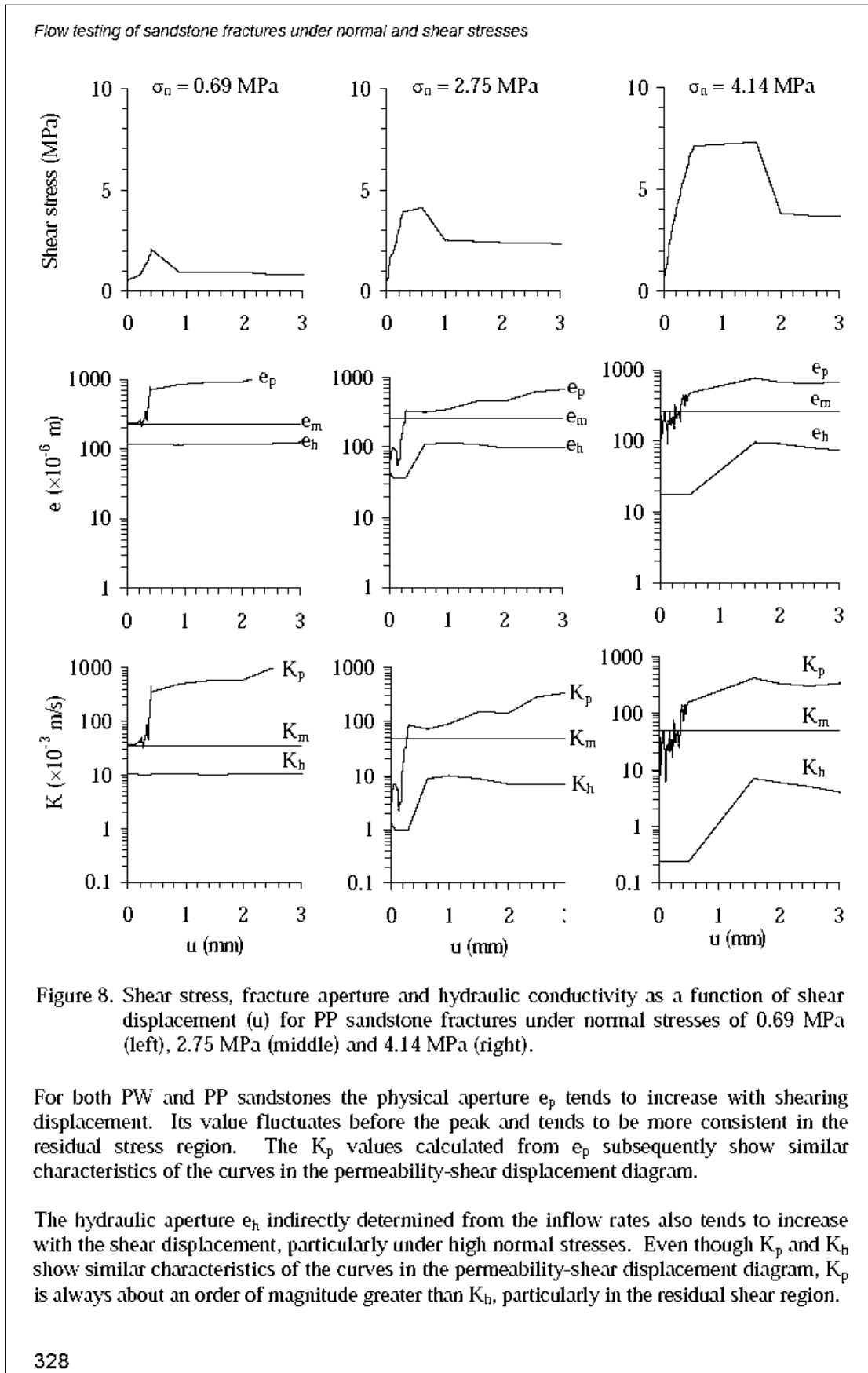




Figure 9. Example of post-test fracture surfaces in a PW sandstone specimen. The sheared surfaces are indicated by white areas.

Figures 10 and 11 plot the hydraulic conductivity derived from e_h as a function of normal stress σ_n . The fracture permeability values under no shear stress, immediately before the peak stress, and under the residual shear stress are compared. The fracture permeability under residual shear region is greater than that under no shear and that immediately before peak stress. It is not very sensitive to the normal stress – showing a slightly decrease with increasing the normal stress. The magnitudes of fracture permeability under no shear and under peak stress are similar. Both tend to decrease exponentially with the normal stress. As a result the difference between the permeability under residual shear stress and that under peak stress becomes larger as the normal stress increases. The results agree reasonably well with those obtained by Lee & Cho (2002) and Son et al. (2004).

This suggests that under a given normal stress, the fracture permeability immediately before peak stress will remain similar to that under no shear stress. After the fracture is displaced beyond the peak stress its permeability will however notably increase particularly under high normal stresses. The change of the fracture permeability with the normal stress will be presented in the next section.

From the shear stress-displacement diagrams as shown in Figures 7 and 8, the joint shear stiffness for various normal stresses has been calculated at the 50% peak stress using an equation (Indraratna & Ranjith, 2001):

$$k_s = \tau_s / \delta_s \quad (6)$$

where k_s is the joint shear stiffness (MPa/m), τ_s is the shear stress (MPa), δ_s is the shear displacement (m). Table 3 summarizes the results for PW and PP sandstones. The joint shear stiffness tends to increase with the normal stresses.

Flow testing of sandstone fractures under normal and shear stresses

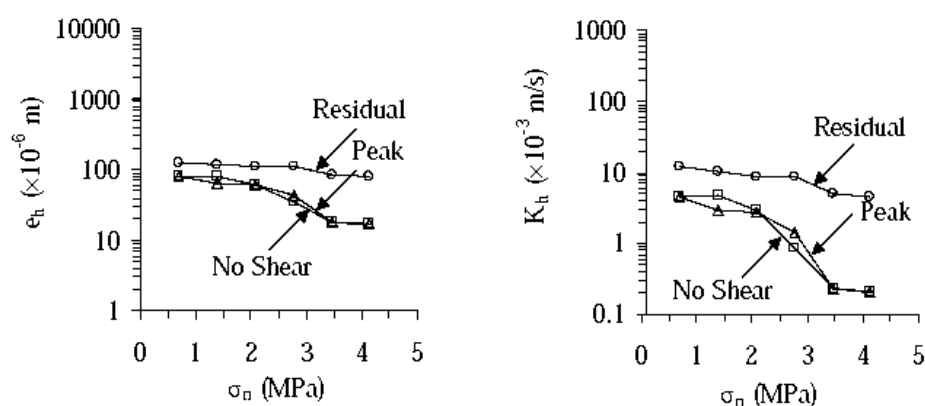


Figure 10. Hydraulic aperture (left) and hydraulic conductivity (right) as a function of applied normal stress for PW sandstone specimens.

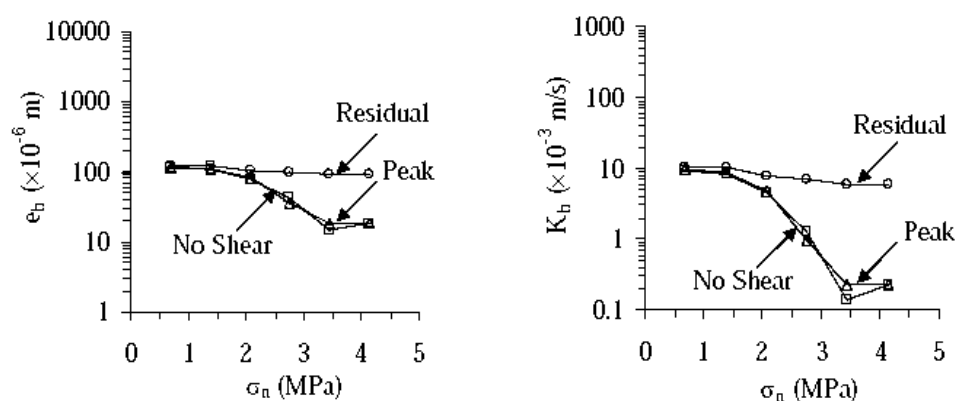


Figure 11. Hydraulic aperture (left) and hydraulic conductivity (right) as a function of applied normal stress for PP sandstone specimens.

Table 3. Joint shear stiffness for PP and PW sandstones.

PP	K_s (GPa/m)	PW	K_s (GPa/m)
PPSS-DS-01	5.17	PWSS-DS-01	11.49
PPSS-DS-02	6.47	PWSS-DS-02	12.93
PPSS-DS-03	11.34	PWSS-DS-03	10.34
PPSS-DS-04	14.13	PWSS-DS-04	8.08
PPSS-DS-05	8.62	PWSS-DS-05	6.47
PPSS-DS-06	9.42	PWSS-DS-06	6.90
Average	9.19 ± 3.25	Average	9.37 ± 2.62

5 FLOW TESTING ON SANDSTONE FRACTURES UNDER NORMAL STRESSES

Falling head flow tests have been performed to determine the fracture permeability in PW, PP, PK and SK sandstone specimens under normal stresses. One cycle of loading and unloading has been made during the flow test. During loading the normal stresses are

progressively increased from 0.35, 0.69, 1.03, 1.39, 1.72 to 2.06 MPa. During unloading the normal stresses are reduced from the maximum to the minimum while the flow rates are continuously measured. The tested fractures are tension-induced fractures with a nominal area of 15×15 cm. The flow test arrangement is similar to the flow test under shear stresses. A minimum of 3 specimens have been tested for each sandstone type.

The hydraulic aperture e_h and hydraulic conductivity K_h of the fractures are plotted as a function of the normal stress in Figure 12. They are calculated by using equations (4) and (6). For all sandstone types the fracture hydraulic conductivities exponentially decrease with increasing the normal stresses. Their permeability is in the range between 100×10^{-6} m/s and 10000×10^{-6} m/s. A permanent fracture closure is usually observed after unloading as evidenced by the permanent reduction of the fracture permeability (flow rate). The joint normal stiffness is calculated by an equation (Indraratna & Ranjith, 2001):

$$k_n = \sigma_n / \delta_n \quad (7)$$

where k_n is the joint normal stiffness (MPa/m), σ_n is the normal stress (MPa), δ_n is the joint deformation or closure (m). Table 4 summarizes the results. Due to the permanent closure of the fracture under the normal stresses the normal stiffness determined from the loading curves is significantly less than that from the unloading curves.

6 DISCUSSIONS AND CONCLUSIONS

The hydraulic conductivities of the intact PW and PP sandstones decreases with increasing volumetric strain before dilation strength probably due to the closure of voids and micro-cracks, and increases with the dilation strain after the dilation strength due to the initiation and propagation of cracks and fractures. The hydraulic conductivity of the PW sandstone decreases from about 100×10^{-9} m/s to about 50×10^{-9} m/s as the confining pressures increase from 3.45 MPa to 20.7 MPa. The flow rates measured during unloading show a permanent reduction of the rock permeability, suggesting that a permanent collapse of the pore spaces has occurred.

Both physical and hydraulic apertures (e_p and e_h) increase with shearing displacement, particularly under high normal stresses. The hydraulic conductivity derived from the actual aperture measurement (K_p) is about an order of magnitude greater than that indirectly determined from the flow rate (K_h), particularly in the residual shear region. The magnitudes of fracture permeability under no shear and under peak stress are similar. The K_p values in the residual shear region are greater than that immediately before peak stress. Both tend to decrease exponentially with the normal stress. The difference between the permeability under residual shear stress and that under peak stress becomes larger as the normal stress increases. For all sandstones tested here the fracture hydraulic conductivities exponentially decrease with increasing the normal stresses. Their permeability is in the range between 100×10^{-6} m/s and 10000×10^{-6} m/s. A permanent fracture closure is usually observed after unloading as evidenced by the permanent reduction of the flow rate.

More testing is required to develop mathematical relationships between the fracture hydraulic conductivity (or hydraulic apertures) with the applied normal stresses for the peak and the residual regions. Such relations would be useful in predicting the fracture permeability in rock mass around underground excavations or in the slope embankments where displacement of fractures usually occur.

Flow testing of sandstone fractures under normal and shear stresses

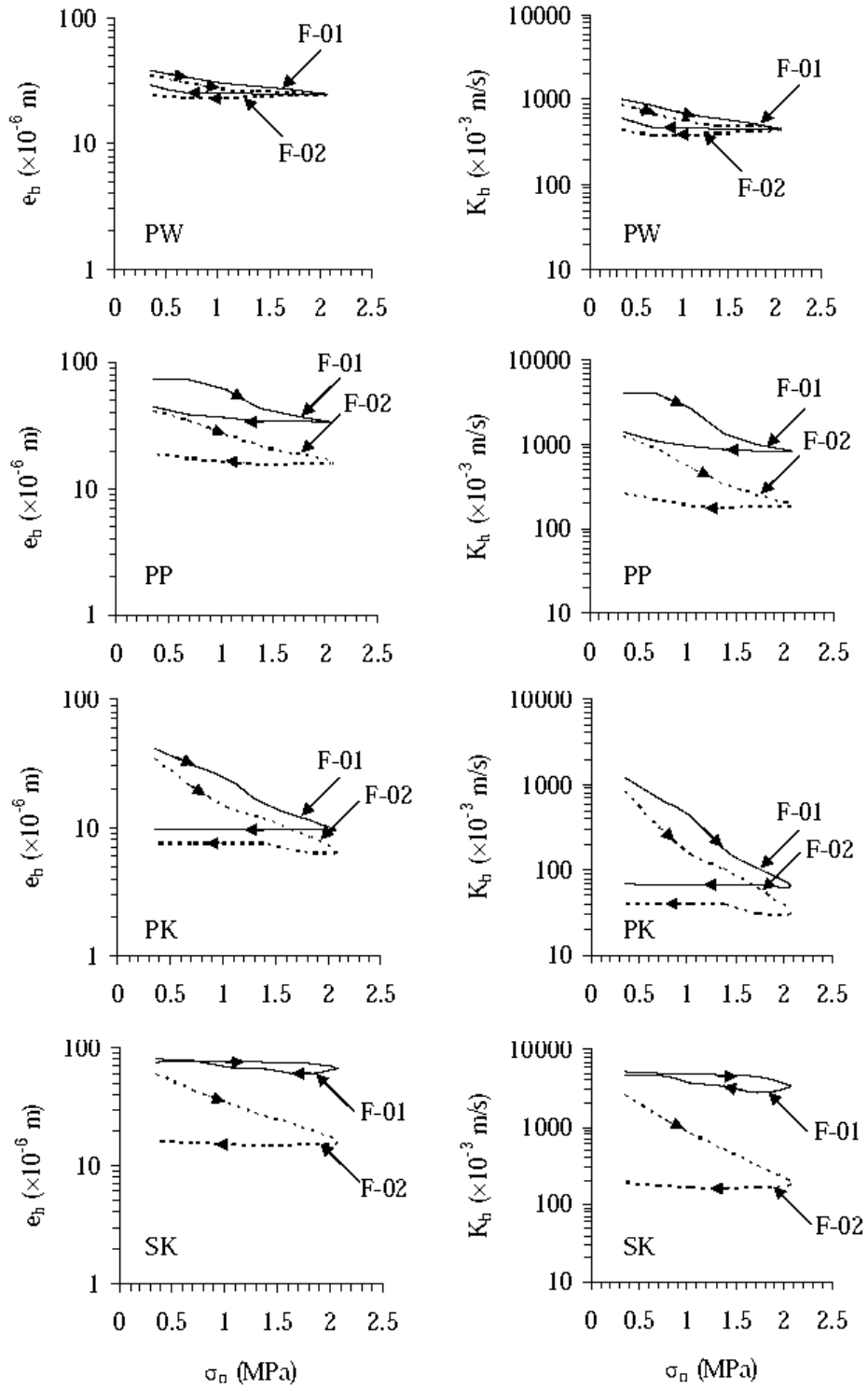


Figure 12. Hydraulic aperture (e_h) and hydraulic conductivity (K_h) as a function of normal stress (σ_n) for fracture in PW, PP, PK and SK sandstones.

Table 4. Joint normal stiffness for PW, PP, PK and SK sandstones.

K_n (GPa/m)	PW	PP	PK	SK
Loading	427.2±533.7	85.2±43.2	72.3±45.1	48.5±20.3
Unloading	1548.9±1817.4	1837.9±3875.5	18504.3±4296.8	211±905.9

ACKNOWLEDGMENT

This research is funded by Suranaree University of Technology. Permission to publish this paper is gratefully acknowledged.

REFERENCES

- Auradou, A., Drazer, G., Boschan, A., Hulin, J.P. & Koplik, J., 2006. Flow channeling in a single fracture induced by shear displacement. *Geothermics*. 35(5-6): 576–588.
- Baghbanan, A. & Jing, L., 2008. Stress effects on permeability in a fractured rock mass with correlated fracture length and aperture. *International Journal of Rock Mechanics & Mining Sciences*. 45(8): 1320-1334.
- Bandis, S.C., Barton, N.R. & Christianson, M., 1985. Application of a new numerical model of joint behaviour to rock mechanics problems. *Proc. Int. Symp. On Fundamentals of Rock Joints*, Bjorkliden.
- Bandis, S.C., Lumsden, A.C. & Barton, N.R., 1983. Fundamentals of rock joint deformation. *Int. J. Rock Mech. Min. Sci. Geomech. Abstr.* 20: 249-268.
- Barton, N. & Bakhtar, K., 1983. Rock joint description and modeling for the hydrothermomechanical design of nuclear waste repositories (Contract Report, submitted to CANMET). *Mining Research Laboratory*, Ottawa, Parts 1-4: 270; Part 5: 105.
- Ferfera, F.M.R., Sarda, J-P., Bouteca, M. & Vincke, O., 1997. Experimental study of monophasic permeability changes under various stress paths. *Int. J. Rock Mech. & Min. Sci.* 34: 3-4.
- Heiland, J., 2003. Permeability of triaxially compressed sandstone: Influence of deformation and strain-rate on permeability. *Pure appl. Geophys.* 160: 889-908.
- Indraratna, B. & Ranjith, P.G., 2001. Laboratory measurement of two-phase flow parameters in rock joints based on high pressure triaxial testing. *Journal of Geotechnical and Geoenvironmental Engineering*. 127(6): 530-542.
- Indraratna, B., & Ranjith, P., 2001. *Hydromechanical Aspects and Unsaturated Flow in Joints Rock*. Lisse: A. A. Balkema.
- Iscan, A.G., Kok, M.V., & Bagc, A.S., 2006. Estimation of permeability and rock mechanical properties of limestone reservoir rocks under stress conditions by strain gauge. *Journal of Petroleum Science and Engineering*. 53: 13-24.
- Lee, H. S. & Cho, T.F., 2002. Hydraulic characteristics of rough fractures in linear flow under normal and shear load. *Rock Mechanics and Rock Engineering*. Springer-Verlag Wien. 35(4): 299-318.
- Maini, Y.N.T., 1971. *In situ hydraulic parameters in jointed rock-their measurement and interpretation*. Ph.D. Thesis. Imperial College, London. 321 p.
- Niemi, A.P., Vaattinen, T.A., Vuopio, J.A. & Polla, J.P., 1997. Simulation of heterogeneous flow in a natural fracture under varying normal stress. *International of Rock Mechanics and Mining Sciences*. 34(3-4): 565.

Flow testing of sandstone fractures under normal and shear stresses

- Oda, M., Takemura, T., & Aoki, T., 2002. Damage growth and permeability change in triaxial compression tests of Inada granite. *Mechanics of Materials* 34 (2002) 313–331.
- Pusch, G. & Weber, J.R., 1998. Correlation of rock permeability and anisotropic stress conditions for the integration of rock mechanical and hydraulic flow models. *SCA Paper 9826*.
- Pyrak-Noltea, L.J. & Morrisa, J.P., 2000. Single fractures under normal stress: The relation between fracture specific stiffness and fluid flow. *International Journal of Rock Mechanics and Mining Sciences*. 37(1): 245-262.
- Shangxian, Y. & Shangxu W., 2006. Effect and mechanism of stresses on rock permeability at different scales. *Science in China: Series D Earth Sciences* 2006. 49(7): 714-723.
- Son, B. K., Lee, Y. K. & Lee, C.I., 2004. Elasto-plastic simulation of a direct shear test on rough rock joints. *International Journal of Rock Mechanics & Mining Sciences*. 41: 1-6.
- Xiao, Y.X., Lee, C.F. & Wang, S.J., 1999. Assessment of an equivalent porous medium for coupled stress and fluid flow in fractured rock. *International of Rock Mechanics and Mining Sciences*. 36(7): 871-881.
- Zeigler, B. 1976. *Theory of Modelling and Simulation*. New York: John Wiley and Sons.
- Zhou, J. J. & Shao, J. F., 2006. micromechanical study of damage growth and permeability variation in brittle rocks. *Studia Geotechnica et Mechanica*. Vol. 28, No. 1, 2006.
- Zhu, W., Montési, Laurent G. J. & Wong, T.F., 2002. Effects of stress on the anisotropic development of permeability during mechanical compaction of porous sandstones. *Geological Society, London, Special Publications*; 2002; v. 200; p. 119-136.

BIOGRAPHY

Mr. Natthawat Akkrachattrarat was born on July 24, 1985 in Surin province, Thailand. He received his Bachelor's Degree in Engineering (Geotechnology) from Suranaree University of Technology in 2006. For his post-graduate, he continued to study with a Master's degree in the Geological Engineering Program, Institute of Engineering, Suranaree university of Technology. During graduation, 2007-2009, he was a part time worker in position of research assistant at the Geomechanics Research Unit, Institute of Engineering, Suranaree University of Technology. He has published one technical papers related to rock mechanics, titled **“Flow Testing of Sandstone Fractures under Normal and Shear stresses”** published in the Proceeding of the Second Thailand symposium on rock mechanics, Chonburi, Thailand.